NASA CONTRACTOR REPORT

NASA CR-2048

ULTIMATE WIND SENSING CAPABILITIES OF THE JIMSPHERE AND OTHER RISING BALLOON SYSTEMS

by James K. Luers and Charles D. MacArthur

Prepared by
UNIVERSITY OF DAYTON
Dayton, Ohio 45409
for George C. Marshall Space Flight Center

NATIONAL AERONAUTICS AND SPACE ADMINISTRATION • WASHINGTON, D. C. • JUNE 1972

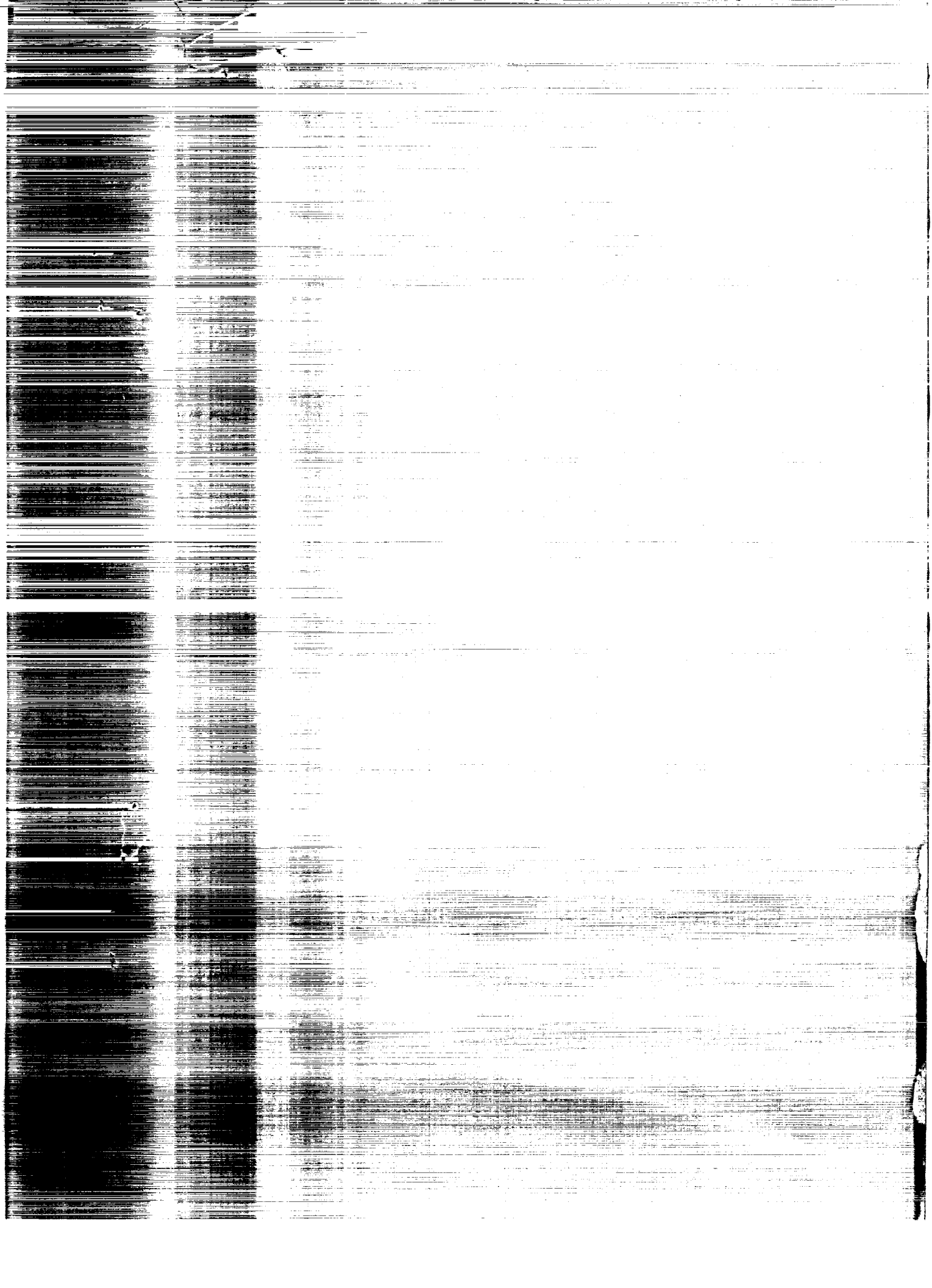

TECHNICAL REPORT STANDARD TITLE PAGE

1. REPORT NO.	2. GOVERNMENT ACCESSION NO.	3. RECIPIENT'S CATALOG NO.
NASA CR-2048		

4. TITLE AND SUBTITLE

ULTIMATE WIND SENSING CAPABILITIES
OF THE JIMSPHERE AND OTHER RISING BALLOON SYSTEMS

5. REPORT DATE: June 1972

6. PERFORMING ORGANIZATION CODE

7. AUTHOR(S): James K. Luers and Charles D. MacArthur

8. PERFORMING ORGANIZATION REPORT #

9. PERFORMING ORGANIZATION NAME AND ADDRESS
University of Dayton
Research Institute
Dayton, Ohio 45409

10. WORK UNIT NO.

11. CONTRACT OR GRANT NO.: NAS8-26600

12. SPONSORING AGENCY NAME AND ADDRESS
NASA
Washington, D. C. 20546

13. TYPE OF REPORT & PERIOD COVERED: CONTRACTOR REPORT

14. SPONSORING AGENCY CODE

15. SUPPLEMENTARY NOTES

16. ABSTRACT

The error in the magnitude of the horizontal wind field as computed for balloons with linear and quadratic rise rates ascending through a light, moderate, or severe wind field has been derived. The linear and quadratic rise rate functions chosen span the set of all practical rise rate functions for a rising balloon. The rise rate function of the Jimsphere is analyzed as a special case. Figures are presented which show the wind error versus altitude for each rise rate, and each wind field, assuming linear smoothing. The results and figures presented are useful in determining the ultimate capability of rising balloon systems in general and for the Jimsphere system in particular for measuring wind from the surface to 18 kilometers. Using the figures presented, one can estimate the wind accuracy that can be achieved by any type of rising balloon by knowing only its rise rate behavior versus altitude. In addition, the figures can be used in balloon design to determine what rise rate function is needed to achieve specified accuracies. For a specified rise rate function, the radius of a smooth and roughened sphere needed to achieve the desired rise rate at various altitudes has been derived. Since the rise rate depends largely upon drag coefficient, two different drag coefficient curves were assumed - one for a smooth and one for a roughened sphere. Tables are presented which show the balloon radius for smooth and roughened spheres needed to achieve two-meter-per-second to 20-meter-per-second rise rates at 10 and 14 km altitudes. The wind-following capability for balloons of each radius was also determined. Even balloons of very large diameter are shown to provide excellent response to fine scale wind fluctuations.

17. KEY WORDS	18. DISTRIBUTION STATEMENT
Wind Profiles, Rise Rate, Balloon Sensor Self-Induced Balloon Motion	

19. SECURITY CLASSIF. (of this report)	20. SECURITY CLASSIF. (of this page)	21. NO. OF PAGES	22. PRICE
Uncl	Uncl	111	$3.00

*For sale by the National Technical Information Service, Springfield, Virginia 22151

FOREWORD

This report was prepared by the University of Dayton Research Institute for the National Aeronautics and Space Administration, George C. Marshall Space Flight Center, Huntsville, Alabama under Contract NAS8-26600. Dr. George H. Fichtl of Marshall Space Flight Center was the Technical Monitor of the contract. The authors wish to thank Mrs. Nancy Fratini, Mr. Christopher Johnston, and Mr. C. Frank Ball for their assistance in preparing the computer programs used in this study. We are indebted to them for many helpful comments and suggestions.

TABLE OF CONTENTS

LIST OF FIGURES

LIST OF TABLES

LIST OF SYMBOLS

A	Cross sectional area of balloon
A_s	Surface area of balloon
A, A'	Amplitude of wind field and balloon response respectively
A, B	Coefficients of linear segment of wind field
b	Constant of integration
C_D	Drag coefficient of balloon
D_B	Amplification factor of balloon response
D_f	Amplification factor of filter response
E	Dynamic error
g	Gravitational acceleration
K, K_1, K_2	Constants
m'	Apparent mass of balloon
m_{gas}	Mass of gas contained in balloon
m_{skin}	Mass of balloon skin
N	Number of points fit by linear polynomial smoothing
q, q^*	Constants
r	Radius of spherical balloon
R	Reynolds number
R, E, A	Radar spherical coordinates
S, S'	Length of linear smoothing intervals
ΔS	Thickness of the skin of the balloon
t	Time in seconds
$\Delta t, \Delta t'$	Radar time constants
V	Volume of balloon
W	Wind magnitude
W_x, W_y	Wind components in the x and y directions
$\vec{W}_t$	True wind vector
$\vec{W}$	Measured wind vector
W_x, W_y	x and y components of the measured wind vector

x, y, z	Cartesian coordinates of balloon
$\dot{x}, \dot{y}, \dot{z}$	Cartesian balloon velocities
$\ddot{x}, \ddot{y}, \ddot{z}$	Cartesian balloon accelerations

Greek Symbols

α, β, γ	Coefficients of linear and quadratic rise rate functions
θ	Wind direction
λ	Wavelength of wind field
μ	Coefficient of viscosity of air
ρ	Density of air
ρ_{gas}	Density of gas contained in balloon
ρ_{skin}	Density of skin of balloon
σ_w	RMS error in wind magnitude
$\sigma_R, \sigma_E, \sigma_A$	RMS errors in radar spherical coordinates
$\sigma_x, \sigma_{\dot{x}}$	Standard deviation of the error in x and $\dot{x}$
ω	2π times the frequency

INTRODUCTION

The FPS-16 radar/Jimsphere rising balloon system is one of the most accurate operational methods of obtaining detailed wind profile measurements from the surface to eighteen kilometers. At present, the system can routinely provide wind speed measurements to an RMS accuracy of about 0.5 meter per second with a vertical spatial frequency resolution of about one cycle per 100 meters [1]. Such wind data is sufficiently accurate to allow computation of the important structural loads on space vehicles during the critical, high dynamic pressure regions of flight. The ultimate accuracy achievable by the FPS-16/Jimsphere system depends upon such factors as the influence of noise in the radar data, the noise suppression capability and frequency response of the data smoothing method, the geometry of the balloon trajectory, and, of course, the ability of the balloon to respond to changes in the wind field (balloon response). The first purpose of this study is to investigate the effects of these and other factors on the accuracy of the FPS-16/Jimsphere system in order to determine its ultimate wind measuring ability. The second purpose is to examine the wind measuring ability of rising balloons possessing rise rates other than the nominal five meter per second constant rate of the Jimsphere. The main emphasis will be placed upon the influences of radar noise, trajectory geometry, balloon rise rate, and smoothing techniques. In the first section of the report, the accuracy of the present system will be examined. The second section is devoted to an investigation of variable rise rates and their effects on the system accuracy. Previous studies of the balloon response and other aerodynamic characteristics will be briefly reviewed.

ACCURACY OF THE PRESENT FPS-16/JIMSPHERE SYSTEM

Sources of Error

To determine the ultimate accuracy of the Jimsphere system the nature of the sources of error must be considered. Since the central principle of the Jimsphere system is the determination of winds from time history of balloon position data provided by a tracking radar, the ability of the balloon to respond to the wind and the ability of the radar to provide an accurate track are of great importance. Accordingly, much study has been devoted to the Jimsphere's aerodynamic characteristics and the effects of radar error. A brief examination of some of the conclusions reached is given below.

Response of the Jimsphere to the Wind Field - Several investigators have presented analyses of the dynamic response of rising balloons and falling spheres to variations in the wind field [Ref. 1-6]. Reed [2] and Eckstrom [3] considered responses to linear wind speed variations, while Luers and Engler [4] examined the response to sinusoidal changes of wind speed with altitude. Zartarian and Thompson [1] considered wind profiles of both sinusoidal and linear character for the Jimsphere and ROSE rising balloons. In each investigation the response to vertical variations of totally horizontal winds was examined under the assumptions of no vertical winds, constant rise rate, an absence of lift forces, and motion confined to a vertical plane. In particular, Zartarian and Thompson show that the Jimsphere's response to both types of wind field is quite good. A measure of response is the dynamic error, E_d, which is defined as the horizontal sensor velocity subtracted from the true horizontal wind velocity ($E_d = W_x - \dot{x}$). Zartarian and Thompson have shown that this dynamic error for linear wind fields is given by $E_d = \alpha L$ where α is the wind shear (meters/second) and L is the "lag distance", a function of the balloon rise rate, mass, and the mass of displaced air. The Jimsphere lag distance is about 1.5 meters so that even in a wind field of an unusually large shear of 0.1 sec^{-1} the dynamic error in wind speed is only 0.15 meter per second, which is much smaller than other errors in the system. The dynamic error for wind fields with a sinusoidal wind speed variation with

altitude is given by a considerably more complicated expression [1]. A more preferable method of expressing the response to sinusoidal variations is to give the amplification factor, D_B, and phase angle, φ_B, of the balloon's motion. The amplification factor is the ratio of the amplitude of the balloon's motion to that of the wind, or $D_B = \text{Amp}(\dot{x})/\text{Amp}(W_x)$ and the phase angle is the angle (in degrees) by which the balloon's sinusoidal motion lags the wind's.

Figure 1, abstracted from [1], presents the variation of D_B and φ_B with the wavelength of the wind field for two representative altitudes, 9 and 14 kilometers. From the figure we see that D_B is above 0.9 and φ_B below 15^o for wavelengths longer than 30 meters, and that D_B is very near 1.0 and φ_B near 1^o and 2^o at wavelengths longer than 90 meters. If we adopt a criterion of a 10% allowable error in amplitude, it can then be said that the Jimsphere is an adequate sensor (in terms of dynamic response) for sinusoidal wind variations of wavelengths as short as approximately 30 meters. At these wavelengths the balloon motion is about 15^o "behind" the wind motion. For these reasons the Jimsphere is usually assumed to be a perfect wind sensor for large horizontal variations in the wind field. Thus, the balloon's horizontal velocity components are taken as those of the wind.

DeMandel and Krivo [5] have investigated the ability of the Jimsphere system to detect vertical winds and have concluded that up to 15 kilometers the system is capable of resolving vertical wavelengths greater than 250 meters with an RMS vertical wind speed accuracy of five centimeters per second. Fichtl [6] has analyzed the Jimsphere response to vertical variations of both the horizontal and vertical components of the wind in light of the proposed use of the Jimsphere system for the detection of clear air turbulence. His study shows that it may be possible to use the Jimsphere to detect turbulence (at least below 13 kilometers) if proper data reduction techniques can be developed and careful attention is paid to the balloon's response characteristics.

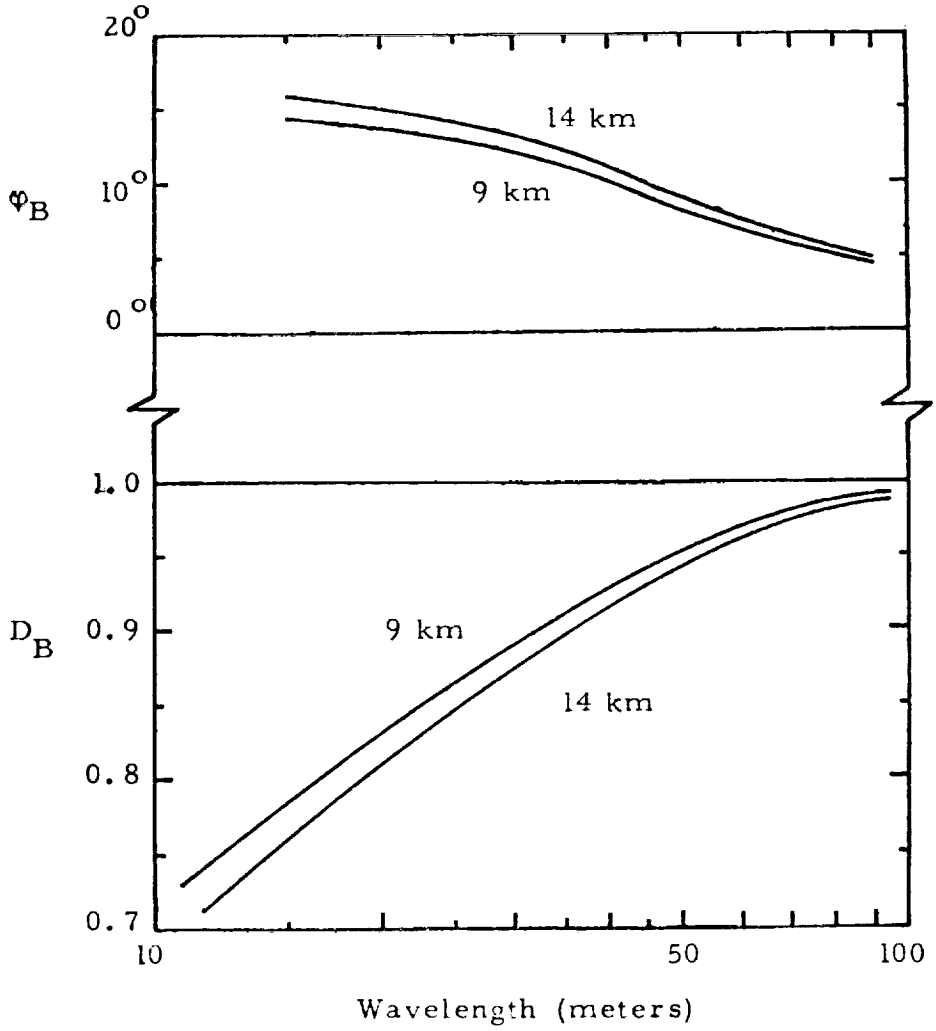

Figure 1. Amplification Factor and Phase Angle of the Jimsphere Response.

Self-Induced Motion - Included in any discussion of the aerodynamics of rising spherical balloons must be a mention of the phenomenon of self-induced motion. A number of investigations of the self-induced motion of balloons have been made [Ref. 7-12]. Most recently Fichtl et al. [12] have examined the aerodynamic characteristics and self-induced motion of the Jimsphere, which was designed expressly for reducing the self-induced motions originally observed in the smooth-skinned ROSE series of balloons. Fichtl's work shows that the Jimsphere can be expected to execute self-induced, oscillatory motion, predominately in the horizontal plane, at frequencies in

the vicinity of 0.21 Hz. The exact frequency (or wavelength) of the oscillations depends upon Reynolds number, but wavelengths usually between 21 and 26 meters may be expected assuming a constant rise rate of five meters per second. Certainly the effects of these motions must be taken into account if data processing methods are to be devised to resolve the finer details of wind profiles.

Radar Errors - Radar tracking of the Jimsphere is presently accomplished with the AN/FPS-16 radar, a high accuracy, monopulse, range-tracking radar. A detailed error analysis of the FPS-16 has been given by Barton [13]. The performance of this radar in tracking superpressure balloons has been examined by Zartarian and Thompson [1], Scoggins [14], and Engler, et al. [15, 16]. The errors associated with the radar may be generally divided into two groups: noise errors and bias errors. Of these, noise errors are of much greater importance since the noisy position data must be smoothed and differentiated to obtain winds. The noise error in the winds is a direct effect of the original noise in the position data. Bias errors, however, have virtually no effect on wind computations due to the nature of the differentiation process. A further distinction can be made between "fixed (noise) errors" which have approximately constant values and "variable (noise) errors" whose magnitudes depend upon the operating conditions of the radar, the state of the atmosphere, etc. Fixed errors therefore constitute a lower limit on the error values for any tracking condition. A comprehensive description of the fixed and variable errors is given in [1]. For the purposes of this study, the values of noise error have been assumed to represent good tracking conditions. For good tracking conditions, i.e., clear weather, slant ranges less than 100 kilometers, elevation angles above 10^{o}, etc., the RMS noise errors of five meters in range (σ_R) and 0.1 mils in elevation and azimuth (σ_E and σ_A) have been used. These values are approximately those specified by the manufacturer, and may be somewhat conservative (especially for range measurements below 50 kilometer slant ranges where values of σ_R as small as 1.5 meters have been quoted [1], [15]). The

character of the noise is assumed to be thermal, so that no correlation among individual errors exists. For simplicity, the values of the RMS noise errors (σ_R, σ_E, and σ_A) are assumed constant throughout the measurement space of the radar. The limits of this space are taken to be: a maximum slant range of 150 kilometers, 360° in azimuth angle, and 5° to 85° in elevation angle. In reality, of course, these limits may be severely reduced by atmospheric conditions, clutter, etc. In order to take this into account we have noted situations where the slant ranges or elevation angles under consideration exceed 100 km. or fall below 10° respectively. In these long slant range and/or low elevation angle situations the noise error will be quite dependent on the radar's environment.

The servobandwidth setting at which the radar is operated is critical in determining how quickly the radar can respond to changes in the target position. This response is in turn reflected in the independence of the successive data points which result from the digitization of the analog tracking signals. Low bandwidth settings serve to reduce noise error but make the response sluggish and consequently introduce correlated servo response errors in the digitized data. High bandwidth settings reduce these errors but increase the effects of thermal noise. Engler, et al. [15, 16] have studied this problem in tracking with the AN/FPS-16 and have observed that for the medium bandwidth setting of five, correlation (or dependence) may exist between data points as much as 2.0 seconds apart. With high bandwidth settings, e.g., 7.5, the time between independent points (the time constant of the radar) drops to about 0.3 second. At the upper limit of 10, 0.1 second independent points may be observed, but the situation is complicated by the fact that the servo system may now be underdamped. One solution to this problem has been to average five consecutive 0.1 second data points to obtain independent 0.5 second data [17]. In this work both 0.1 second and 0.5 second sample rates have been examined in the hope that most situations will be covered.

Development of Methods for Predicting Error in Wind Measurements

The function of the data reduction process is to abstract the desired wind information from the raw data in the most accurate and efficient manner possible. In this section we will examine the propagation of errors through the data reduction process to the final wind measurements. It will be assumed that the data reduction process consists of fitting raw coordinate data points with a linear polynomial by the method of least squares, and using the first derivative of this polynomial as the value of the velocity at the center of the smoothing interval. This smoothing technique has been described by Engler, Luers, and McCloskey [15], who have shown that linear polynomial smoothing is a most desirable method in terms of reducing noise error for determining wind data for ascending balloon sensors.

The nature of the noise error in the radar generated balloon coordinates will be assumed to be random and Gaussian with no correlation among different radar spherical coordinates at the same point in time and between values of the same coordinate at successive time points. These assumptions, while not always completely valid as mentioned above, usually suffice for FPS-16 data, provided that the radar has been properly operated and maintained.

A final assumption will be made that the wind field in which the balloon flies will have no vertical components. Although, as mentioned above, some study has been given to the use of the Jimsphere as a sensor of vertical winds, the present operational system is intended as a purely horizontal wind sensor. Therefore, we will confine our analysis to errors in the measurement of horizontal winds.

Derivation of Error Expressions - The coordinate system used in the error analysis is shown in Figure 2. Raw radar data consists of a time series of sets of the three values: range, R, elevation angle, E, and azimuth angle, A.

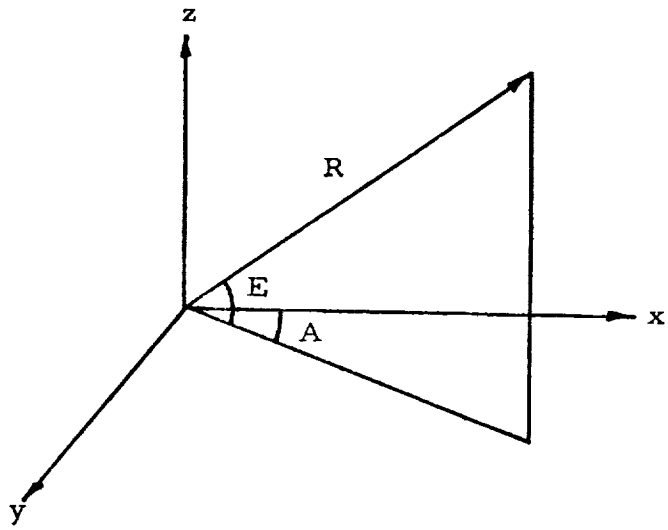

Figure 2. Rectangular and Spherical Coordinate Systems

The relation of R, E, and A to the rectangular coordinate system, is given by

$$\begin{aligned} x &= R \cos E \cos A \\ y &= R \cos E \sin A \\ z &= R \sin E \end{aligned} \qquad (1)$$

(For the purposes of this analysis correction for the earth's curvature has been ignored.)

Applying the differential error approximation, small errors in x, y, and z can be given in terms of errors in R, E, and A by

$$\begin{aligned} dx &= (\cos E \cos A)dR - (R \sin E \cos A)dE - (R \cos E \sin A)dA \\ dy &= (\cos E \sin A)dR - (R \sin E \sin A)dE + (R \cos E \cos A)dA \\ dz &= (\sin E)dR + (R \cos E)dE \end{aligned} \qquad (2)$$

The definition of the error variance (mean square error) of a quantity q is:

$$\sigma_q^2 = \langle (dq)^2 \rangle - \langle dq \rangle^2$$

where $< dq >$ denotes the expected value of an error dq. If the errors in R, E, and A are assumed to be random then $<dR> = <dE> = <dA> = 0$. The error variances (mean square errors) in x, y, and z, denoted by σ_x^2, σ_y^2, and σ_z^2, can be obtained from Equations (2) by squaring and taking the expected value of both sides. The expected value of the cross terms (i.e., those containing dRdE, dRdA, and dEdA) on the right hand side will be zero by the assumption of independence of errors in the radar measured coordinates. The error variances in the rectangular position coordinates are then

$$\sigma_x^2 = (\cos^2 E \cos^2 A)\sigma_R^2 + (R^2 \sin^2 E \cos^2 A)\sigma_E^2 + (R^2 \cos^2 A \sin^2 E)\sigma_A^2$$

$$\sigma_y^2 = (\cos^2 E \sin^2 A)\sigma_R^2 + (R^2 \sin^2 E \sin^2 A)\sigma_E^2 + (R^2 \cos^2 A \cos^2 E)\sigma_A^2$$

$$\sigma_z^2 = (\sin^2 E)\sigma_R^2 + (R^2 \cos^2 E)\sigma_E^2 \quad . \tag{3}$$

To obtain velocity, the position coordinates are numerically differentiated by fitting a linear polynomial to a given number, N, of points and using the value of the derivative of the polynomial as the velocity at the midpoint of the N point interval. The data fitting (or smoothing) is accomplished using a least squares - Legendre polynomial technique as described in reference [15]. It can be shown that the error variance in velocity resulting from this technique is given by

$$\sigma_{\dot{x}}^2 = \left[\frac{12}{N(N^2-1)\Delta t^2} \right] \sigma_x^2 \tag{4}$$

where $\sigma_{\dot{x}}^2$ is the variance of x velocity errors, σ_x^2 the variance of x position errors, N the number of points in the fitting interval, and Δt the time spacing of these points. Similar expressions apply to the velocity error variances in y and z. It should be noted that the Legendre polynomial smoothing technique, and hence Equation (4), are applicable only if the data points are equally spaced in time, which is the usual case with FPS-16/Jimsphere data. As previously mentioned, the Jimsphere may be assumed to be a perfect wind sensor so that $W_x = \dot{x}$ and $W_y = \dot{y}$, and

$$\sigma_{wx}^2 = \sigma_{\dot{x}}^2 \tag{5a}$$

$$\sigma_{wy}^2 = \sigma_{\dot{y}}^2 \quad . \tag{5b}$$

We have, by our assumption of a purely horizontal wind field, included in Equations (5) only x and y wind component errors. It may be mentioned that the error in z position, σ_z, will introduce uncertainty in the altitude at which to assign a wind measurement. However, the uncertainty in z is normally so small (usually one or two meters at most) compared to the total 18 kilometer altitude of the flight that the error is negligible.

$$\sigma_{wx}^2 = \left[\frac{12}{N(N^2-1)\Delta t^2}\right]\left[\cos^2 E \cos^2 A\, \sigma_R^2 + R^2(\sin^2 E \cos^2 A\, \sigma_E^2 + \cos^2 E \sin^2 A \sigma_A^2)\right] \tag{6a}$$

$$\sigma_{wy}^2 = \left[\frac{12}{N(N^2-1)\Delta t^2}\right]\left[\cos^2 E \sin^2 A\, \sigma_R^2 + R^2(\sin^2 E \sin^2 A\, \sigma_E^2 + \cos^2 E \cos^2 A \sigma_A^2)\right] \tag{6b}$$

The methods of using σ_{wx} and σ_{wy} to specify errors in measured wind profiles are presented in the following section.

Specifying the Accuracy of Wind Measurements - A complete description of a wind measurement at a given altitude must include both a wind speed and a wind direction or heading. Owing to this vector property of the wind field, several different methods of specifying the accuracy of a wind measurement are possible. In this section we will examine these methods.

Figure 3 shows a measurement of the wind vector, $\vec{W}$, at an altitude, z. The true value of the wind is shown by the vector $\vec{W}_t$ which may not have the same magnitude or direction as $\vec{W}$. If there are no vertical winds, both $\vec{W}_t$ and $\vec{W}$ lie in a plane parallel to that of the x and y axes and may be resolved into x and y components along these directions. The angles made by $\vec{W}_t$ and $\vec{W}$ with the x axis (clockwise being positive) are denoted as θ_t and θ, respectively. The noise errors in the components of $\vec{W}$ have been given in Equations (6). The problem, therefore, is how to use these component errors to provide an estimate of the error in the measurement of the wind vector.

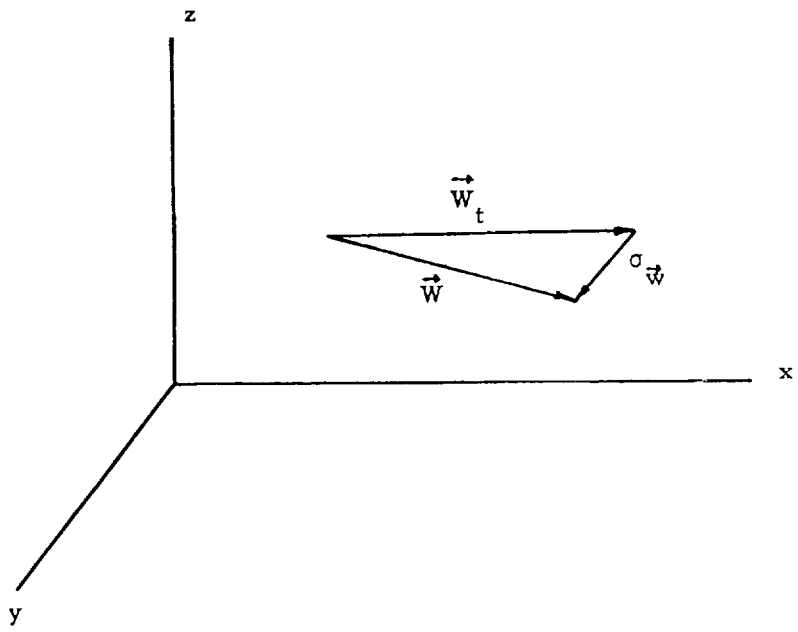

Figure 3. Relationship of the True, Measured, and Error Standard Deviation Wind Vectors.

The first attempt at specifying the accuracy of a wind measurement might be to just give the RMS errors σ_{wx} and σ_{wy}, in other words, giving the accuracy of the x (zonal or downrange) and y (meridianal or crossrange) components of the wind. This approach is not desirable for two reasons. First, of course, it does not give a direct estimate of the accuracy of the measurement of the actual wind field at an altitude, and, second, the values of σ_{wx} and σ_{wy} are dependent on the orientation of the coordinate system to the wind vector. It has been shown above that σ_{wx}^2 can be written as

$$\sigma_{wx}^2 = K[\cos^2 E \cos^2 A \sigma_R^2 + R^2(\sin^2 E \cos^2 A \sigma_E^2 + \cos^2 E \sin^2 A \sigma_A^2)] \quad (7a)$$

and

$$\sigma_{wy}^2 = K[\cos^2 E \sin^2 A \sigma_R^2 + R^2(\sin^2 E \sin^2 A \sigma_E^2 + \cos^2 E \cos^2 A \sigma_A^2)] \quad (7b)$$

where K is a constant which depends only upon the smoothing technique.

Examination of Equations (7a) and (7b) shows that, as might be expected, the values of σ_{wx}^2 and σ_{wy}^2 depend on the azimuth angle, A. Therefore, this method of specifying the wind accuracy is dependent on the x-y orientation of the coordinate system, which is not desirable.

The dependence on the coordinate system may be eliminated by adding (7a) and (7b), that is, let

$$\sigma_{\vec{W}}^2 = \sigma_{wx}^2 + \sigma_{wy}^2 \tag{8}$$

where $\sigma_{\vec{W}}^2$ is to be defined as an estimate of the error in the wind measurement. Substitution in (8) from (7a) and (7b) results in

$$\sigma_{\vec{W}}^2 = 2K[\cos^2 E\,\sigma_R^2 + R^2(\sin^2 E\,\sigma_E^2 + \cos^2 E\,\sigma_A^2)] \tag{9}$$

from which we see that the dependence on A has been eliminated. By giving $\sigma_{\vec{W}}^2$, the mean square error, or $\sigma_{\vec{W}}$, the RMS error, of a wind measurement, reference need not be made to a particular x-y coordinate system.

The approach of Equation (8), however, also has some drawbacks. Equation (8) is not a measure of the expected error in the magnitude of W or its direction, but a combination of both. In Figure 3 the measured wind vector $\vec{W}$ is shown as the sum of the true wind vector, $\vec{W}_t$, and a vector representing the error standard deviation, $\vec{\sigma}_{\vec{W}}$. The magnitudes of the x and y components of $\vec{\sigma}_{\vec{W}}$ are σ_{wx} and σ_{wy} so that the mean square error of Equation (8) is the squared magnitude of the "vector deviation" of wind measurement, $\sigma_{\vec{W}} = |\vec{\sigma}_{\vec{W}}|$. The value of $\sigma_{\vec{W}}$ is seen to depend on both the errors made in the determination of magnitude and direction of W. In many applications there is a need to know the error in the magnitude of direction of W separately. This information is not supplied explicitly by giving wind error (as has been done previously [16, 18]) as defined by

$$\sigma_{\vec{W}} = \sqrt{\sigma_{wx}^2 + \sigma_{wy}^2} = \sqrt{\sigma_{\dot{x}}^2 + \sigma_{\dot{y}}^2} \quad .$$

To obtain separate expressions for the RMS errors in the magnitude and direction of $\vec{W}$, we can express the magnitude, $W = |\vec{W}|$, and angular direction, θ, as

$$W = (W_x^2 + W_y^2)^{1/2} \tag{10a}$$

and

$$\theta = \tan^{-1} \frac{W_y}{W_x} \tag{10b}$$

where W_x and W_y are the magnitudes of the x and y components of $\vec{W}$. Applying the differential error approximation, errors in W and θ may be given in terms of errors in W_x and W_y as:

$$dW = \frac{\partial (W_x^2 + W_y^2)^{1/2}}{\partial W_x} dW_x + \frac{\partial (W_x^2 + W_y^2)^{1/2}}{\partial W_y} dW_y$$

$$dW = \frac{W_x}{W} dW_x + \frac{W_y}{W} dW_y \tag{11a}$$

and

$$d\theta = \frac{\partial}{\partial W_x} \left(\tan^{-1} \frac{W_y}{W_x} \right) dW_x + \frac{\partial}{\partial W_y} \left(\tan^{-1} \frac{W_y}{W_x} \right) dW_y$$

$$d\theta = \frac{1}{W^2} \left[W_x dW_y - W_y dW_x \right] . \tag{11b}$$

Squaring (11a) and (11b) gives

$$(dW)^2 = \frac{W_x^2 dW_x^2 + W_y^2 dW_y^2 + 2W_x W_y dW_x dW_y}{W^2} \tag{12a}$$

and

$$(d\theta)^2 = \frac{W_x^2 dW_y^2 + W_y^2 dW_x^2 - 2W_x W_y dW_x dW_y}{W^4} . \tag{12b}$$

Taking the expected value of each side of Equations (12a) and (12b),

$$\sigma_w^2 = \frac{W_x^2}{W^2}\,\sigma_{wx}^2 + \frac{W_y^2}{W^2}\,\sigma_{wy}^2 + \frac{2W_xW_y}{W^2} < dW_x dW_y > \qquad (13a)$$

and

$$\sigma_\theta^2 = \frac{W_y^2}{W^4}\,\sigma_{wx}^2 + \frac{W_x^2}{W^4}\,\sigma_{wy}^2 - \frac{2W_xW_y}{W^4} < dW_x dW_y > \qquad (13b)$$

where the term $< dW_x dW_y >$ is, in effect, the correlation in the errors in W_x and W_y. This term may be expressed in terms of σ_R^2, σ_E^2, and σ_A^2 in much the same manner as σ_{wx}^2 and σ_{wy}^2,

$$< dW_x dW_y > = \left[\frac{12}{N(N^2-1)\Delta t^2}\right]\left[\sin A\cos A(\cos^2 E\,\sigma_R^2 + R^2\sin^2 E\,\sigma_E^2 - R^2\cos^2 E\,\sigma_A^2)\right]. \qquad (14)$$

Substituting (6a), (6b), and (14) into (13a) and (13b) after some simplification yields

$$\sigma_w^2 = \left[\frac{12}{N(N^2-1)\Delta t^2}\right]\frac{1}{W^2}\left[(W_x\cos A + W_y\sin A)^2(\cos^2 E\,\sigma_R^2 + R^2\sin^2 E\,\sigma_E^2) + (W_x\cos A - W_y\sin A)^2 R^2\cos^2 E\,\sigma_A^2\right] \qquad (15a)$$

and

$$\sigma_\theta^2 = \left[\frac{12}{N(N^2-1)\Delta t^2}\right]\frac{1}{W^4}\left[(W_y\cos A - W_x\sin A)^2(\cos^2 E\,\sigma_R^2 + R^2\sin^2 E\,\sigma_E^2) + (W_y\sin A + W_x\cos A)^2 R^2\cos^2 E\,\sigma_A^2\right]. \qquad (15b)$$

Equation (15a) gives the mean square error in the direction of the wind vector V both in terms of the radar errors. It can be shown that σ_w^2 and σ_θ^2 have the desirable property of being independent of azimuth angle. Computing the wind error as in (15a) and (15b) allows one to quote a wind measurement and its accuracy as a wind speed of, say, W meters per second $\pm\sigma_w$ meters per second and a direction of $\theta^\circ \pm \sigma_\theta^\circ$. We believe that this method of specifying wind

error is most desirable, and we will use Equations (15) as the definitions of wind error in the remainder of the report.

The quantities σ_w and σ_θ may be combined, if desired, to give the magnitude of the vector deviation, $\sigma_{\vec{w}}$, as given by Equation (8). If we return to σ_w and σ_θ as given by Equations (13) and multiply both sides of (13b) by W^2 and then add it to (13a) we see that

$$\begin{aligned}
\sigma_{\vec{w}}^2 &= \sigma_w^2 + W^2\sigma_\theta^2 \\
&= \left[\frac{W_x^2}{W^2} + \frac{W_y^2}{W^2}\right]\sigma_{wx}^2 + \left[\frac{W_y^2}{W^2} + \frac{W_x^2}{W^2}\right]\sigma_{wy}^2 \\
&\quad + \left[\frac{2W_xW_y}{W^2} - \frac{2W_xW_y}{W^2}\right]\langle dW_x dW_y\rangle \\
&= \sigma_{wx}^2 + \sigma_{wy}^2 \quad .
\end{aligned}$$

Thus, we have re-expressed Equation (8) in terms of the more useful quantities σ_w^2 and σ_θ^2.

Frequency Response - An important property of any smoothing method is its frequency response or attenuation characteristics. Engler and Luers [3] have presented a method of finding the attenuation of the first derivative for smoothing and differentiating sinusoidal position data by the linear fitting technique.

Figure 4 from [3] shows the attenuation factor D_f as a function of the "fractional smoothing wavelength", Q_f, which is the fraction of a wavelength over which the smoothing interval is taken. The attenuation factor gives the magnitude of the velocity resulting from the smoothing in terms of the true (sinusoidal) velocity, i.e., $\dot{x}_s = D_f\dot{x}_t$ where $\dot{x}_t$ is the true velocity and $\dot{x}_s$ is the velocity resulting from the smoothing. The curve of Figure 4 may be used to find the frequency response of a filter of any given length. The attenuation, D_f, for a given wavelength, λ_o, is given by the equation of the curve as shown with $Q_f = S/\lambda_o$, where S is the smoothing interval length

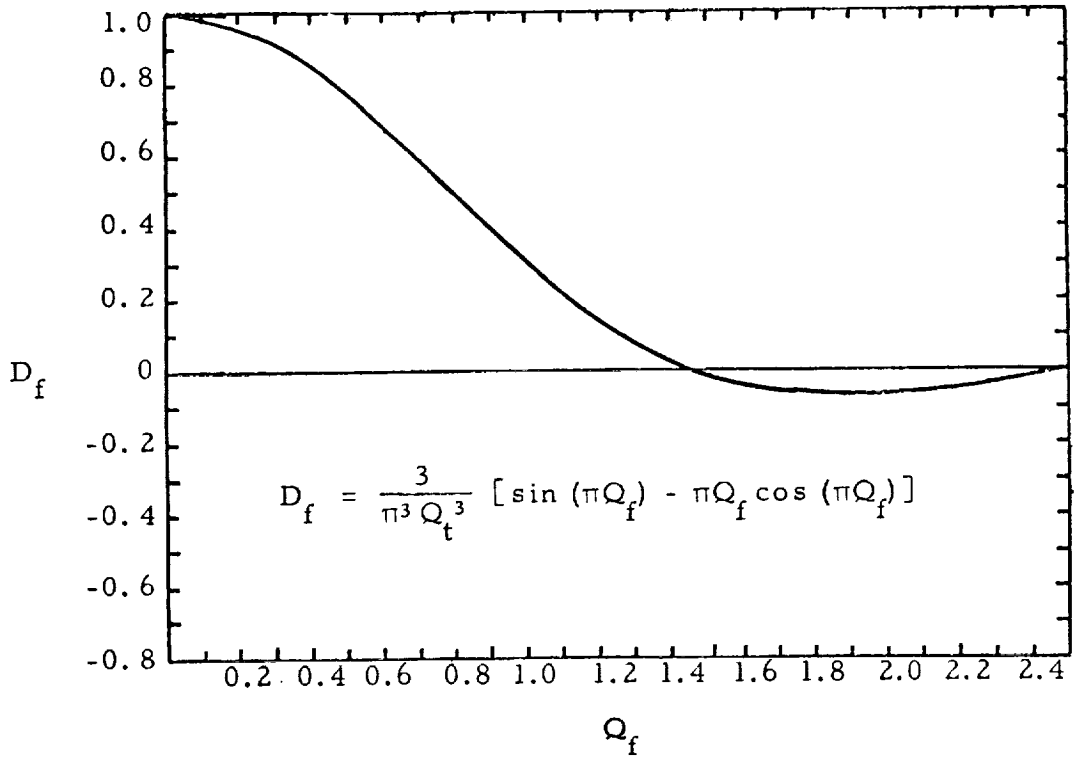

Figure 4. The Attenuation Factor, D_f, vs. the Fractional Smoothing Wavelength, Q_f, for Linear Smoothing.

in meters. For values of Q_f from 0 to about 1.43 the effect of the smoothing is to continually decrease the amplitude at a given wavelength without producing a phase shift. At $Q_f = 1.43\ \lambda_o$ the smoothing has completely removed oscillations of this wavelength from the data. Above $Q_f = 1.43$ the attenuation factor becomes negative and the oscillations appear again but are 180^o out of phase with the true velocity sine curve.

Error Analysis of Selected Wind Profiles

The method of error analysis derived in the previous sections has been applied to various wind profiles selected to be generally representative of those encountered in measurements by the FPS-16/Jimsphere system. Our main purpose is to show how the errors in wind speed and direction depend upon such factors as wind direction and magnitude (or alternatively the geometry of the balloon trajectory), sample rate, smoothing interval length, and radar noise error. The frequency response functions will also be presented for the smoothing intervals used.

Constant direction wind fields - a "worst case" analysis - We consider first situations in which the wind direction is constant over the entire 18 kilometer ascent. The launch point of the balloon is assumed, as in all cases, to be at the radar site. As mentioned above, the quantities σ_w and σ_θ are independent of azimuth angle so, for simplicity, the wind direction may be taken as parallel to the x (downrange) axis. Equations (15) will then reduce to

$$\sigma_w^2 = \sigma_{wx}^2 = \left[\frac{12}{N(N^2-1)\Delta t^2}\right]\left[\cos^2 E\,\sigma_R^2 + R^2 \sin^2 E\,\sigma_E^2\right] \qquad (16a)$$

and

$$\sigma_\theta^2 = \frac{\sigma_{wy}^2}{W_x^2} = \left[\frac{12}{N(N^2-1)\Delta t^2}\right]\left[R^2 \cos^2 E\,\sigma_A^2\right] \quad . \qquad (16b)$$

For any given smoothing interval length, time constant, and wind speed vs. altitude profile, the Jimsphere will have, at a given altitude, the largest slant range and smallest elevation angle when the flight is made in a wind field of constant direction. Therefore, we see immediately upon examining (16b) that the value of σ_θ is a maximum when the wind field has constant direction. It is not difficult to show that σ_w in (16a) also takes on maximum values when R is large and E is small.

Equations (16) were used to compute the RMS error in wind speed and direction versus altitude for three constant direction wind profiles. The

profiles, shown in Figure 5 and Table 1, were from the "Design Scalar Wind Speed Profile Envelopes (Steady State) for the Eastern Test Range" presented on page 5.172 of "Terrestrial Environment (Climatic) Criteria Guidelines for Use in Space Vehicle Development," 1969 Revision, NASA TM 53872 [19]. The "severe" and "moderate" profiles are the 95th and 50th percentiles, respectively. The "light" profile was obtained by taking wind speed values of about half of the "moderate" values. The values of the radar errors used were those mentioned above for "good" tracking conditions, namely $\sigma_R = 5$ meters and $\sigma_E = \sigma_A = 0.10$ mils. Two values of the sample rate were used, two points per second ($\Delta t = 0.5$) and 10 points per second ($\Delta t = 0.1$). All smoothing was assumed to be by linear least squares fitting with Legendre polynomials, with the slope of the line taken as the velocity at the midpoint of the smoothing interval. A number of smoothing intervals were examined. Their lengths in meters and the number of 0.1 or 0.5 second points which they contain are given in Table 2. In every case a constant rise rate of 5.0 meters per second was assumed.

TABLE 1

CONSTANT DIRECTION WIND PROFILES

Altitude Range (kilometers)	Shears (1/sec)		
	Light	Moderate	Severe
0 to 10	0.0017	0.0041	0.0060
10 to 14	0.0	0.0	0.0
14 to 18	-0.0017	-0.0052	-0.0083
Ground Wind Speed(m/s)	3.3	6.0	15.0

The results of these calculations are shown in Figures 6 through 13. Two types of plots are presented: 1) the variation of RMS wind speed error (σ_w) and the RMS wind direction error (σ_θ) with altitude and 2) the variation of σ_w and σ_θ with smoothing interval length for several representative altitudes. The plots of σ_w and σ_θ versus altitude are divided into two groups, the first

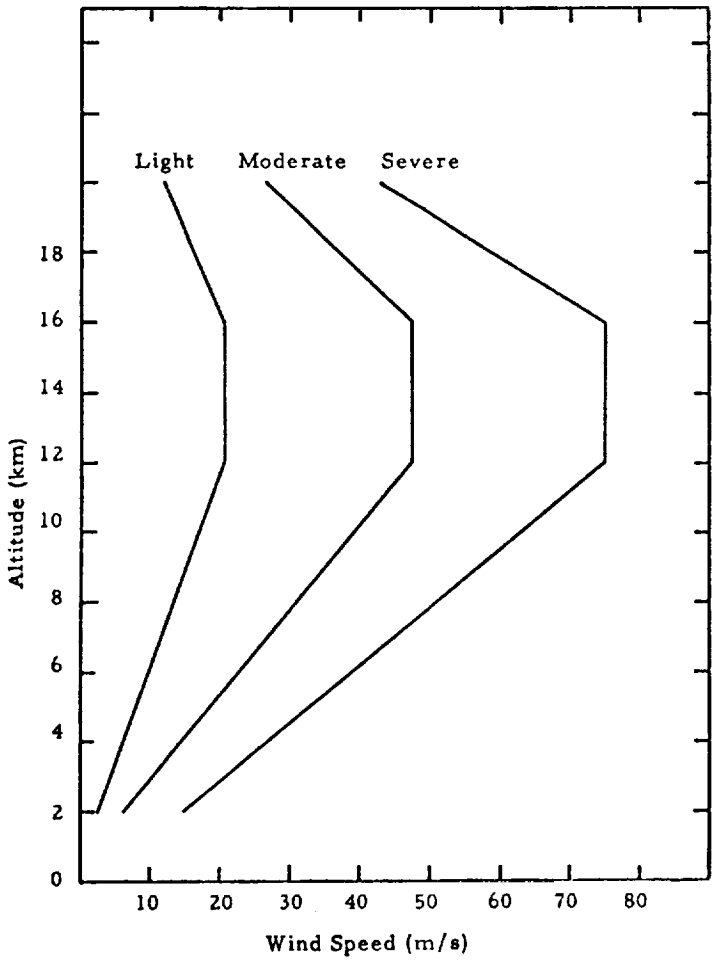

Figure 5. Constant Direction Wind Profiles.

TABLE 2

SMOOTHING INTERVALS

Interval Length (Meters)	Number of 0.1 Second Data Points	Number of 0.5 Second Data Points
10	21	5
25	51	11
37.5	76	16
50	101	21
100	201	41

in Figures 6 through 8, for a time constant (Δt) of 0.5 and the second, Figures 9 through 11, for $\Delta t = 0.1$. All three wind profiles are included in each group. Four plots of σ_w and σ_θ versus smoothing interval are given in Figures 12 and 13, all for the light wind profile. Finally, in Figure 14 the X-Z balloon trajectories for the three wind fields are shown along with several elevation angles for comparison. In some figures, sections of the curves are shown as broken lines and vertical broken lines appear at certain altitudes. The broken sections of the curves indicate slant ranges above 100 km. The curves are terminated prematurely if the slant range exceeds 150 km. The left most vertical line indicates an elevation angle of 10° and the right most vertical line an elevation of 5°.

The effects of the variations of altitude, smoothing interval length, and time constant expected from an examination of Equations (16) are apparent in the figures. In all the plots of σ_w and σ_θ versus altitude we see that σ_w shows a small increase with increasing altitude whereas σ_θ increases rapidly with altitude. These variations may be understood by examining the terms $(\cos^2 E\,\sigma_R^2 + R^2 \sin^2 E\,\sigma_E^2)$ of (14a) and $(R^2 \cos^2 E\,\sigma_A^2)/W_x^2$ of (14b). For the first few kilometers of the flight, elevation angles are relatively large (30 to 50°) and slant ranges small (1 to 3 or 4 kilometers). In these regions more of the balloon motion appears as elevation angle change than later where, at higher altitudes and larger slant ranges, elevations are small (5 to 10°) and almost constant. If the terms $(\cos^2 E\,\sigma_R^2)$ and $(R^2 \sin^2 E\,\sigma_E^2)$ of σ_w^2 are evaluated for various altitudes, it will be seen that the former is always much greater than the later. Therefore, the behavior of σ_w^2 is primarily that of $(\cos^2 E\,\sigma_R^2)$ and, since σ_R^2 is always constant, almost that of $\cos^2 E$. So, at low altitudes, σ_w increases as elevation decreases with z, and at medium and high altitudes σ_w becomes almost constant as more and more of the balloon motion lies along the slant range direction. The expression for σ_θ^2 does not contain the $\cos^2 E\,\sigma_R^2$ term, but contains the term $(R^2 \cos^2 E\,\sigma_A^2)/W_x^2$. The behavior of this term is to constantly increase with increasing altitude and range so that σ_θ always increases. For the particular wind profile shapes

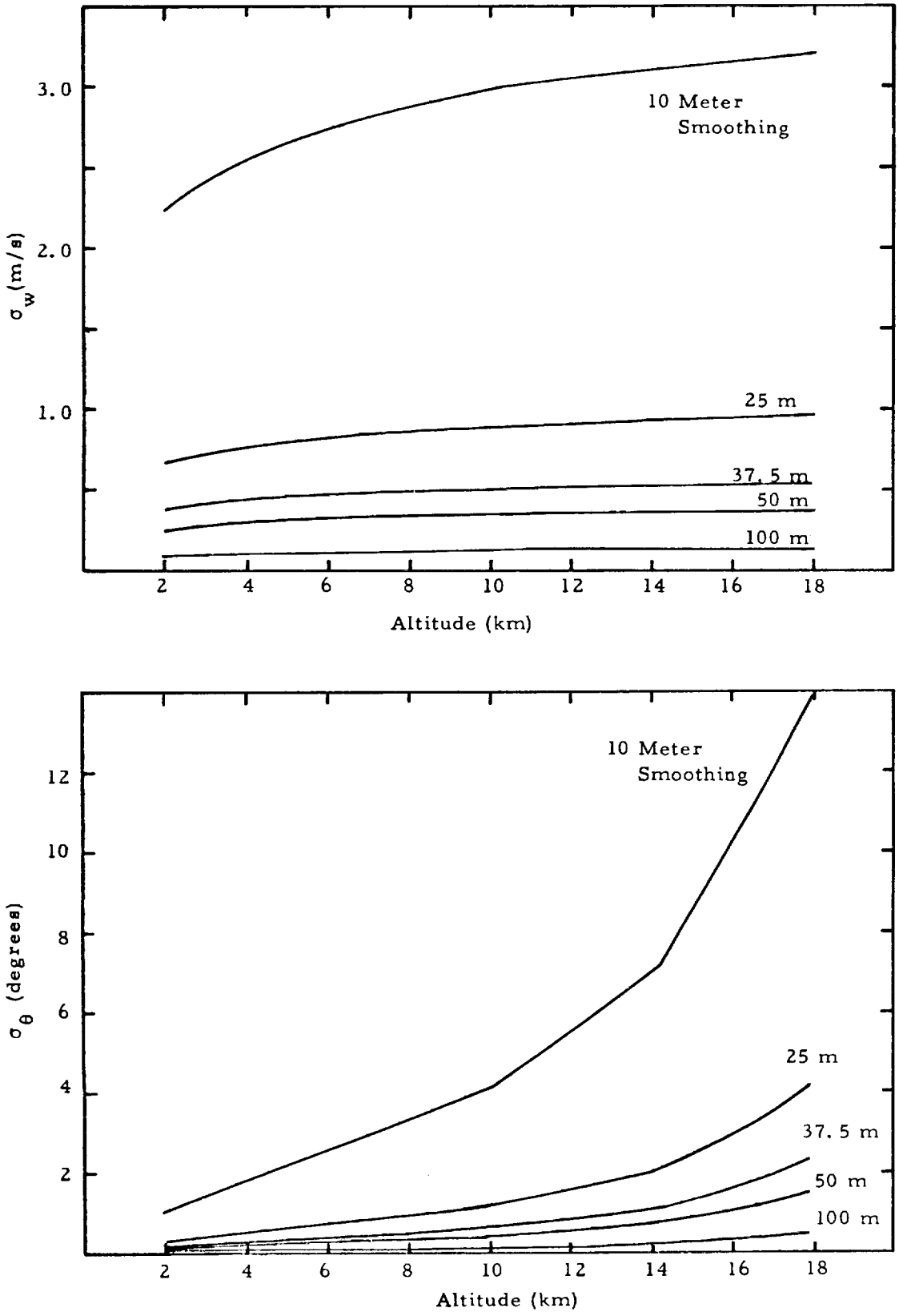

Figure 6. Wind Speed and Direction Error vs. Altitude for the Light Wind Profile (Δt = 0.5 second).

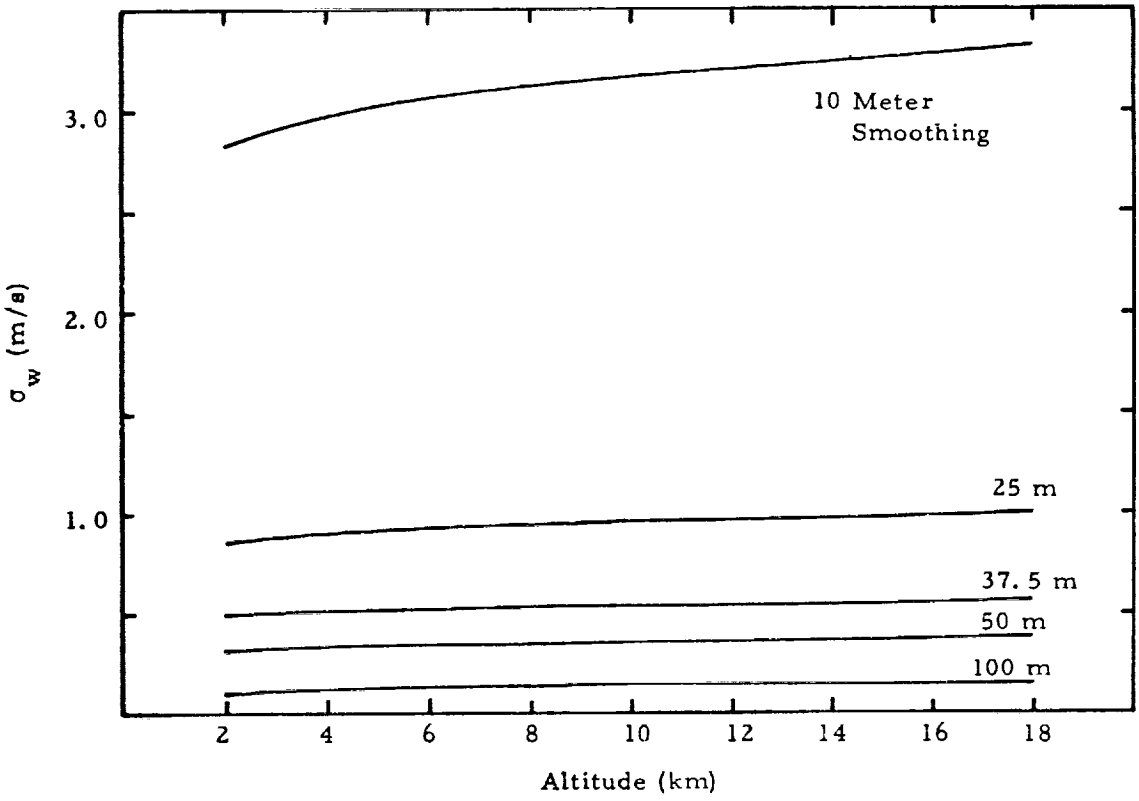

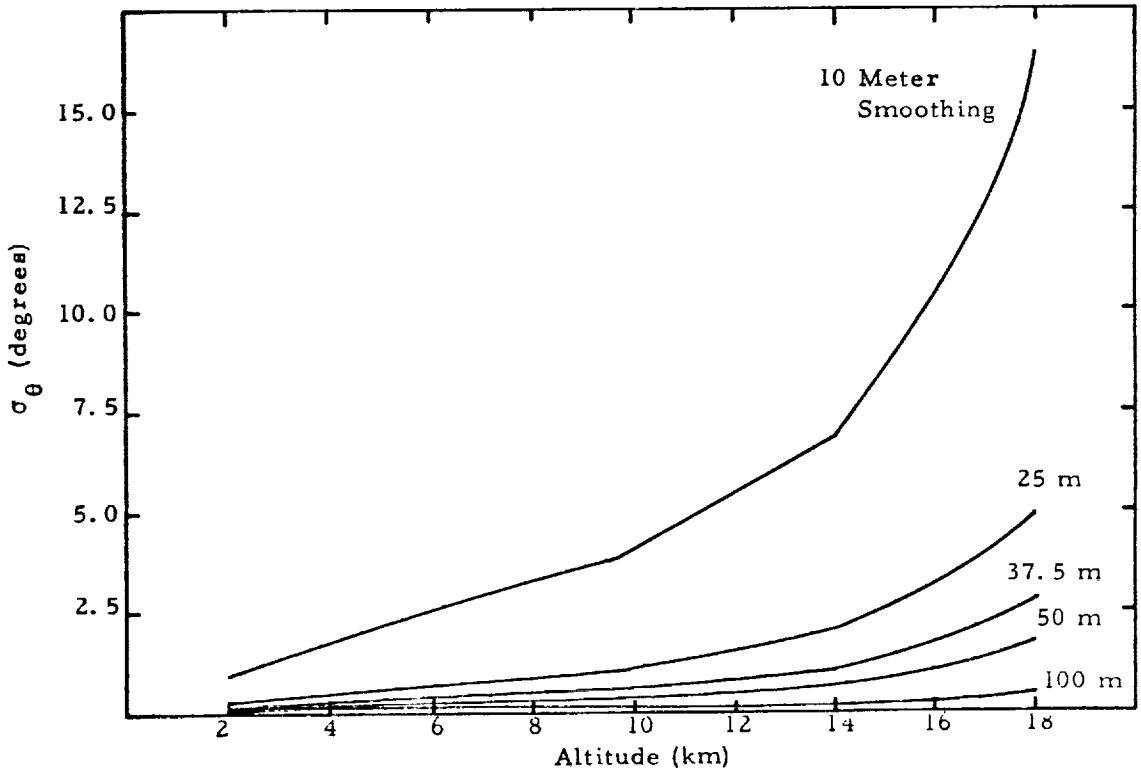

Figure 7. Wind Speed and Direction Error vs. Altitude for the Moderate Wind Profile (Δt = 0.5 second).

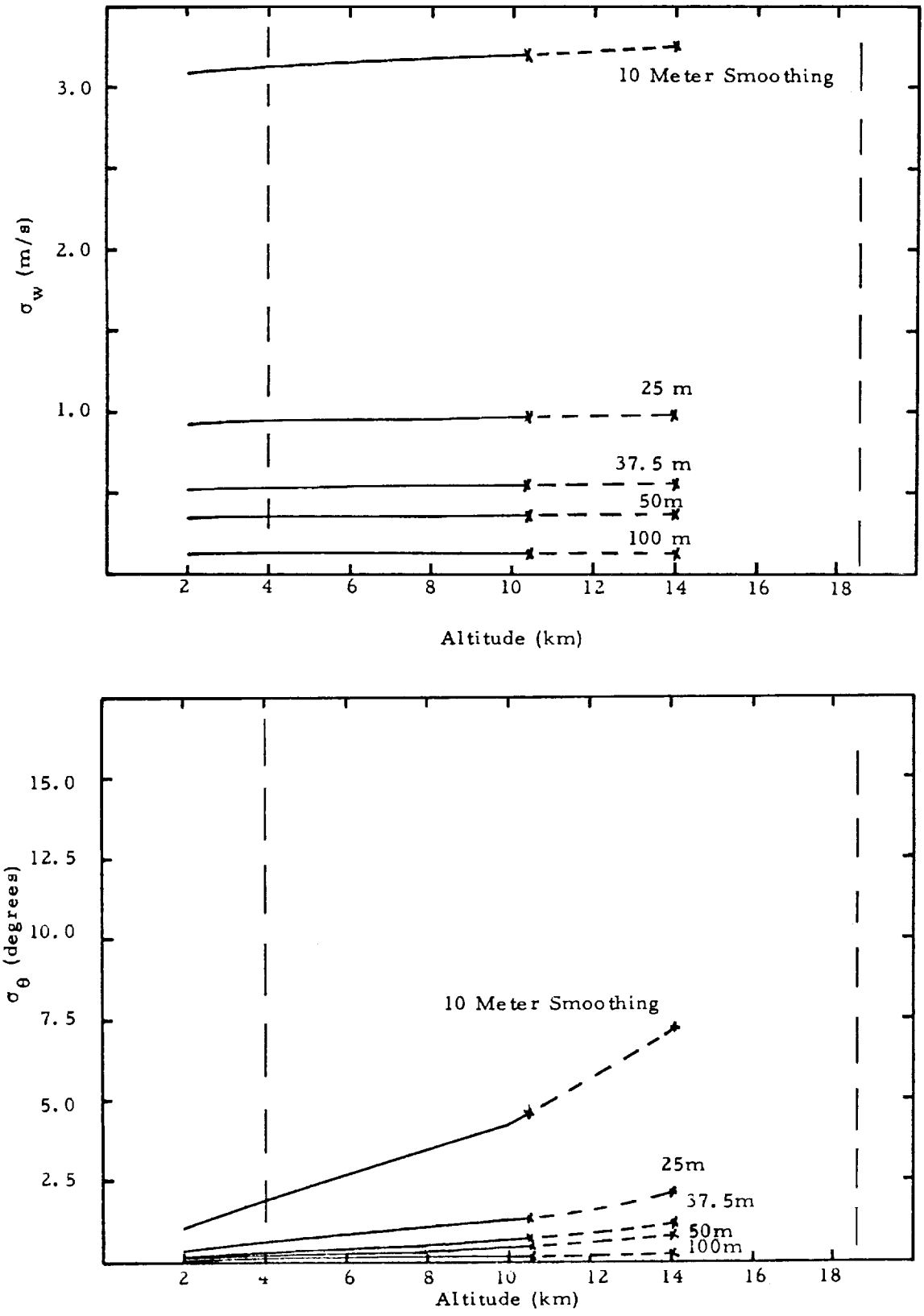

Figure 8. Wind Speed and Direction Error vs. Altitude for the Severe Wind Profile (Δt = 0.5 second).

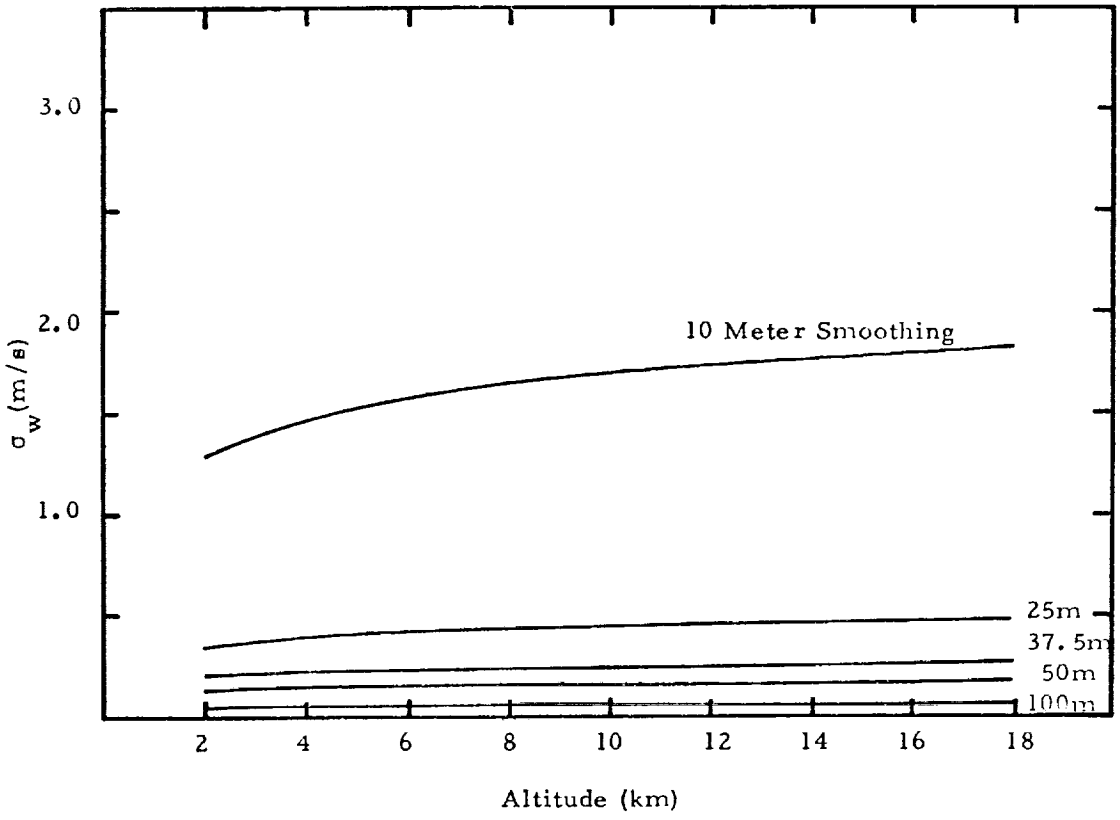

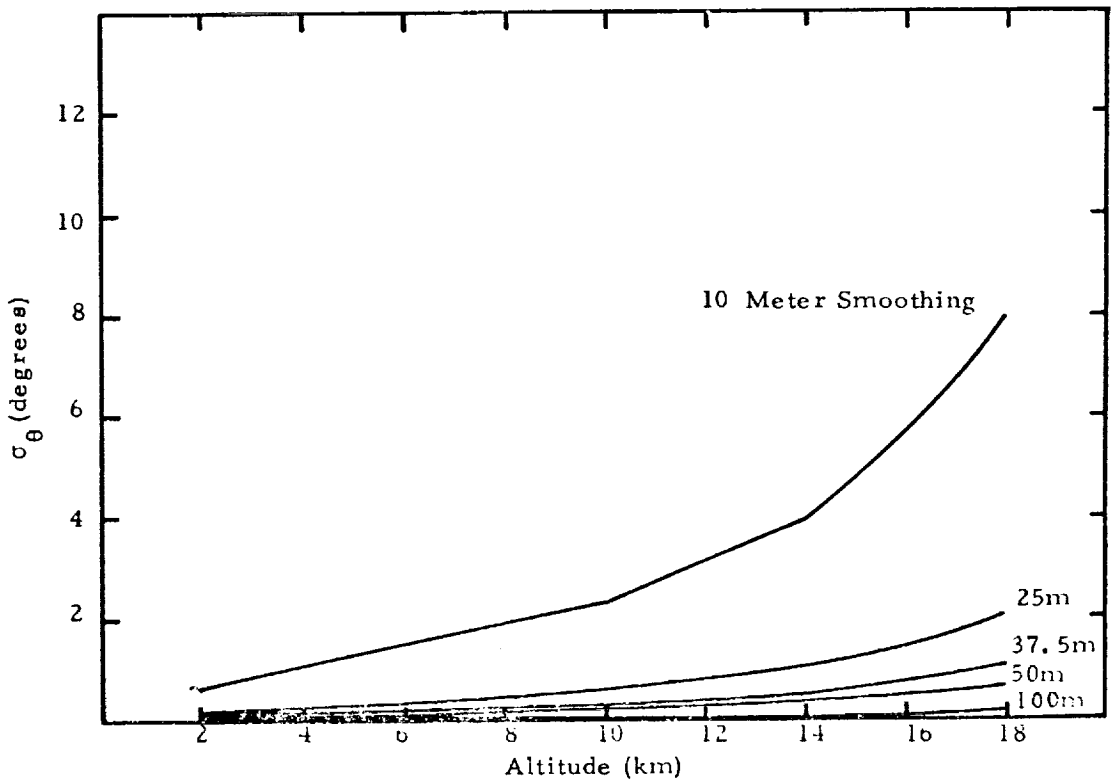

Figure 9. Wind Speed and Direction Error vs. Altitude for the Light Wind Profile (Δt = 0.1 second).

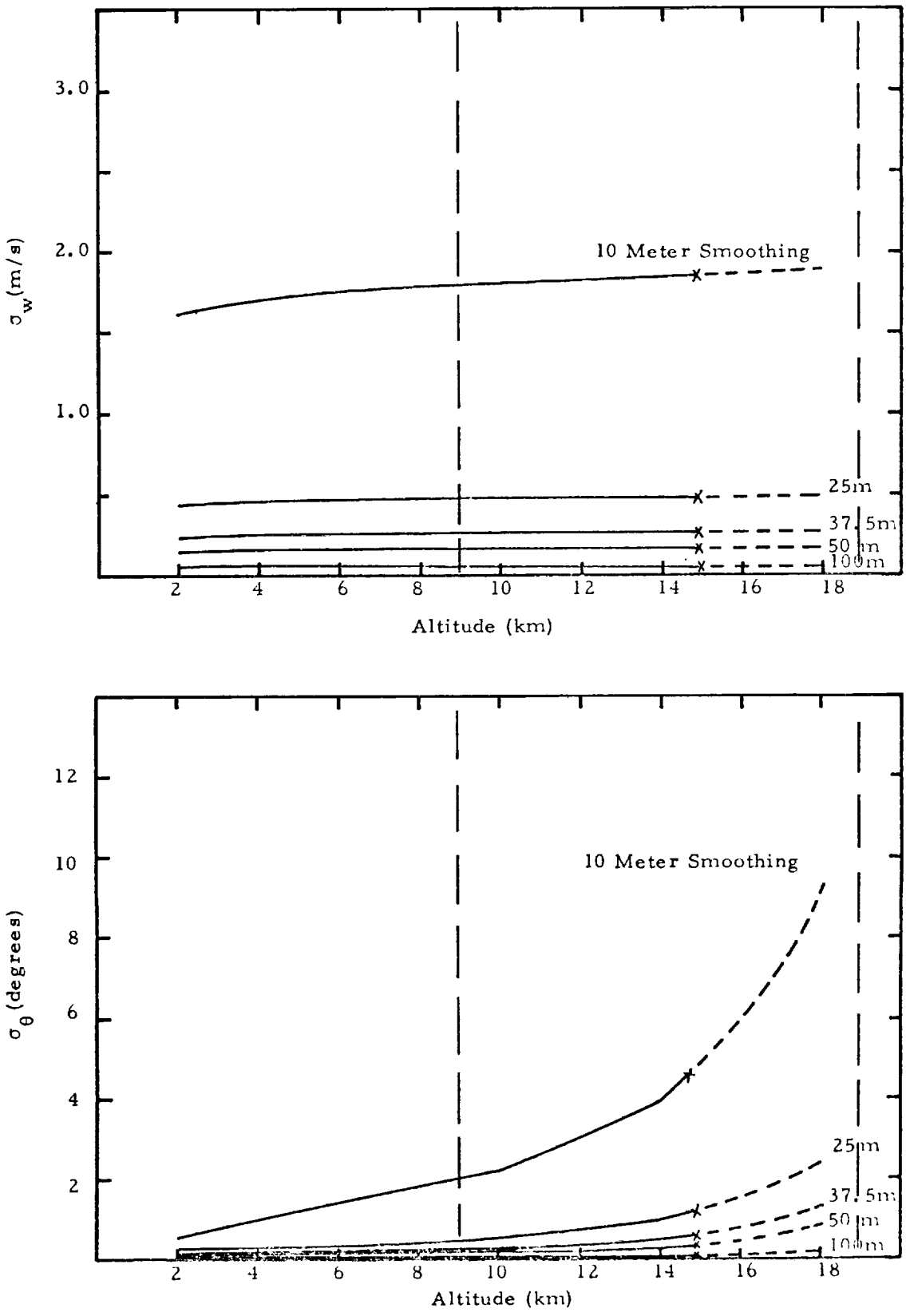

Figure 10. Wind Speed and Direction Error vs. Altitude for the Moderate Wind Profile ($\Delta t = 0.1$ second).

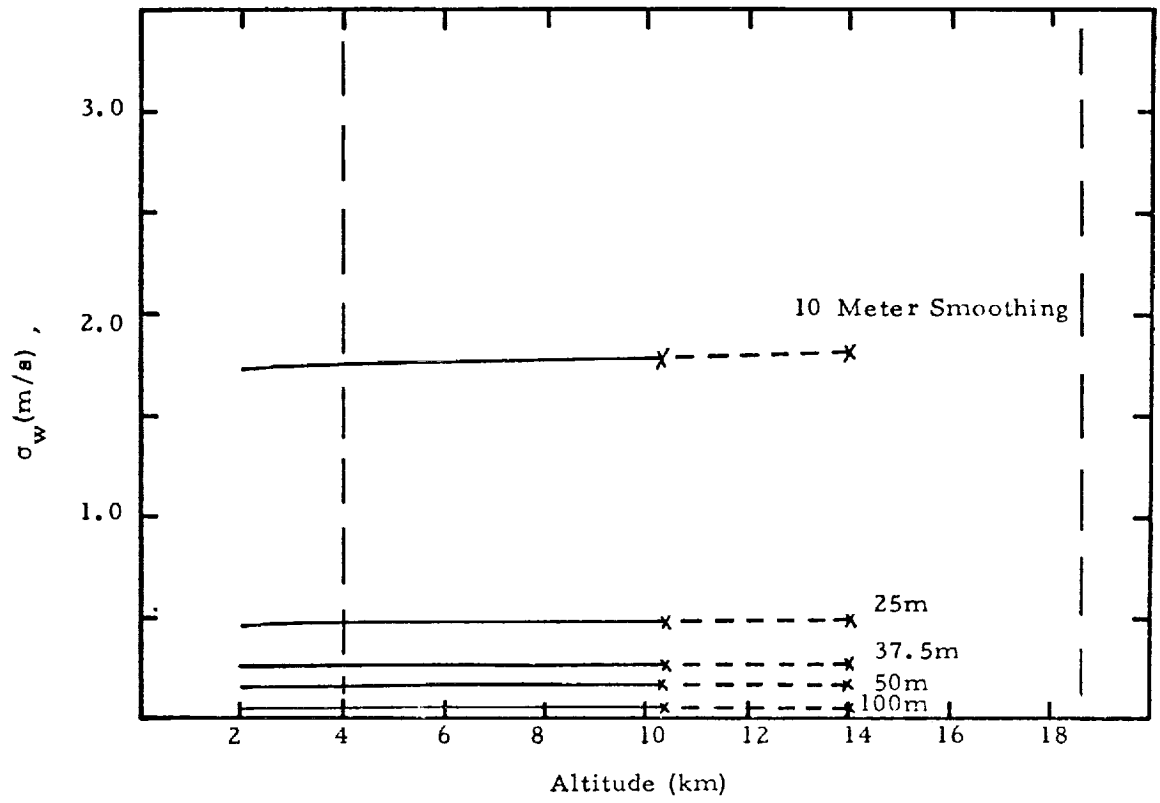

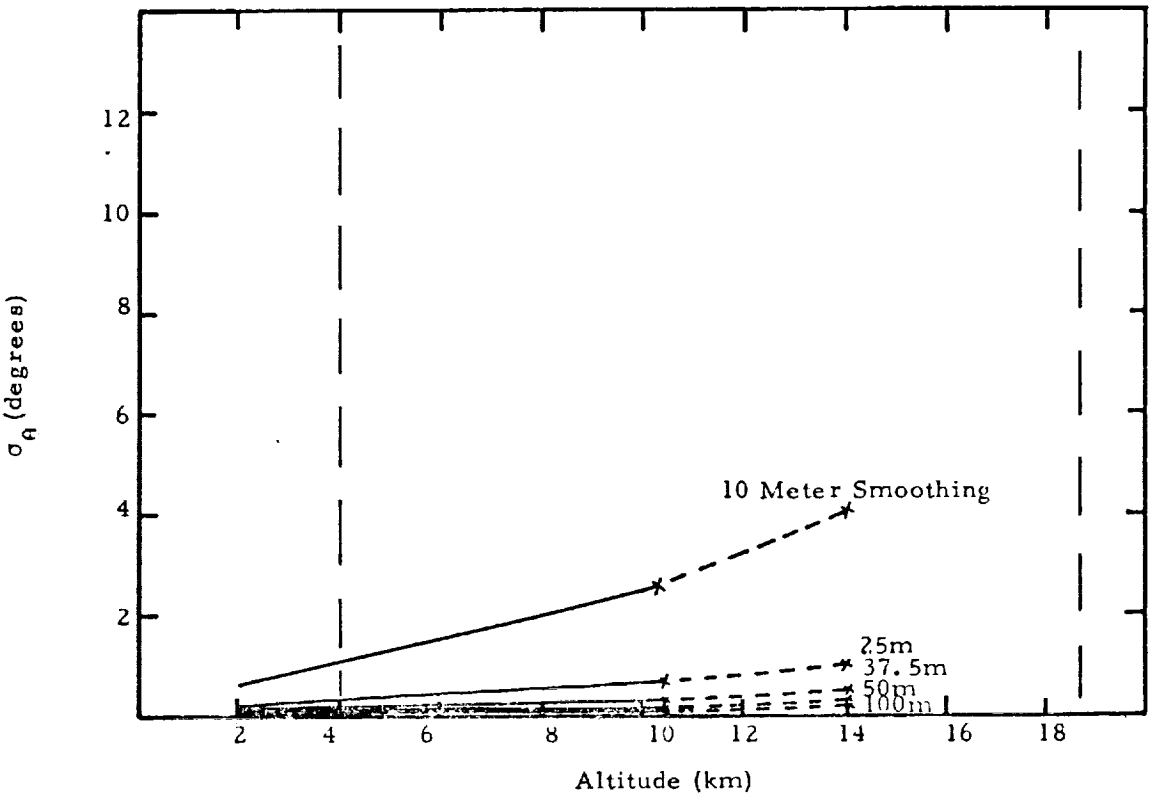

Figure 11. Wind Speed and Direction Error vs. Altitude for the Severe Wind Profile (Δt = 0.1 second).

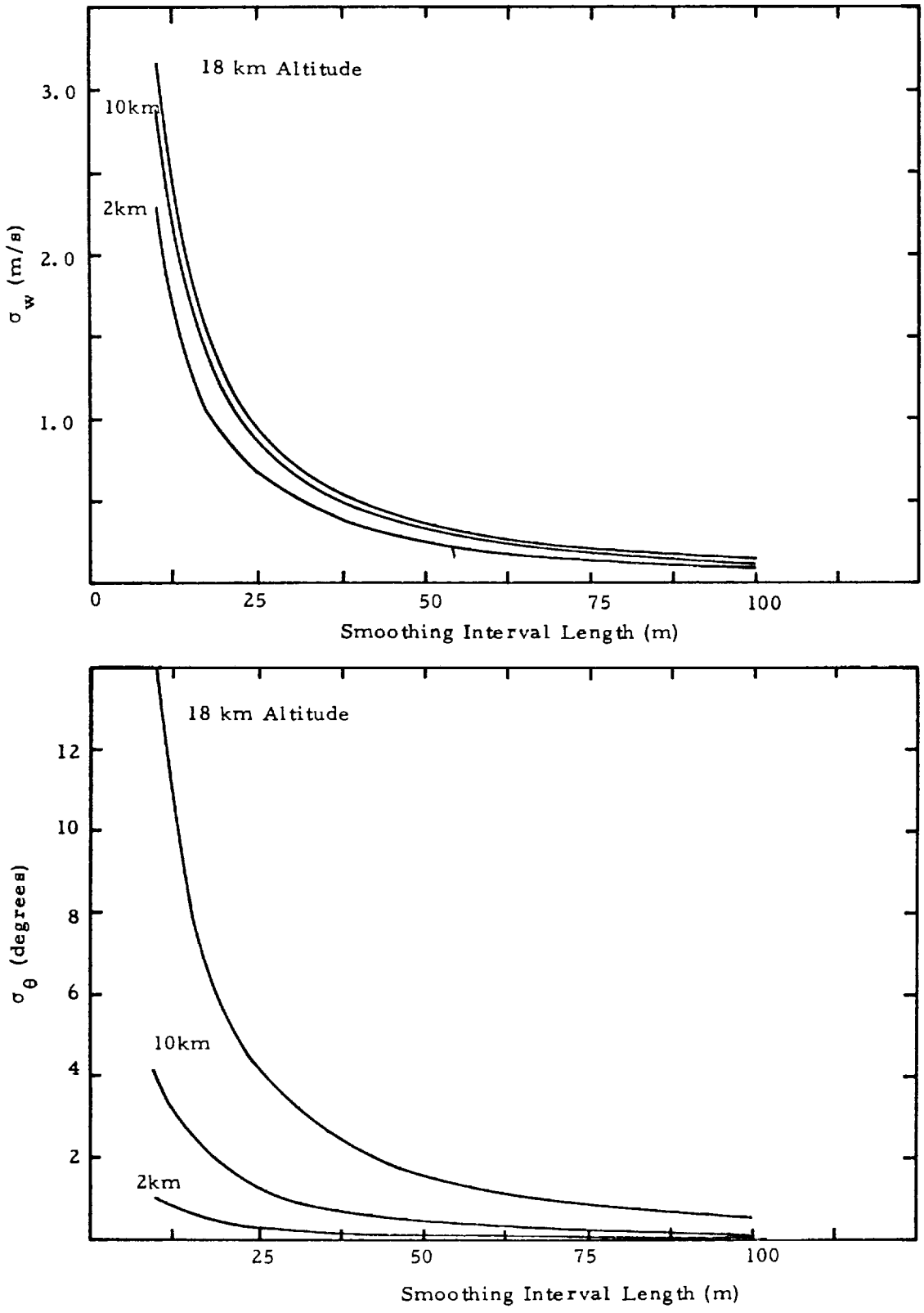

Figure 12. Wind Speed and Direction Error vs. Smoothing Length for the Light Wind Profile (Δt = 0.5 second).

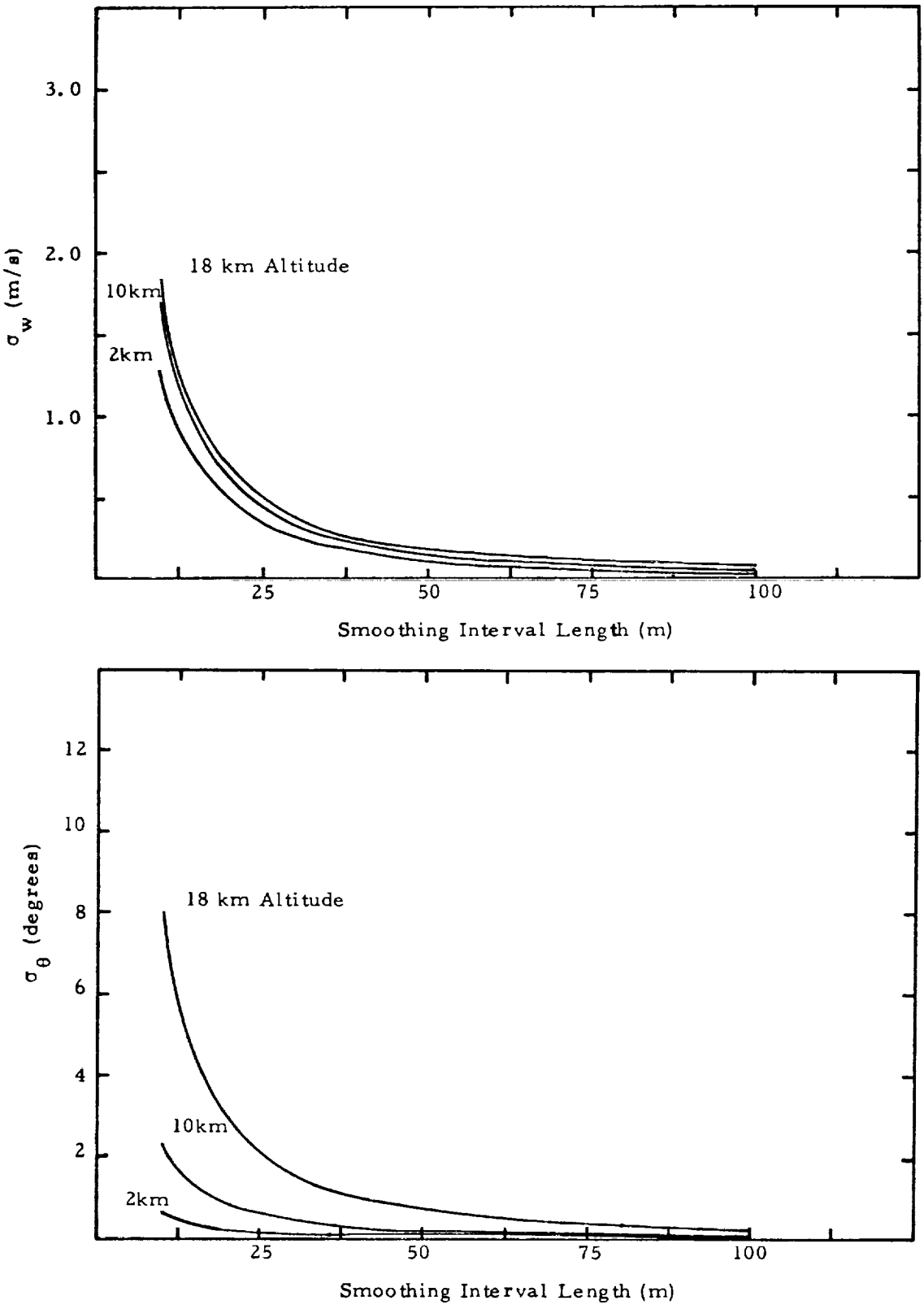

Figure 13. Wind Speed and Direction Error vs. Smoothing Length for the Light Wind Profile (Δt = 0.1 second).

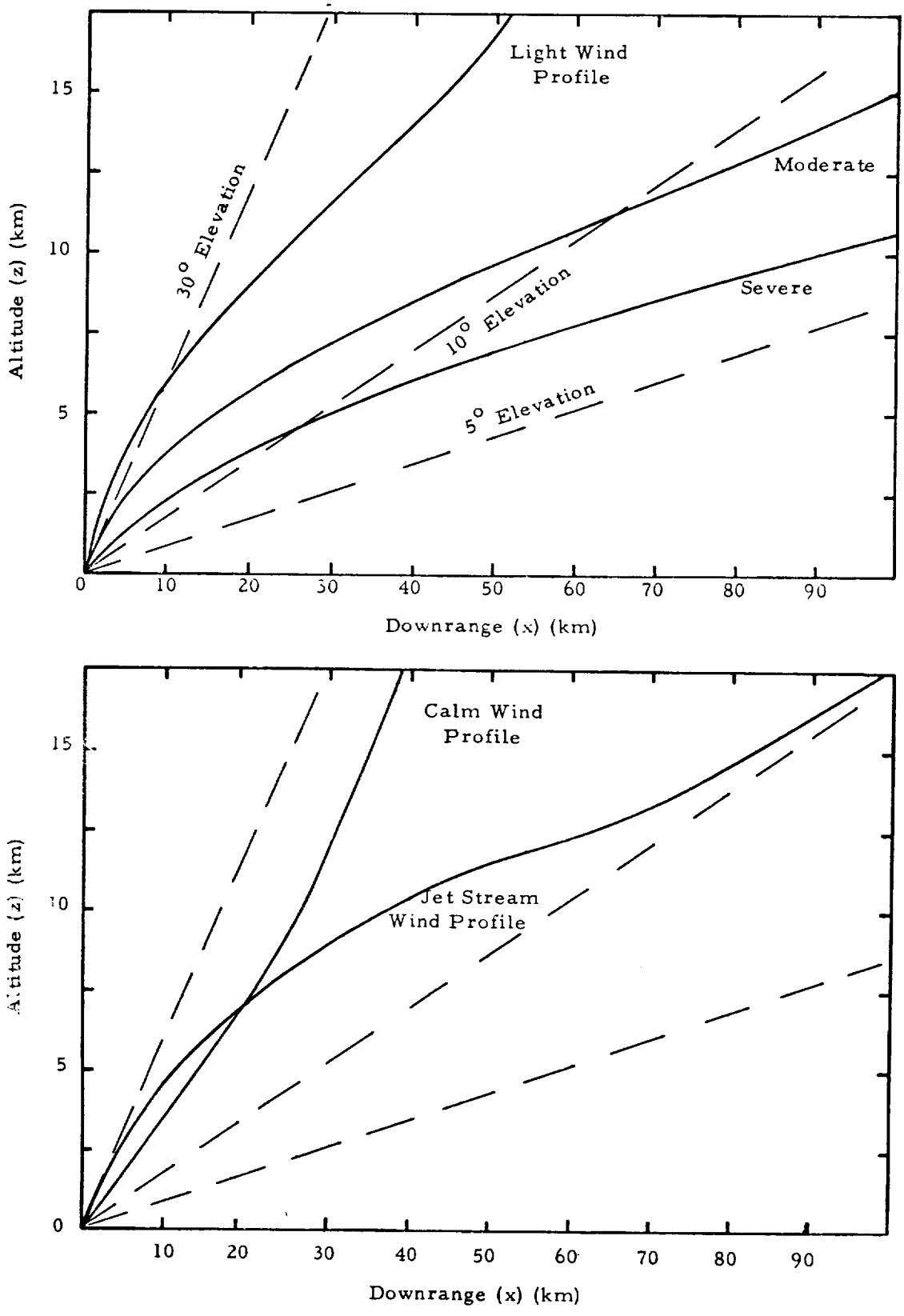

Figure 14. Trajectories of Five Flights with Constant Wind Direction.

used in our examples, W_x increases to 10 kilometers, then remains constant to 14 kilometers and finally decreases thereafter. Being the denominator of the fraction, the added effect of W_x is to slow the increase of σ_θ to ten kilometers, not effect the value between ten and 14 kilometers, and then to aid the growth of σ_θ to 18 kilometers. The light wind profile shows the altitude effect on σ_w to the greatest degree since large values of elevation and smaller slant ranges occur in that case. The altitude effect on σ_θ is largest in the severe profile where large slant ranges cause large direction errors.

The effects of smoothing interval length and time constant enter through the term $\left[\frac{12}{N(N^2-1)\Delta t^2}\right]$ in both Equations (16). Holding the time constant, Δt, fixed and increasing the length of the smoothing interval, i.e., increasing the number of points, N, makes the term smaller and so decreases the value of σ_w and σ_θ. Since N appears to approximately the third power in the denominator the decrease is quite rapid at first and much slower later, as noted in Figures 12 and 13. For example, in the light wind case with a Δt of 0.5 second, increasing the smoothing interval from 10 to 25 meters reduces the RMS wind speed error from about 3.0 meters per second (at 10 kilometers) to about 0.9 meters per second, while an increase from 35 meters to 50 meters results in a decrease from about .60 meter per second to about 0.35 meter per second. To hold the smoothing interval length fixed and vary the time constant requires not only varying Δt but changing the number of points, N, in a consistent manner. For example, smoothing over 25 meters of altitude requires 51 0.1 second data points or 11 0.5 second data points (see Table 2). The increased number of points obtained by using a smaller value of Δt serves to reduce the value of the term $(12/N(N^2-1)\Delta t^2)$ since N appears to power one higher than Δt. The smoothing interval length, S, in meters may be expressed as $S = (N-1)\Delta t\dot{Z}$ where $\dot{Z}$ is the rise rate. If we rearrange the above expression as $\Delta t = S/(N-1)\dot{Z}$ and substitute into the factor $12/N(N^2-1)\Delta t^2$, the factor becomes $12(N-1)\dot{Z}^2/N(N+1)S^2$ which for large N is approximately $12\dot{Z}^2/NS^2$. Therefore, if the smoothing interval, rise rate, etc. are fixed and Δt and N allowed to vary, the RMS errors in wind speed and direction are (by Equations (14)) inversely

proportional to the square root of N. For 25 meter smoothing with $\Delta t = 0.1$, the value of $[12/N(N^2-1)\Delta t^2]^{1/2}$ is 0.0951 while for $\Delta t = 0.5$ the value increases to 0.1907. Comparing, for example, the moderate wind profiles for 25 meter smoothing at ten kilometers, we see that the value of σ_w for the half second time constant is 0.95 meter per second while for the tenth second Δt the value is 0.475 meter per second. A 50% increase in accuracy is achieved by using the smaller sample spacing.

Summarizing the constant direction results, the general behavior of the wind speed RMS error for a given smoothing interval and time constant is to remain almost constant over the entire altitude range. The RMS direction error rises throughout the flight, especially sharply above 14 kilometers. Smoothing interval length and sample spacing (time constant) have a large effect on both wind speed and direction error. The best accuracy is achieved when many closely spaced points are used with long smoothing intervals, as must certainly be expected since more data is made available for "averaging out" the random noise errors.

Frequency response. - In choosing a particular smoothing interval length, the attenuation properties of this filter must be considered in addition to the noise suppression ability. For the filter lengths shown in Table 2, Figure 15 presents their frequency responses to sinusoidal oscillations in the data computed by the method outlined in a previous section. The velocity attenuation factor, D_f, is plotted as a function of wavelength. A wind profile may be considered to have an overall shape such as those used above with the smaller details represented by sinusoidal wind oscillations superimposed on the gross profile. This allows the use of Figure 15 with the above noise error plots in an evaluation of a particular smoothing interval.

The figure also shows the response of the balloon (taken from Figure 1) and the wavelength region of the aerodynamic oscillations. With regard to the balloon's response, we see that it is much more responsive to velocity changes than any of the smoothing lengths, so that the ability of the Jimsphere system

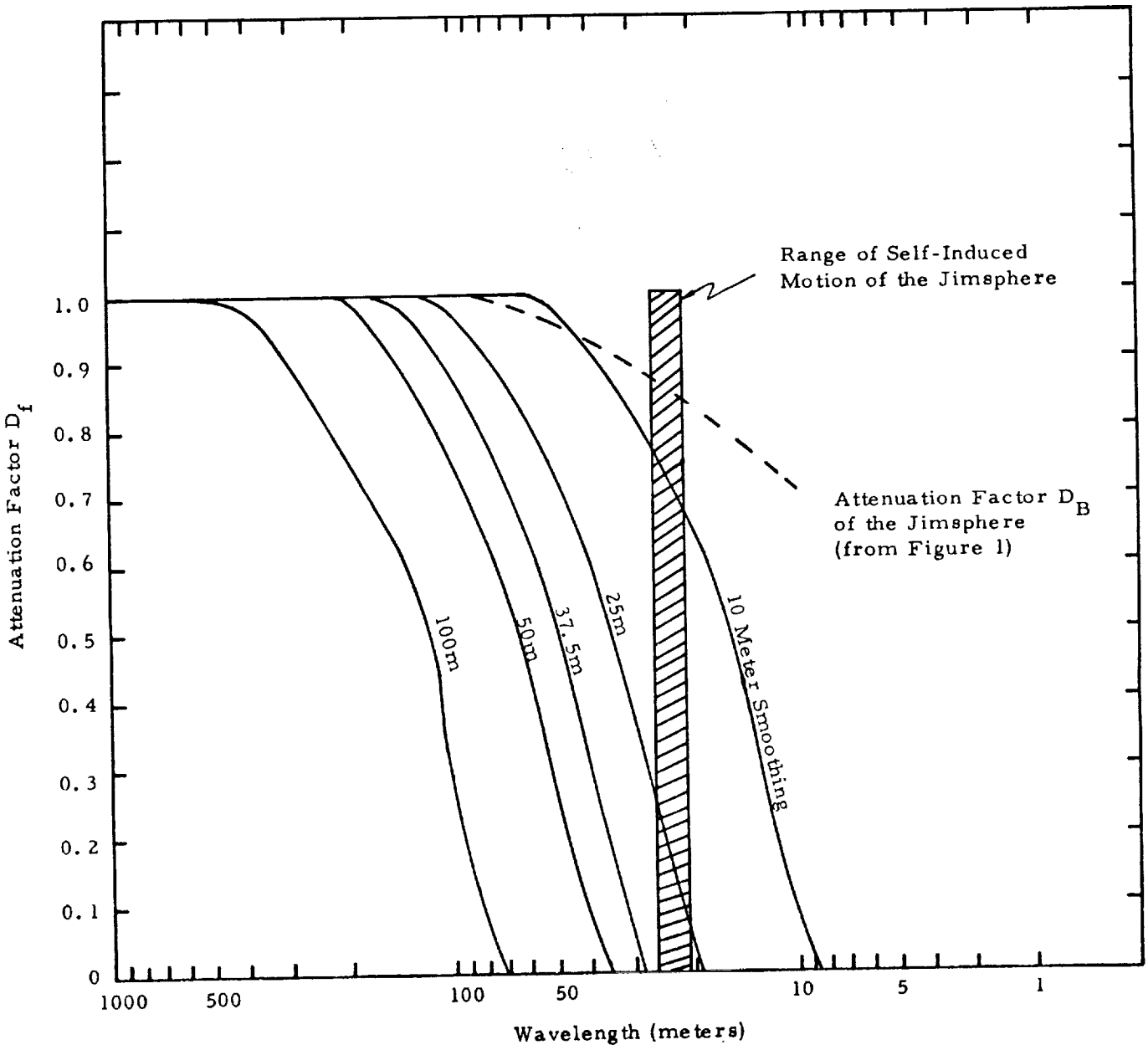

Figure 15. Frequency Response Functions For Various Smoothing Lengths.

to detect fine wind details can be considered to be limited by the attenuation characteristics of smoothing technique. Smoothing out of the self-induced oscillations provides a convenient lower limit for a smoothing length. A length of 37.5 meters (16 0.5 second or 76 0.1 second points) removes almost all of the oscillations in the 26 to 21 meter band, while keeping 90% of the amplitude of 80 meter waves, a good frequency response. Shorter filters, e.g. 25 meters, may be used, but will retain some of the self-induced motion. Longer filters, while further reducing noise error, significantly attenuate longer wavelengths and so destroy much of the fine detail of the wind field.

Varying Direction Wind Fields. - In order to examine the effects of changes in wind direction with altitude, Equations (15) were applied to a wind field in which the direction changes linearly through 90 degrees of azimuth from the surface to 18 km. The wind speed profile employed was the light profile (Figure 5). Figure 16 shows the x-y and x-z paths of the balloon throughout the flight. Plots of the RMS wind speed and direction errors as functions of altitude and smoothing interval were made for several filter lengths using the 0.5 second time constant. These plots are shown in Figures 17 and 18.

The wind speed error for this situation is not very different from the constant direction cases examined above. Values of σ_w are relatively constant throughout the flight, especially for the longer smoothing intervals. Comparing the magnitude of the σ_w for 25 meter smoothing in Figure 17 to the corresponding value for the constant direction case, Figure 6, shows little difference in the values obtained in the two cases. This may again be attributed to the dominance of the terms containing $\cos^2 E \sigma_R^2$ over the terms with $R^2 \sigma_E^2$ and indicates that wind speed error is relatively independent of direction. Similarly when the wind direction errors are compared for the constant and changing direction causes, little difference is found between the two situations. Near the end of the ascent the accuracy of the changing direction case is slightly better than the constant case due to the shorter slant range values involved. The plots

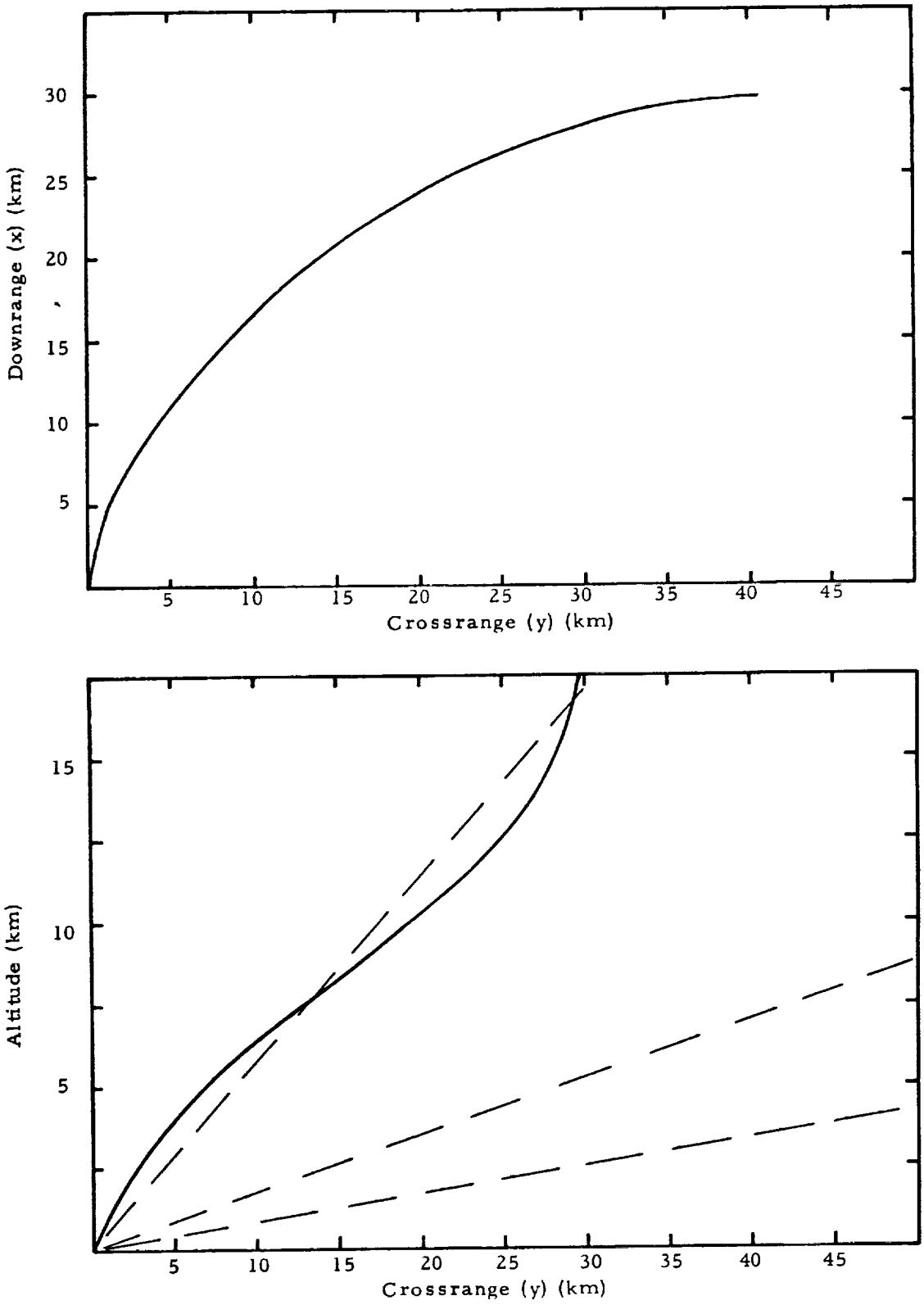

Figure 16. x-y and x-z Trajectories of the Jimsphere for the Varying Direction Wind Field.

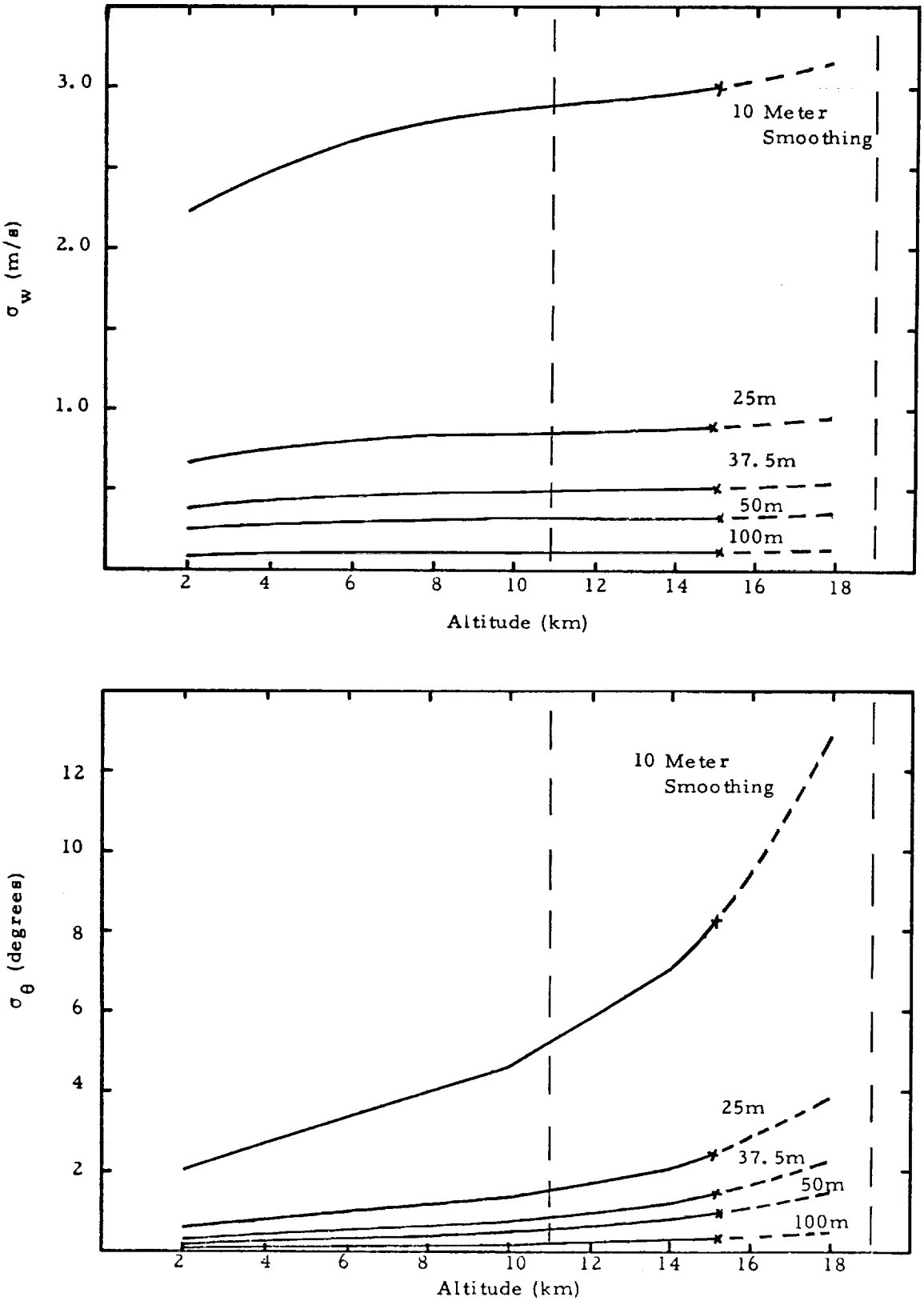

Figure 17. Wind Speed and Direction Error vs. Altitude for the Varying Direction Wind Profile.

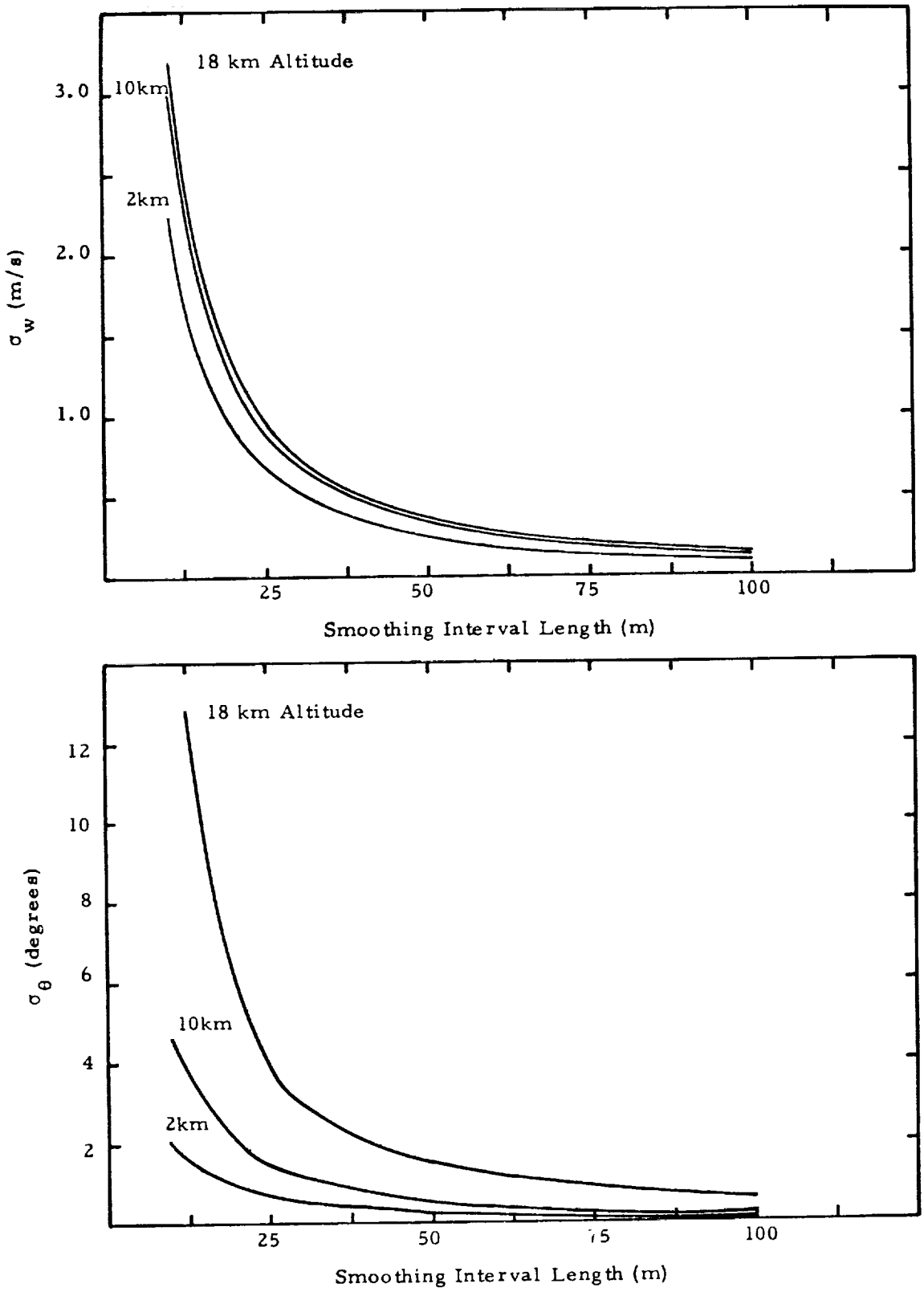

Figure 18. Wind Speed and Direction Error vs. Smoothing Interval for the Varying Direction Wind Profile.

of σ_w and σ_θ vs. smoothing interval are essentially similar to those for constant direction. It should be noted that we have chosen to analyze a case of a "moderate" change in direction with altitude. Situations could be imagined, of course, where the wind direction changes by 180 degrees or more so that larger elevation angles and short slant ranges might occur near the end of the flight. Such situations, however, were not considered to be realistic and so were not examined.

Two "Special Case" Wind Profiles. - Two wind speed profiles of special interest were analyzed assuming constant wind direction. The first profile was that of a "jet stream" situation, a relatively thin layer of high wind speed centered at about 12 km. The second was a "calm" profile in which wind speed remained at a relatively low value over the whole flight. The particular shapes of these profiles were obtained from two actual Jimsphere tests, Nos. 5364 (Jet stream) and 6610 (calm), made in 1966 at the Eastern test range. Figure 19 presents these profiles as taken from pp. 5.196 and 5.197 of [19]. In order to make these profiles able to be input to the computer program which performed the error calculations, they were approximated by profiles composed of linear segments. These segmented profiles are also shown in Figure 20. Plots of σ_w and σ_θ vs. altitude for both profiles are given in Figures 21 and 22. Considering first the jet stream profile, the values of σ_w of each smoothing interval are again relatively constant reflecting the dominance of the $\cos^2 E$ term. The magnitudes of the RMS errors are about the same as the moderate constant direction profile of Figure 7. Direction error shows an overall behavior much like the moderate profile except for a "dip" in the high wind speed region around 12 km. This is explained by noting that the expressions for σ_θ^2 (13b) or (14b) have W^2 in the denominator which, having a large value in these regions, reduces the value of σ_θ. For the calm profile the σ_w curves are very flat. This reflects the rather high ground wind speed and the small shear so that even though the wind speed is low at the upper altitudes the balloon has an appreciable slant range above 2 km. The curves for direction error rise smoothly to values somewhat above the values for the moderate two dimensional case, again showing the effect of large slant range.

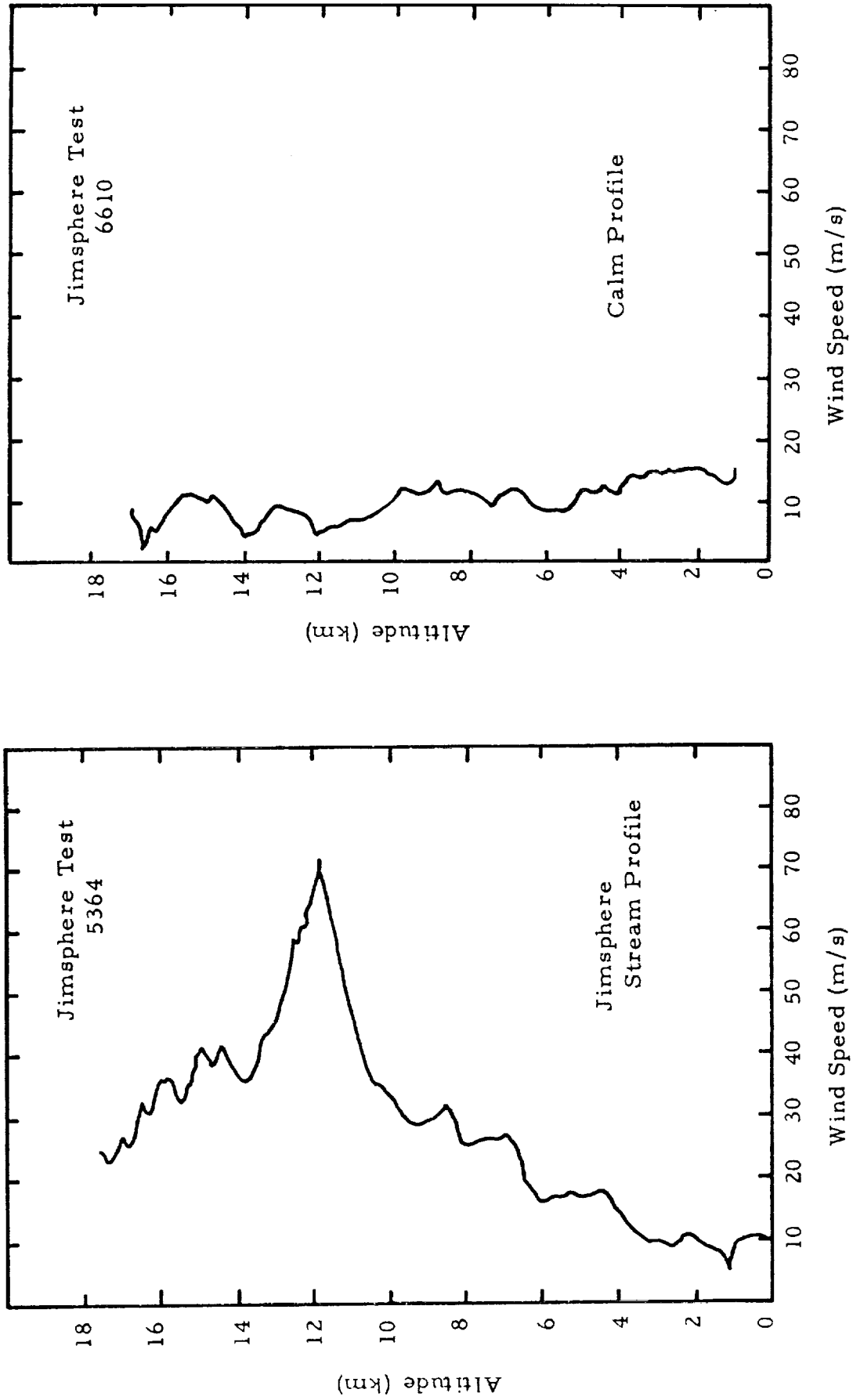

Figure 19. Jet Stream and Calm Wind Profiles.

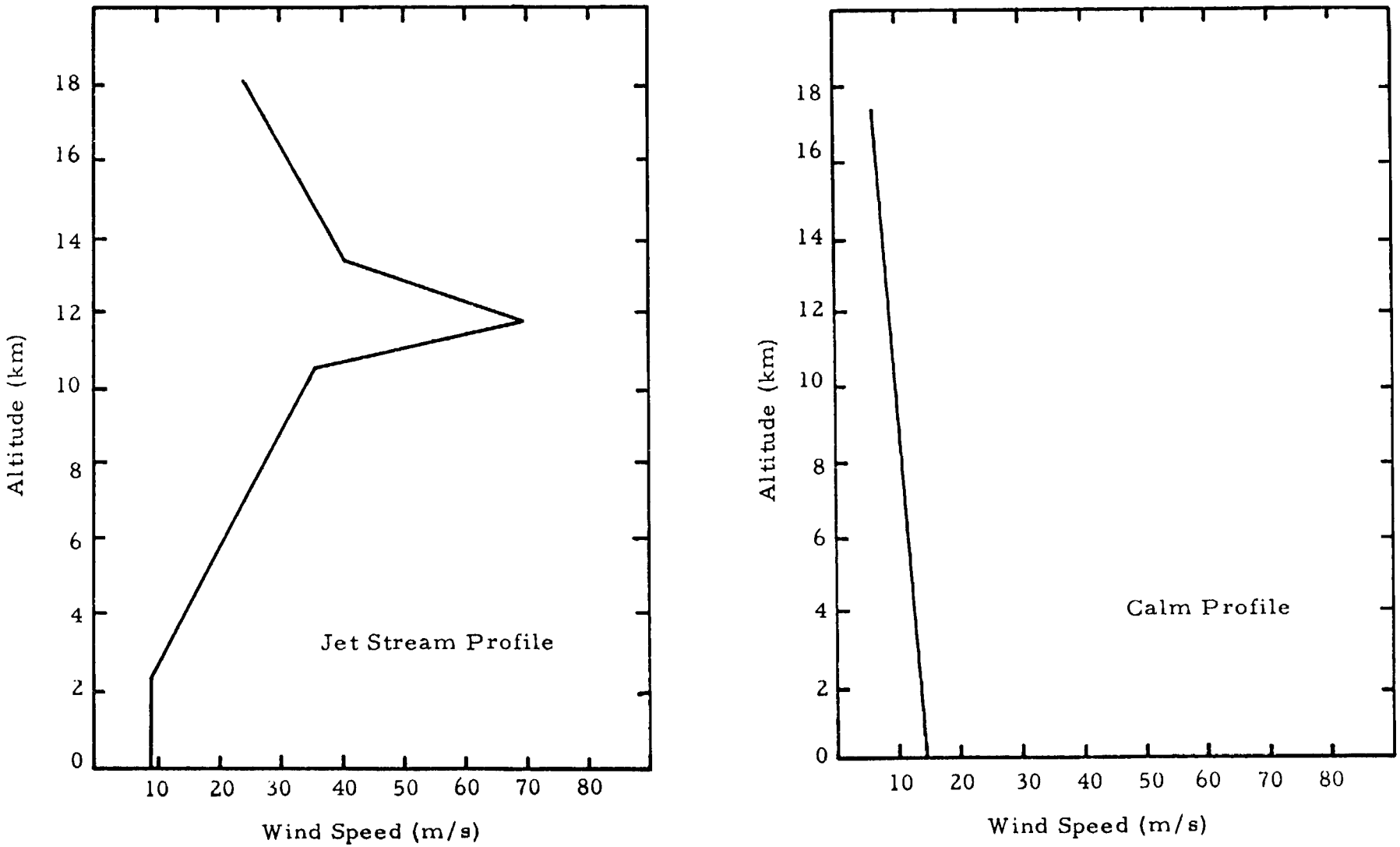

Figure 20. Approximate Jet Stream and Calm Wind Profiles.

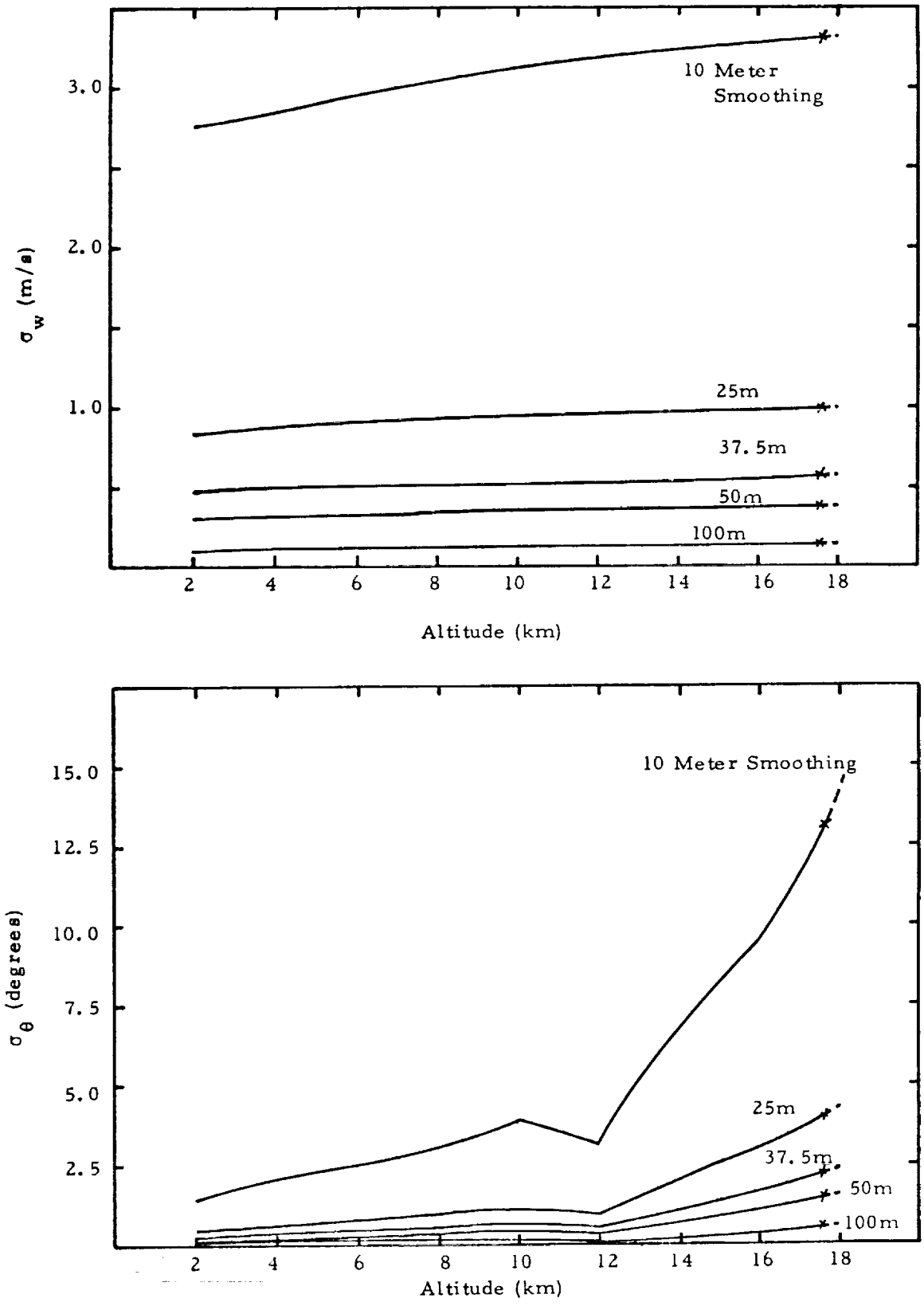

Figure 21. Wind Speed and Direction Error vs. Altitude for the Jet Stream Wind Profile.

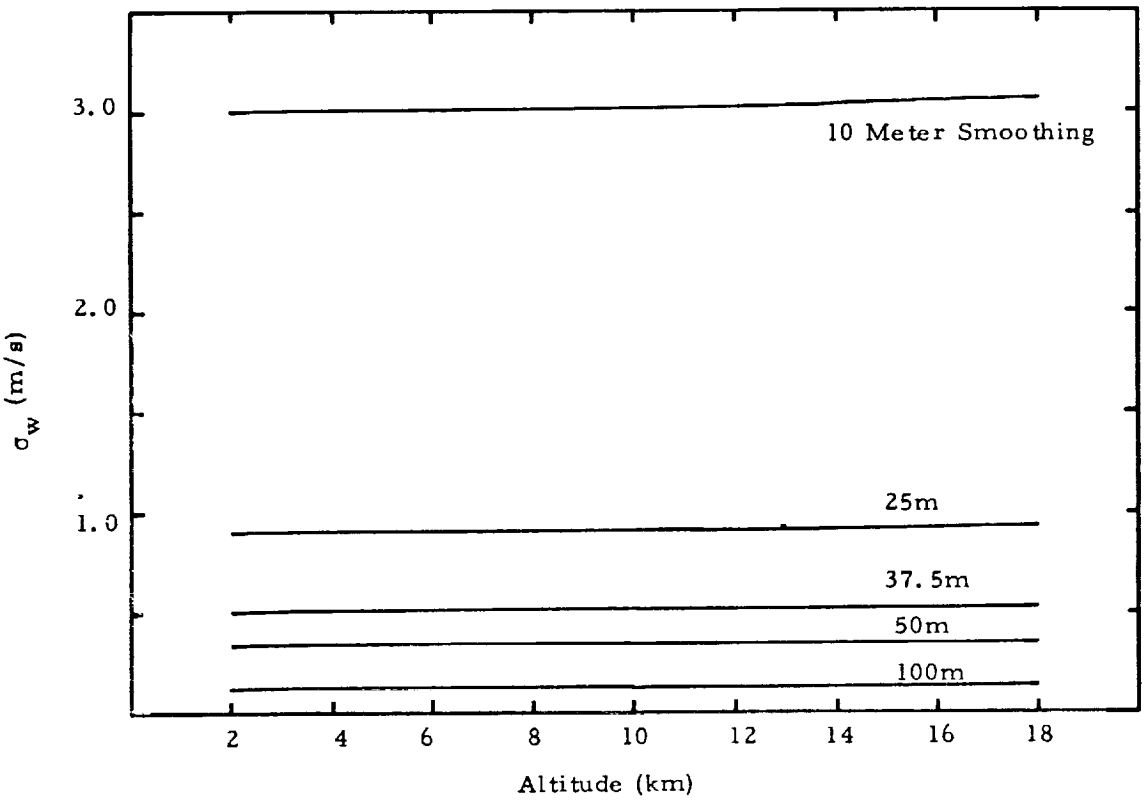

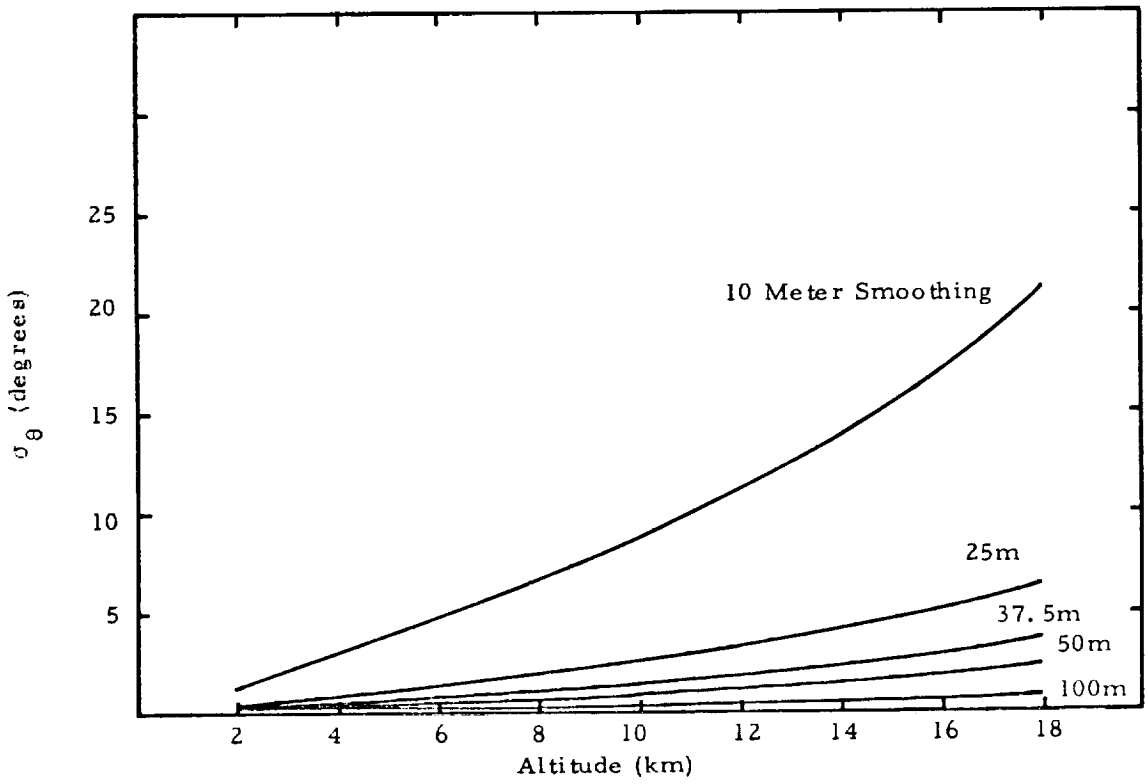

Figure 22. Wind Speed and Direction Error vs. Altitude for the Calm Wind Profile.

Summary. - Several general conclusions based upon the above results can be made concerning the nature of wind errors in the FPS-16/Jimsphere system. These conclusions are listed below.

1. The trajectory of the Jimsphere is usually of such a shape that low elevation angles and small changes in elevation angle occur after the first one or two kilometers of altitude. The majority of the balloon motion is then along the range direction. Consequently, the error in wind magnitude is primarily dependent on the range error, and since range error is independent of range, σ_w is almost independent of altitude (for ranges within the capabilities of the FPS-16 radar). Wind direction error, however, is a strong function of range and thus of altitude.

2. The plots of smoothing interval length vs. RMS error in wind magnitude or direction show that smoothing lengths in the 25 to 50 meter region are most desirable in terms of noise error and frequency response. Filters of these lengths proved a significant reduction in noise error over shorter filters, and are not much poorer than filters of greater length. In particular a filter length of 37.5 meters and a time constant of 0.5 second will provide wind magnitude RMS error below 0.6 meter /second and direction errors below 2.5 degrees (below 1.0 degree for altitudes less than 14 km.) for the severe wind conditions (Figure 8). The 37.5 meter length will smooth out almost all of the self-induced balloon motion and yet retain about 0.9 of the amplitude of waves of 80 meters in length (Figure 15).

The effect on the wind speed and direction errors of a wind field with a moderate change in direction is slight. Similarly the results for two special case profiles were little different from the results obtained with the normal profiles. Both of these observations may be again attributed to the particular shape of the Jimsphere trajectory in which most of the balloon motion lies along the range direction.

3. For a given smoothing interval length, the least squares linear smoothing technique provides RMS errors in wind speed and direction which are inversely proportional to the square root of the number of independent

data points in the interval. It is therefore desirable to obtain the closest possible time spacing of data points when using any length of smoothing interval.

OPTIMUM RISE RATES FOR WIND MEASUREMENTS

For balloon tracking with an FPS-16 radar, there are two quantities that essentially determine the accuracy which is possible for fine scale wind measurements. They are the rise rate of the balloon and the wind field to which the balloon responds. These two quantities determine the geometric position of the balloon relative to the radar site. Light wind fields will result in a shorter distance between the balloon and radar than a severe wind field and consequently, less severe tracking conditions. A fast rise rate will also provide, at a given altitude, less severe tracking conditions than would occur with a slower rising balloon, On the other hand, a fast rise rate is undesirable because, as it passes through a given altitude layer, it provides fewer radar data poi nts than a slower rising balloon. Fewer data points produce less accuracy in a wind measurement. Consequently, for a given wind field, an optimum rise rate exists which provides a balance between desirable and undesirable effects of both fast and slow rise rate balloons. In general, it will be shown that a stronger wind field yields less wind measurement accuracy than a light wind field and that the optimum rise rate is faster for strong wind fields than for light ones.

The error in the wind magnitude has previously been derived as:

$$\sigma_w^2 = \frac{(W_x^2 \sigma_{wx}^2 + W_y^2 \sigma_{wy}^2)}{W^2} + \frac{2W_x W_y}{W^2} < dW_x dW_y > \qquad (13a)$$

where

$$W^2 = W_x^2 + W_y^2 \quad .$$

The optimum rise rate for a given wind field is defined as that rise rate which minimizes Equation (13a). The error in wind direction has not been incorporated into a definition of optimum rise rate for two reasons: a) Meteorologists are generally more interested in having a very accurate estimate of wind magnitude that may be in error by a few degrees direction than the converse

and b) the error in wind direction is even more sensitive to the wind profile than the error in wind magnitude as shown by the factor W^4 in the denominator of Equation (13b).

As in the case of the Jimsphere, the assumption that the balloon is a perfect wind sensor is made throughout this section. That is, the balloon velocity $\dot{X}$ equals the wind velocity W_x, and also, therefore, $\sigma_{\dot{x}} = \sigma_{wx}$. In a later section, the validity of this assumption for various diameter balloons is examined. The error in the wind magnitude (hereinafter referred to as wind error) as given by Equation (13a) is a function of the wind field and the error in the velocity measurements of the balloon.

For linear smoothing over N position points the error in the balloon velocity has already been given by Equation (4) as

$$\sigma_{\dot{x}}^2 = \frac{12\sigma_x^2}{N(N^2-1)\Delta t^2} \tag{4}$$

A substitution of Equation (4) into Equation (13a) shows the minimization of Equation (13a) requires the following:

a) A specification of the wind field by the components W_x and W_y

b) The time constant Δt of the radar

c) A definition of the number of points, N, used in the linear smoothing

d) A determination of σ_x which is a function of the radar capabilities, the balloon rise rate, and the wind field.

The four inputs to Equation (13a), that is, a, b, c, and d, are discussed in the following paragraphs.

Specification of Wind Field - Unique specification of a wind field requires two profiles - a wind magnitude versus altitude profile and a wind direction versus altitude profile. The error in the wind magnitude in general depends on both of these profiles. The only exception to this is if the wind direction is constant at all altitudes (i.e., throughout the flight). For this case, it has been shown that the error in wind magnitude is the same for all

directions so that any direction may be chosen. Each wind profile that exhibits a change in wind direction provides a unique wind error profile. It is obviously impossible to assume all reasonable types of three-dimensional wind profiles and find an optimum rise rate for each. What can be done is to consider wind magnitude profiles only and assume the wind direction is constant, a "worst case" analysis.

The wind profiles used to obtain optimum rise rates will consist of wind magnitude profiles with direction assumed constant and along the X-axis. In this case, the expression for error in wind magnitude, Equation (13a) simplifies to

$$\sigma_w^2 = \sigma_{wx}^2 \quad . \tag{16a}$$

As in the case of the Jimsphere studies, the three wind profiles chosen were the light, moderate, and severe wind profiles presented in Figure 5.

Radar Time Constant Δt - The radar time constant, Δt, is defined as the minimum time spacing between radar measurements that have independent errors. The time constant is dependent upon the servobandwidth of the radar. For an FPS-16 radar and a servobandwidth of 7, Δt is approximately 0.5 second; for a servobandwidth of 10, Δt is approximately 0.1.

Determination of N - The number of points used in smoothing, N, can be chosen so as to provide a wind measurement over a specified altitude layer. N is related to the altitude layer, or smoothing interval by the expression

$$S = (N-1)\Delta t \dot{z} \tag{17a}$$

or

$$N = \frac{S}{\Delta t \dot{z}} + 1 \tag{17b}$$

where S is the smoothing interval defined in units of meters. When minimizing Equation (4) to find an optimum rise rate function for a given wind profile, the smoothing interval will remain fixed for all altitudes. Since the rise rate

of the balloon will vary with altitude, N will be chosen in a compensatory fashion so that the right side of Equation (17a), the smoothing interval, remains constant. A constant altitude smoothing interval provides the same frequency response (ratio of smoothed wind measurement to true wind) at all altitudes. The smoothing interval has initially been chosen as 25 meters. The frequency response function for 25-meter smoothing as well as for ten-meter through 100-meter smoothing has been presented in Figure 14.

Determination of $\sigma_x = f(\sigma_R, \sigma_E, \sigma_A, \dot{Z}, W)$ - In terms of radar errors and the Cartesian Coordinates of the balloon's position σ_x is given by

$$\sigma_x^2 = \frac{X^2}{X^2+Y^2+Z^2} \sigma_R^2 + \frac{X^2 Z^2}{X^2+Y^2} \sigma_E^2 + Y^2 \sigma_A^2 \quad . \tag{18}$$

The factors σ_R, σ_E, and σ_A are nominally taken as:

$$\sigma_R = 5 \text{ meters}$$
$$\sigma_E = .1 \text{ mil}$$
$$\sigma_A = .1 \text{ mil} \quad .$$

The X, Y, Z position of the balloon depends upon the balloon rise rate and the wind. As stated above, the balloon is assumed a perfect horizontal wind sensor so that: $W_x = \dot{X}$ and $W_y = \dot{Y}$. The X and Y position coordinates are obtained by integrating the wind field. That is,

$$X = \int_{t_o}^{t} W_x dt$$

or

$$X = \int_{t_o}^{t} (A z + B) dt \tag{19}$$

where the light, moderate, and severe wind fields given in Figure 5 are specified in terms of linear segments $W_x = Az + B$ for various values of the constants A and B. The integration of Equation (19) requires than z be expressed as a function of time. This is accomplished by taking into account

the balloon rise rate. The balloon rise rate $\dot{z}$ is specified as a function of z. Thus, the differential equation $\dot{z} = f(z)$ can be solved for an expression of $z = f(t)$. A substitution of $z = f(t)$ into Equation (19) allows the determination of x position.

Linear and quadratic functions of altitude have been chosen to define the rise rate. The evaluation of the x-position (Equation (19)) for each of these rise rate functions and the three linear segmented wind fields, light, moderate, and severe, follows.

Linear Rise Rate - Let the rise rate be given by the linear function

$$\dot{z} = \beta z + \gamma$$

where β and γ are constants. The solution for $t = f(z)$ is

$$t = \frac{1}{\beta} \ell n \frac{(\beta z + \gamma)}{\gamma}$$

or for $z = f(t)$ as

$$z = \frac{\gamma(e^{\beta t} - 1)}{\beta} \quad . \tag{20}$$

A substitution of Equation (20) into Equation (19) gives

$$X = \int_{t_o}^{t} \left[\frac{A\gamma}{\beta} (e^{\beta t} - 1) + B \right] dt \quad . \tag{21}$$

The solution of Equation (21) is

$$X = \frac{A\gamma}{\beta^2} (e^{\beta t} - e^{\beta t_o}) + (B - \frac{A\gamma}{\beta})(t - t_o) \quad . \tag{22}$$

Equation (22) expresses the x position of the balloon in terms of the coefficients, A and B, of a linear segment of the wind fields and the coefficients β and γ of the linear rise rate function. A substitution of Equation (22) into Equation (18) allows the estimation of the error in the x position σ_x. A further substitution of Equations (17a) and (18) into Equation (4) determines the wind error as a function of the rise rate parameters. By varying β and γ while holding all

other parameters constant, the minimization of Equation (4) under the specified conditions is permitted. The minimization is achieved under specified conditions of fixed radar errors, a fixed wind field, and a fixed smoothing interval.

Quadratic Rise Rate - For a quadratic rise rate, we have

$$\dot{z} = \alpha z^2 + \beta z + \gamma \quad .$$

The solution for t in terms of z when $\beta^2 - 4\alpha\gamma > 0$ is

$$t = \frac{1}{q} \ell n \left(\frac{2\alpha z + \beta - q}{2\alpha z + \beta + q} \right) + K \tag{23}$$

where K is a constant of integration and given by

$$K = t_o - \frac{1}{q} \ell n \left(\frac{2\alpha z_o + \beta - q}{2\alpha z_o + \beta + q} \right)$$

and

$$q = (\beta^2 - 4\alpha\gamma)^{1/2} \quad .$$

Solving (23) for z explicitly yields:

$$z = \frac{\beta - q - (\beta + q)(e^{qt - qK})}{(2\alpha e^{qt - qK} - 2\alpha)} \quad . \tag{24}$$

Simplifying Equation (24) by introducing new constants gives

$$z = \frac{K_1}{e^{qt} + K_2} - K_1 \frac{e^{qt}}{e^{qt} + K_2}$$

where

$$K_1 = \frac{\beta + q}{2\alpha} \qquad K_2 = - \frac{\beta + q}{\beta - q} \quad . \tag{25}$$

The position x is determined by

$$x = \int_{t_o}^{t} (Az + B)dt$$

or, in terms of Equation (25),

$$x = \int_{t_o}^{t} \left(\frac{AK_1}{e^{qt} + K_2} - \frac{AK_1}{1 + K_2 e^{-qt}} + B \right) dt \quad .$$

Integrating gives

$$x = \frac{AK_1}{K_2} \left[t - \frac{1}{q} \ell n \left(e^{qt} + K_2\right) \right]_{t_o}^{t} - AK_1 \left[t + \frac{1}{q} \ell n \left(1 + K_2 e^{-qt}\right) \right]_{t_o}^{t} + B_t \Big|_{t_o}^{t}$$

or

$$x = \left[\frac{AK_1}{K_2} - AK + B \right] (t - t_o) - \frac{AK_1}{K_2 q} \ell n \left(\frac{e^{qt} + K_2}{e^{qt_o} + K_2} \right)$$

$$- \frac{AK_1}{q} \ell n \left(\frac{1 + K_2 e^{-qt}}{1 + K_2 e^{-qt_o}} \right) \quad . \tag{26}$$

The alternate solution to the differential equation $\dot{z} = \alpha z^2 + \beta z + \gamma$ when $\beta^2 - 4\alpha\gamma < 0$ is given as

$$t = \frac{2}{q^*} \left[\tan^{-1} \left(\frac{2\alpha z + \beta}{q^*} \right) - \tan^{-1} \left(\frac{\beta}{q^*} \right) \right]$$

where

$$q^* = \left(4\alpha\gamma - \beta^2\right)^{1/2} > 0 \quad .$$

Solving for z as a function of t gives

$$z = \frac{q^* \tan\left(q^*/2t + \tan^{-1} \beta / q^*\right) - \beta}{2\alpha} \quad .$$

The position x is determined from

$$x = \int_{t_o}^{t} W_x dt = \int_{t_o}^{t} (Az + B) dt$$

or

$$x = \int_{t_o}^{t} \left[\frac{A}{2\alpha} \left\{ q^* \tan \left(\frac{q^*}{2} t + \tan^{-1} \frac{\beta}{q^*} \right) - \beta \right\} + B \right] dt \quad .$$

The solution is

$$x = \frac{A}{\alpha} \ell n \left\{ \frac{\cos\left(\frac{q^*}{2} t_o + \tan^{-1} \frac{\beta}{q^*} \right)}{\cos\left(\frac{q^*}{2} t + \tan^{-1} \frac{\beta}{q^*} \right)} \right\} - \frac{A\beta}{2\alpha} (t-t_o) + B(t-t_o) \quad . \qquad (27)$$

A substitution of Equations (17) and (18) and either (26) or (27) into Equation (4) allows the wind error to be written in terms of the parameters α, β, and γ of the quadratic rise rate. Numerical minimization of Equation (4) can be achieved by varying these rise rate parameters.

Wind Errors From Linear and Quadratic Rise Rate Functions

Optimum Linear Rise Rate - In order to determine the linear rise rate profile that minimizes wind error, a wide range of surface rise rates and rise rate slopes was examined. Surface rise rates were varied between two meters per second and ten meters per second. Both increasing and decreasing rise rate slopes versus altitude were considered. The constraint that the rise rate could not equal zero below 18 kilometers was invoked in choosing slopes. The linear rise rate functions for surface rise rates from two meters per second to ten meters per second are presented at the left side of Figures 23 through 27. The light, moderate, and severe wind profiles were chosen as wind input. The smoothing interval was fixed at 25 meters. The direction of the wind was chosen as blowing along the X-axis. The Y component of wind was chosen as $W_y = 0$. The simplified equation for error in wind magnitude, Equation (4), is therefore applicable.

Figures 23 through 27 show the wind error for surface rise rates of two through ten meters per second as a function of altitude and rise rate functions for the three wind profiles. The correspondence between rise rate curves and wind error curves is 1-1 order preserving. That is, the first rise rate curve from the left corresponds to the first wind error curve, the second rise rate curve corresponds to the second wind error curve, etc. In all figures presented the dashed lines that sometimes appear on wind error plots indicate slant ranges between 100 kilometers and 150 kilometers - the limiting constraints of the FPS-16 radar. When the slant range exceeds 150 kilometers, the wind error plots are terminated - indicating that radar tracking is no longer feasible. The broken lines indicate elevation angles of 10° and 5°; the first broken line from the right indicating 10° elevation while the second line (when it appears) indicates 5° elevation. The better rise rates on Figures 23 through 27 are those that decrease with altitude.

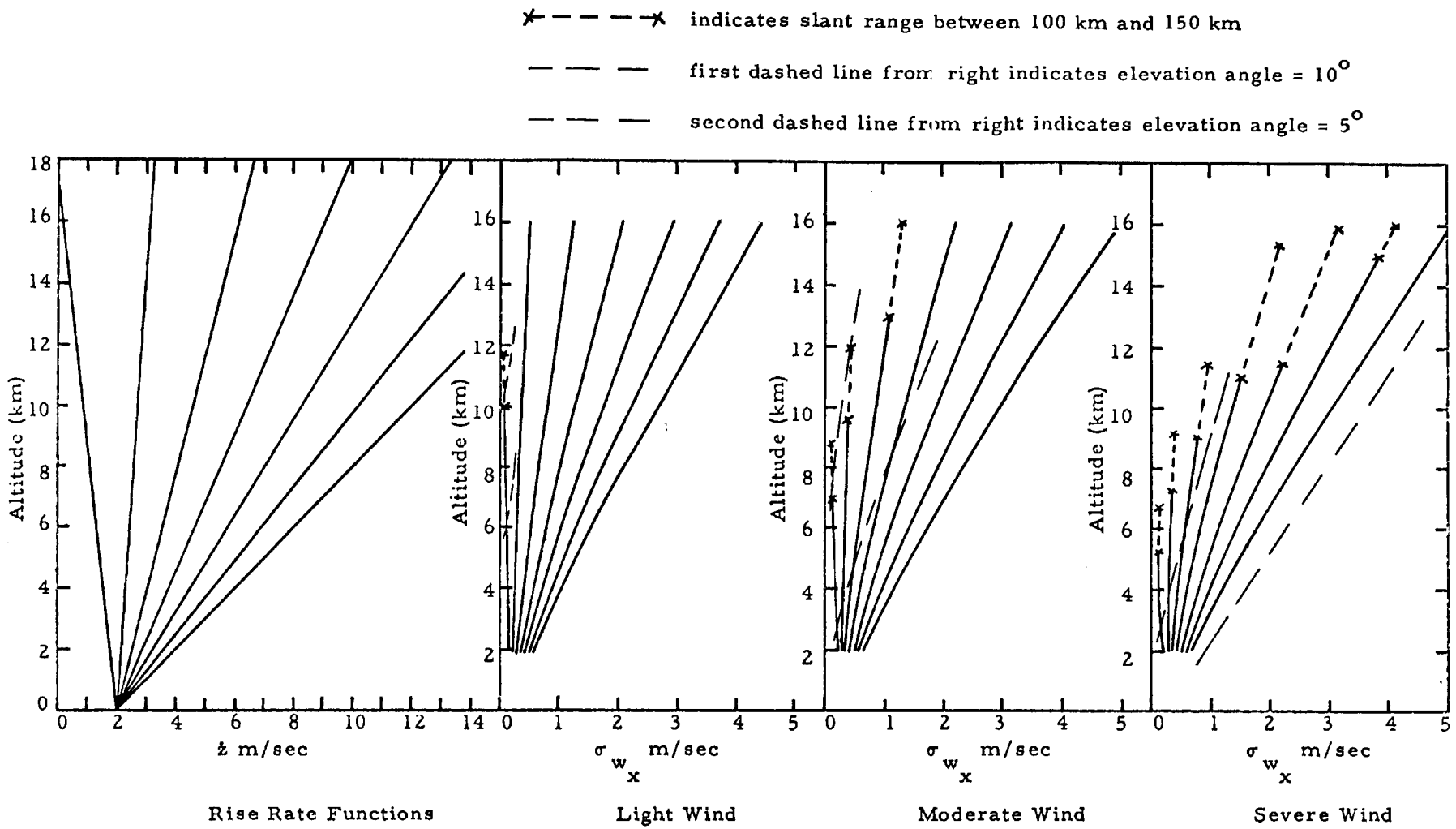

Figure 23. Error in Wind Magnitude for Linear Rise Rate Functions.

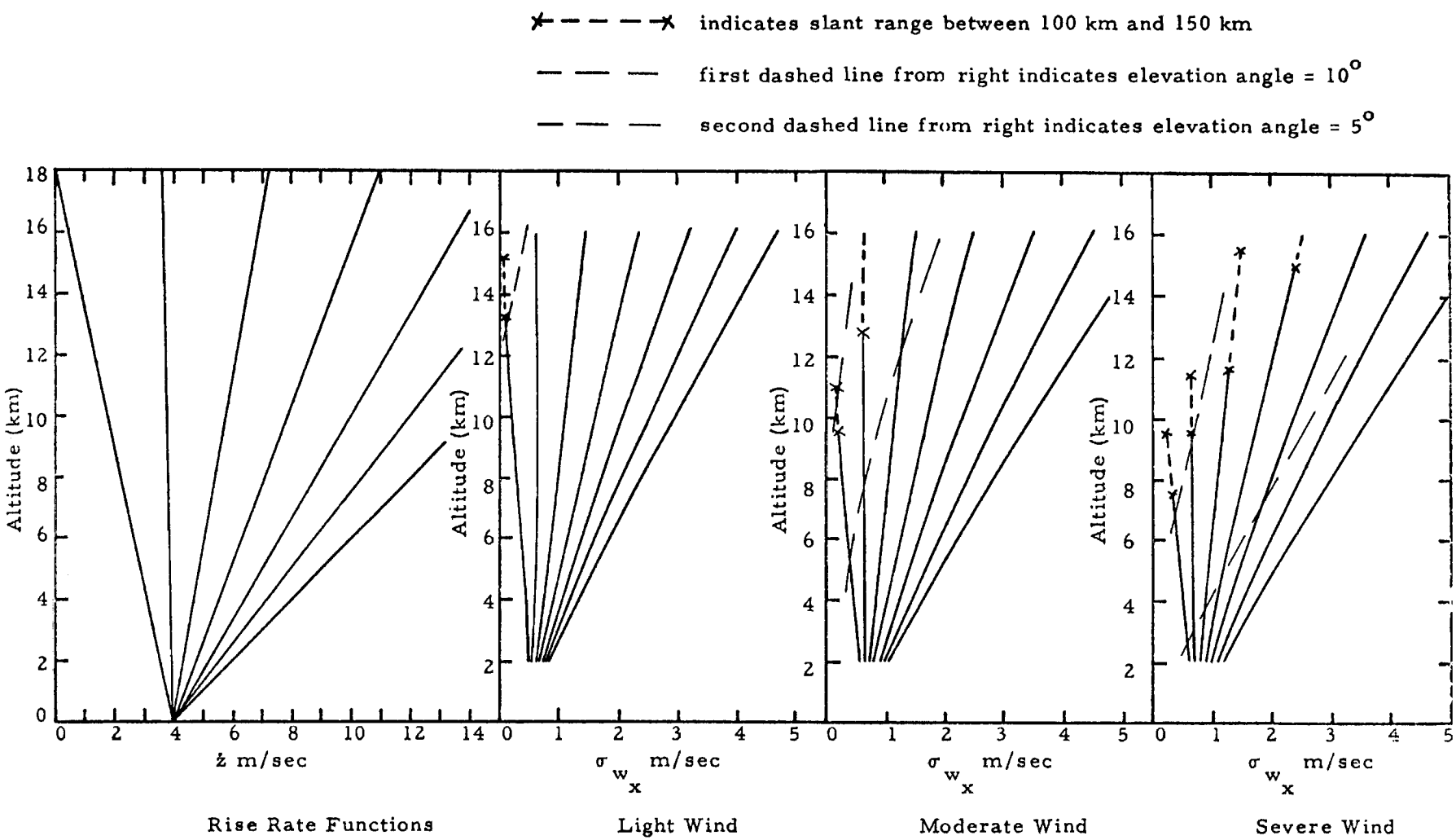

Figure 24. Error in Wind Magnitude for Linear Rise Rate Functions.

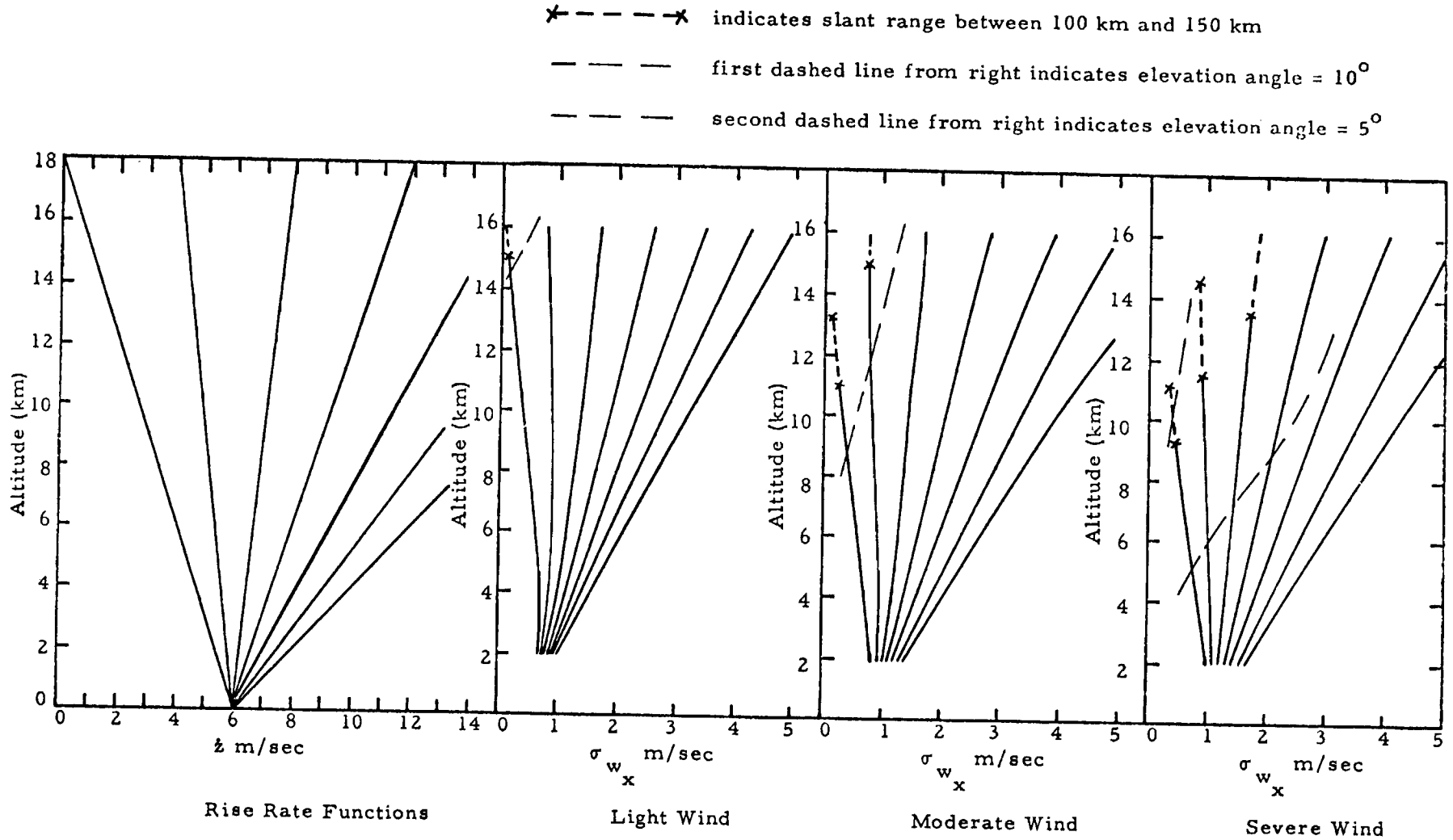

Figure 25. Error in Wind Magnitude for Linear Rise Rate Functions.

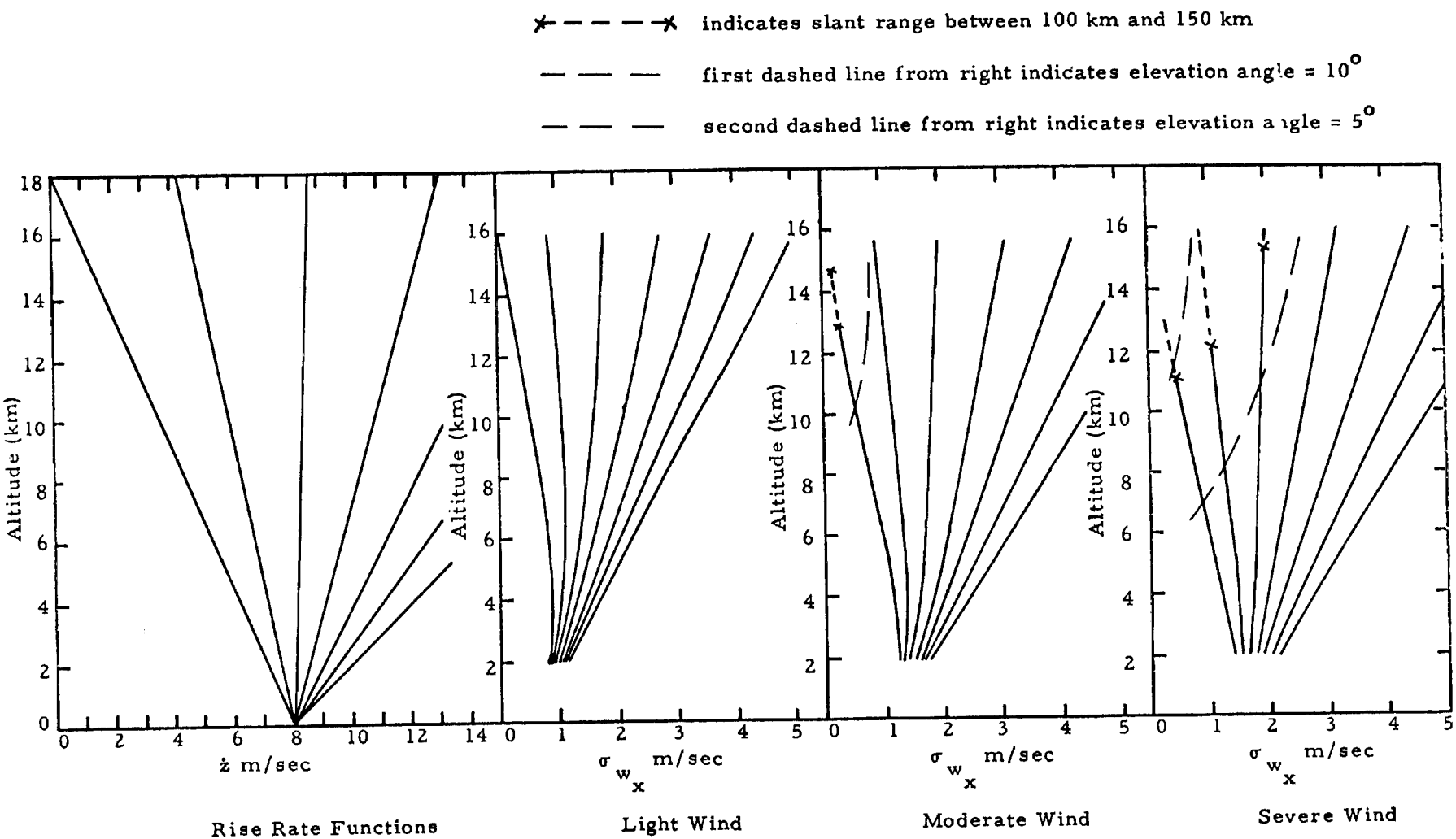

Figure 26. Error in Wind Magnitude for Linear Rise Rate Functions.

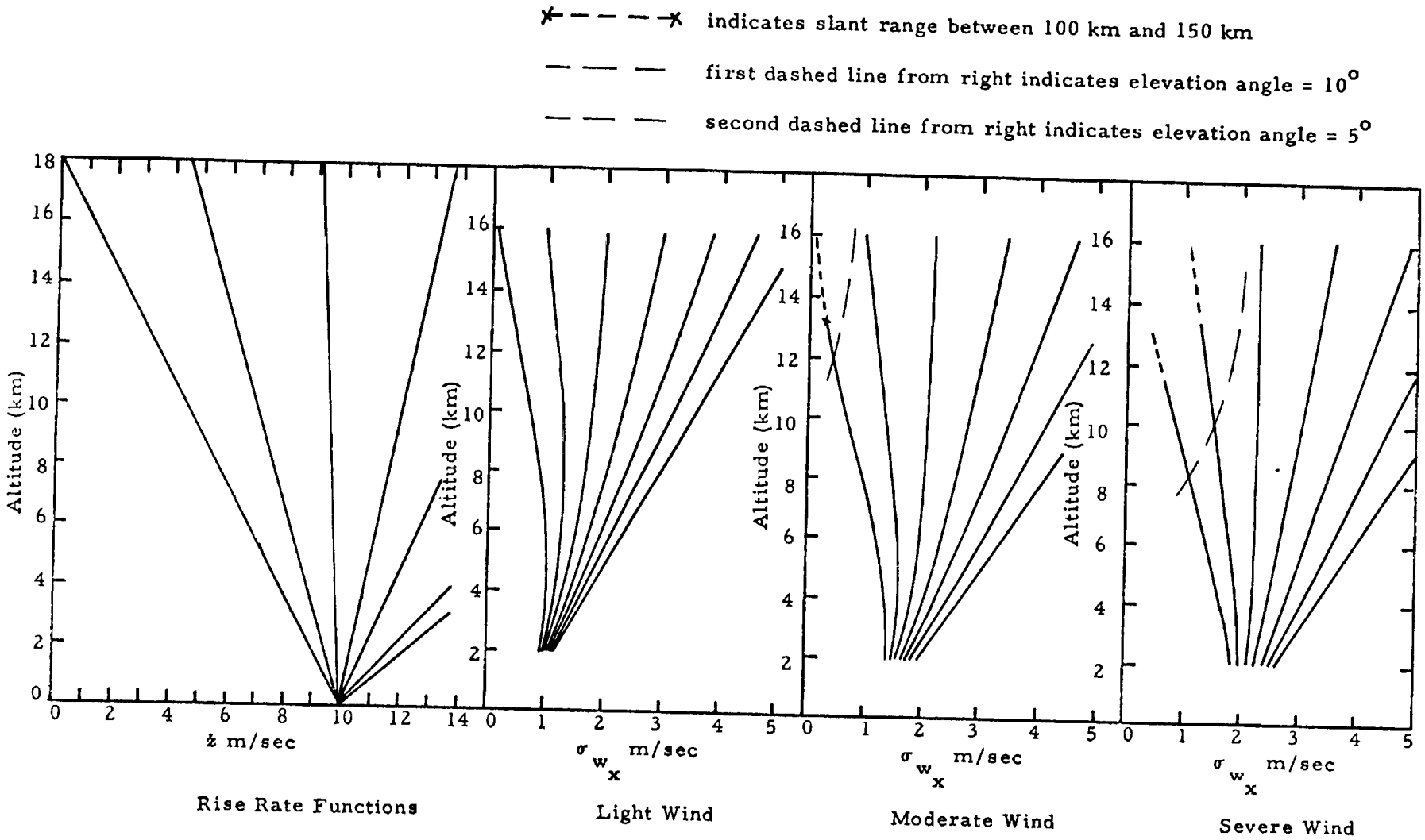

Figure 27. Error in Wind Magnitude for Linear Rise Rate Functions.

Results from these figures show that a linearly increasing rise rate, for any surface rise rate, is undesirable because the wind error increases as altitude increases. Only cases where the rise rate is constant or decreases with altitude show promise of providing acceptable wind errors. However, rise rates which become too slow are also unacceptable because they produce slant ranges and/or elevation angles which exceed FPS-16 tracking capabilities. None of the rise rates, however, will provide even one meter per second accuracy, over 25-meter smoothing, to 16 kilometers, under anything but the light wind condition. The decision as to which is the best or optimum rise rate depends upon the purpose or application of the measurement. For example, if 25 meter winds are only required to 12 kilometers under light to moderate wind fields, rise rate 2, Figure 24 (2nd rise rate from left on Figure 24) and rise rate 1, Figure 25 are desirable. If, on the other hand, data is required to 18 kilometers, neither of these rise rates is satisfactory because of excessive slant ranges. In this case, rise rate number 2, Figure 25 is probably most satisfactory. It is also interesting to note that the normal rise rate of the Jimsphere is between the range of number 2, Figure 24, and number 2, Figure 25, and hence is about the best that can be expected for the light and moderate wind fields.

Optimum Quadratic Rise Rate - In order to determine the quadratic rise rate profile that minimizes wind error a wide range of the quadratic parameters α, β , and γ had to be chosen. The technique used to determine practical bounds for these parameters is the following.

The parameters α, β, and γ of a quadratic function $\dot{z} = \alpha z^2 + \beta z + \gamma$ can be characterized by three geometrically meaningful constraints. They are a) the $\dot{z}$ intercept γ, b) the value of z where the function $\dot{z} = f(z)$ is a maximum or minimum, in particular $z = -\beta/2\alpha$, and c) the value of the function at its maximum or minimum, in particular $\dot{z} = 4\alpha\gamma - \beta^2/4\alpha$ (see Figure 28). By specifying these parameters, γ, $\beta/2\alpha$, and $4\alpha\gamma - \beta^2/4\alpha$, one easily solves for α, β, and γ. The purpose of working with γ, $\beta/2\alpha$, and $4\alpha\gamma - \beta^2/4\alpha$ is for the value of the geometric interpretation. Reality determines guidelines

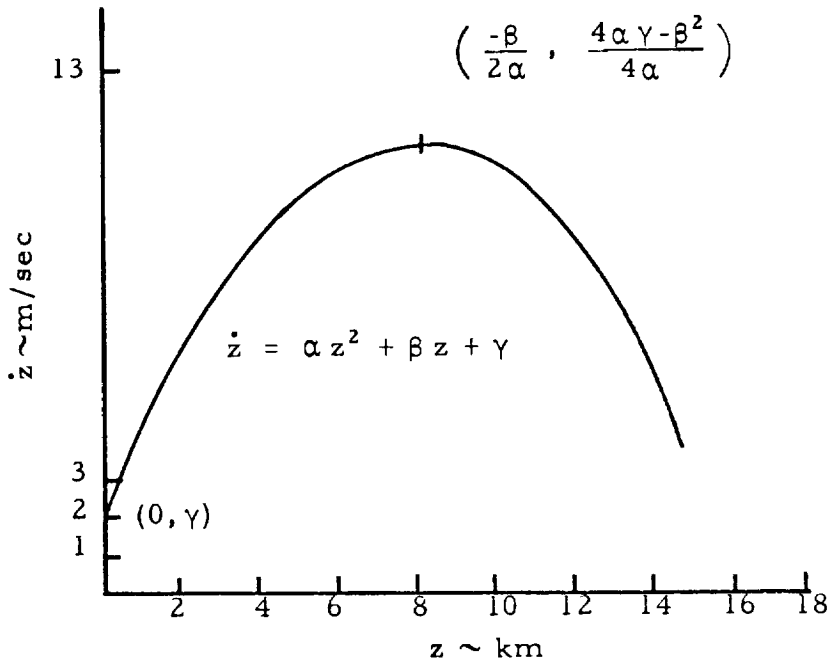

Figure 28. Geometric Interpretation of the Parameters α, β, and γ of a Quadratic Rise Rate Function.

for what types of rise rate functions are physically practical. For a reasonable range of values for surface rise rate the bounds were chosen as two meters per second $\leq \gamma \leq$ 10 meters per second. The range of values for the z altitude where the maximum and minimum rise rate occurs was chosen as two kilometers $\leq -\beta/2\alpha \leq$ 14 kilometers. The range of rise rate values at the maximum or minimum was chosen as $1 \leq 4\alpha\gamma-\beta^2/4\alpha \leq 13$ m/s.

Solving for α and β in terms of $u = -\beta/2\alpha$ and $v = 4\alpha\gamma-\beta^2/4\alpha$ gives

$$\alpha = \frac{\gamma - v}{u^2}$$

and

$$\beta = \frac{2v - 2\gamma}{u} \quad .$$

Figures 29 through 43 show wind errors associated with the quadratic rise rates defined by the ranges of variables specified above. Not all of the defined rise rates are practical. Nevertheless, any practical rise rate is reasonably approximated by at least one of the defined functions.

The wind error plots shown for linear and quadratic rise rate functions (Figures 23 through 27 and 29 through 43) were derived under an assumed radar time constant of $\Delta t = 0.5$ second and fixed smoothing interval of 25 meters. Since an FPS-16 radar may provide a time constant as small as $\Delta t = 0.1$ second under a high servo-bandwidth and optimum tracking conditions, it is of interest to determine the effect of a change in the time constant on wind errors. Of equal interest is the effect a change in the smoothing interval will produce on wind errors. The following two sections are addressed toward these problems.

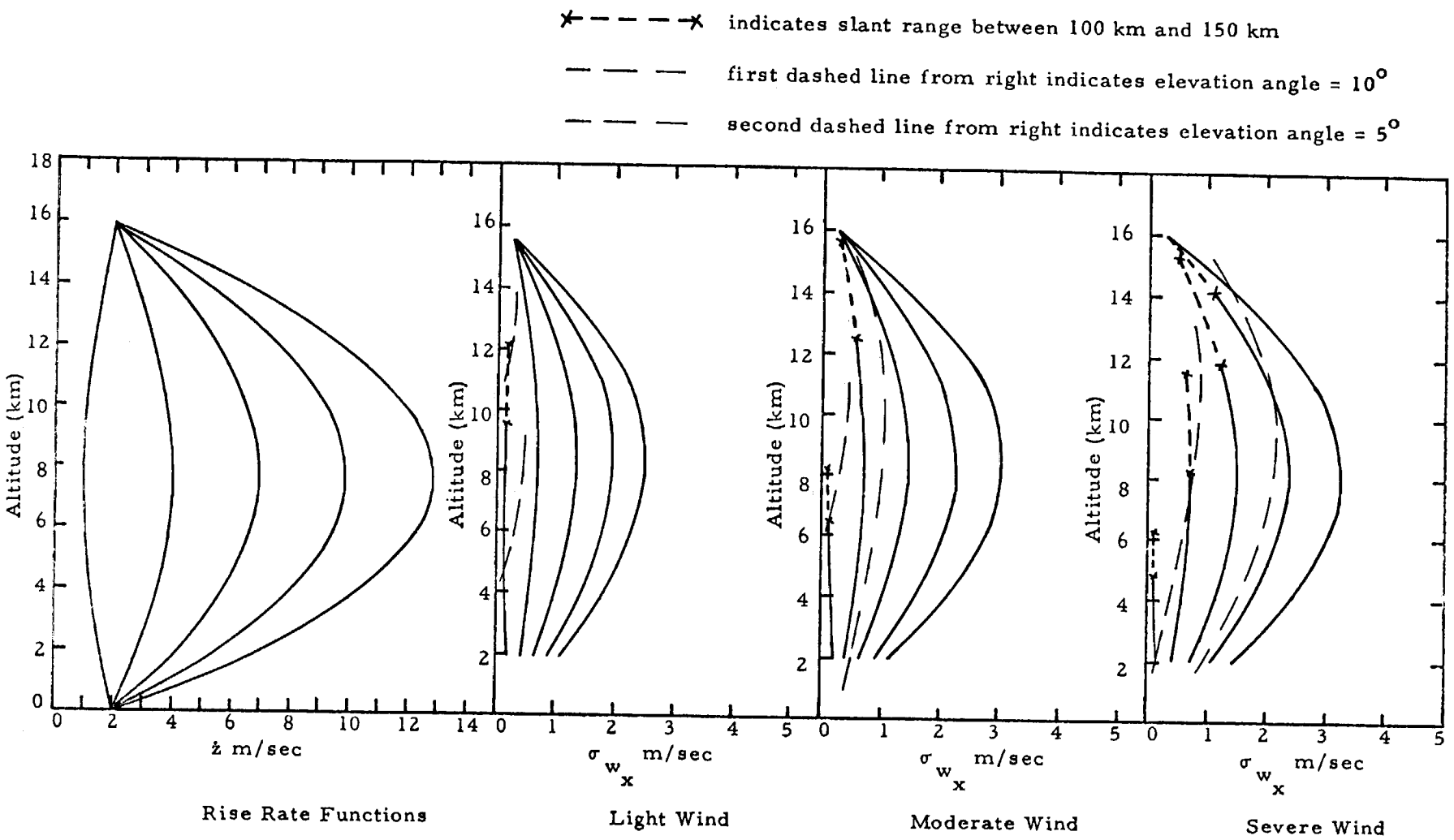

Figure 29. Error in Wind Magnitude for Linear Rise Rate Functions.

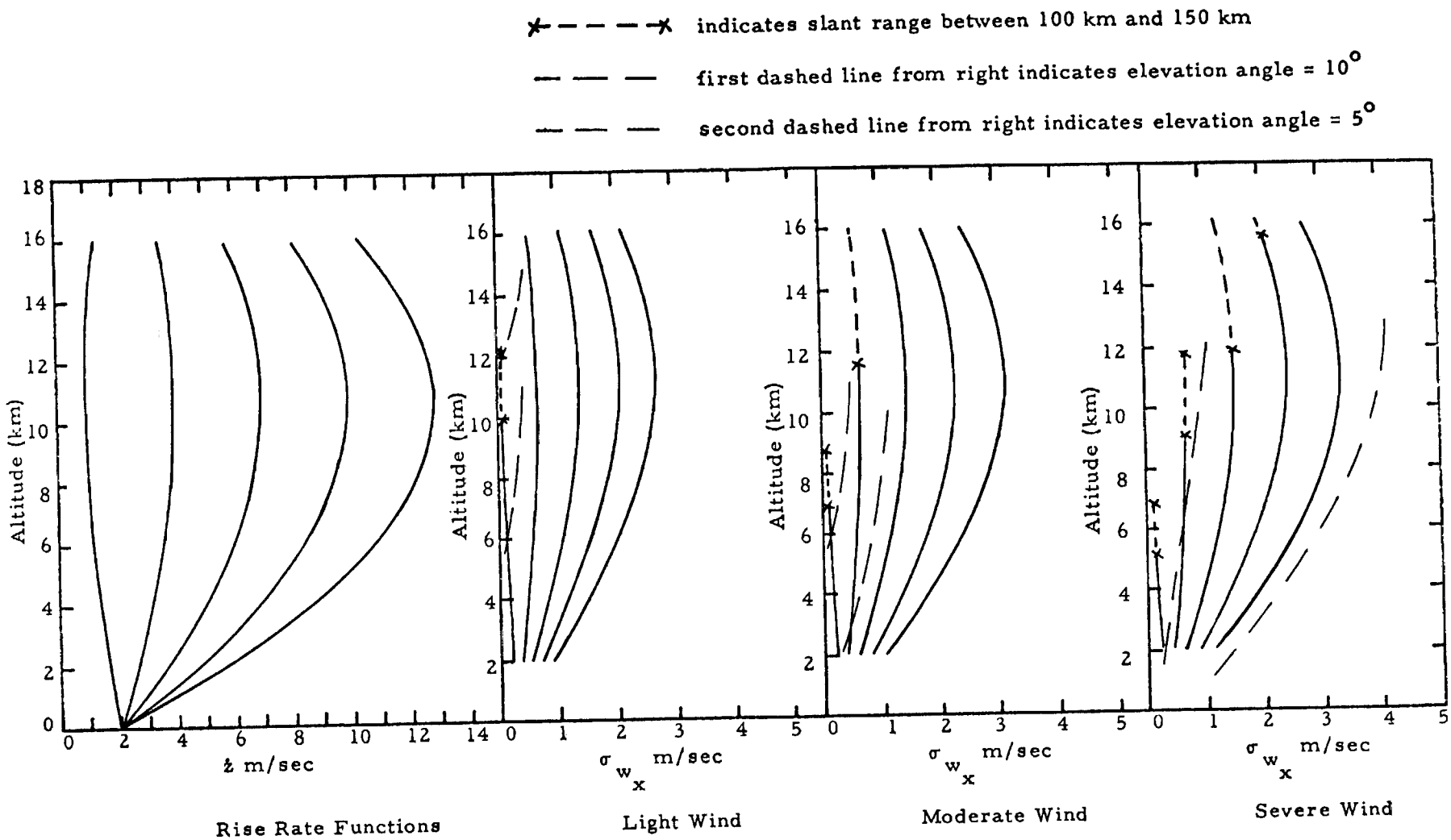

Figure 30. Error in Wind Magnitude for Linear Rise Rate Functions.

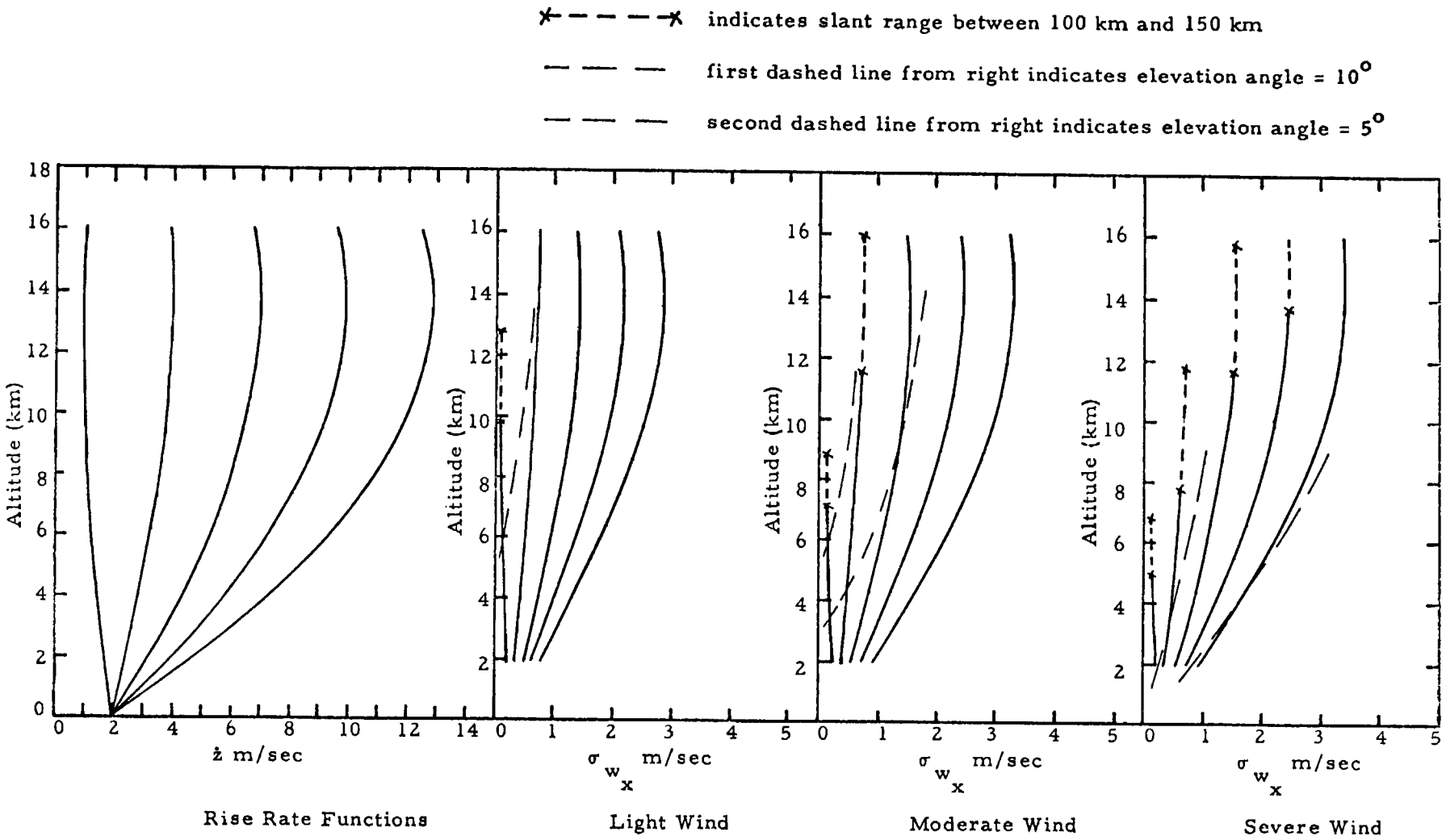

Figure 31. Error in Wind Magnitude for Linear Rise Rate Functions.

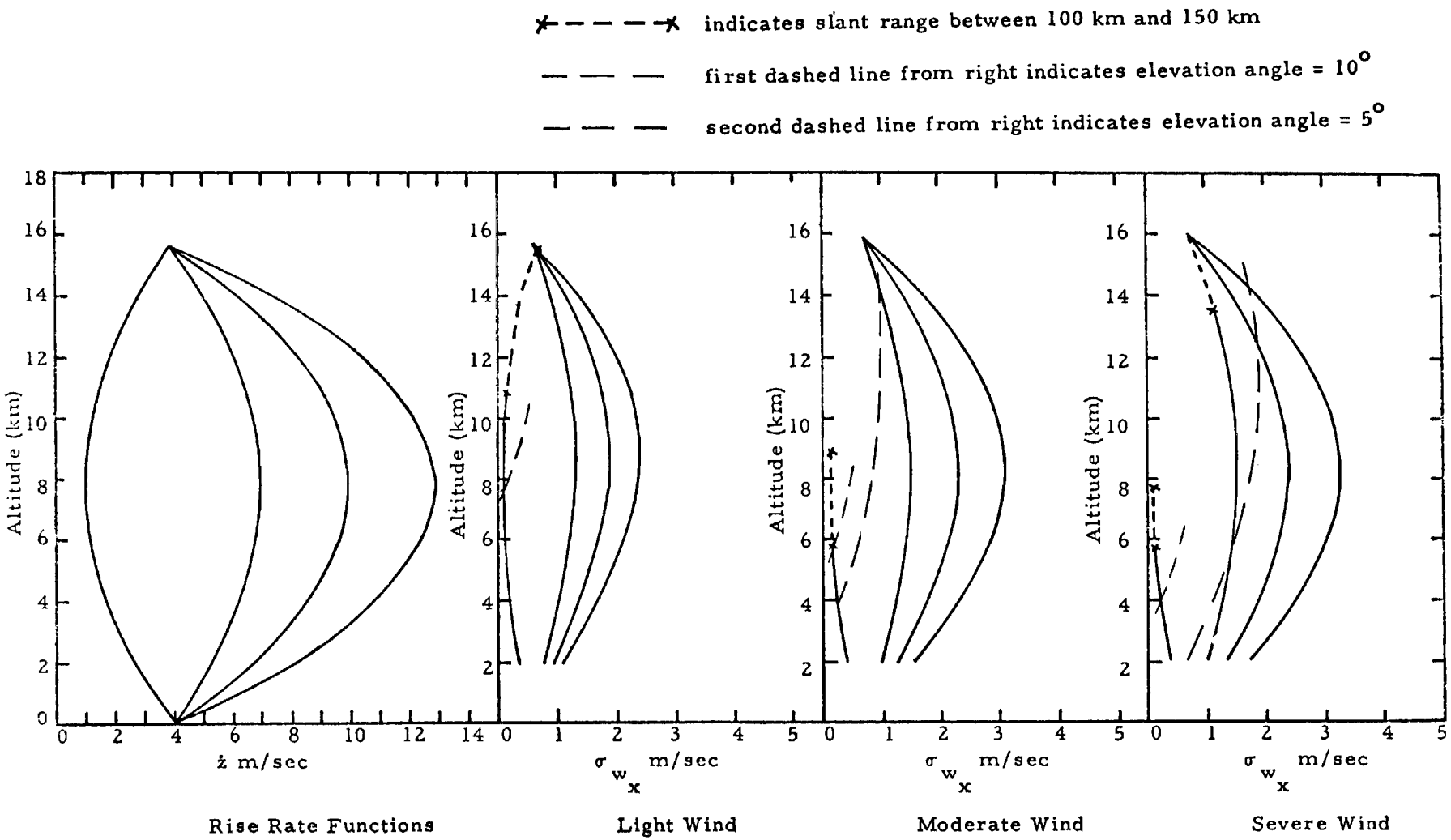

Figure 32. Error in Wind Magnitude for Linear Rise Rate Functions.

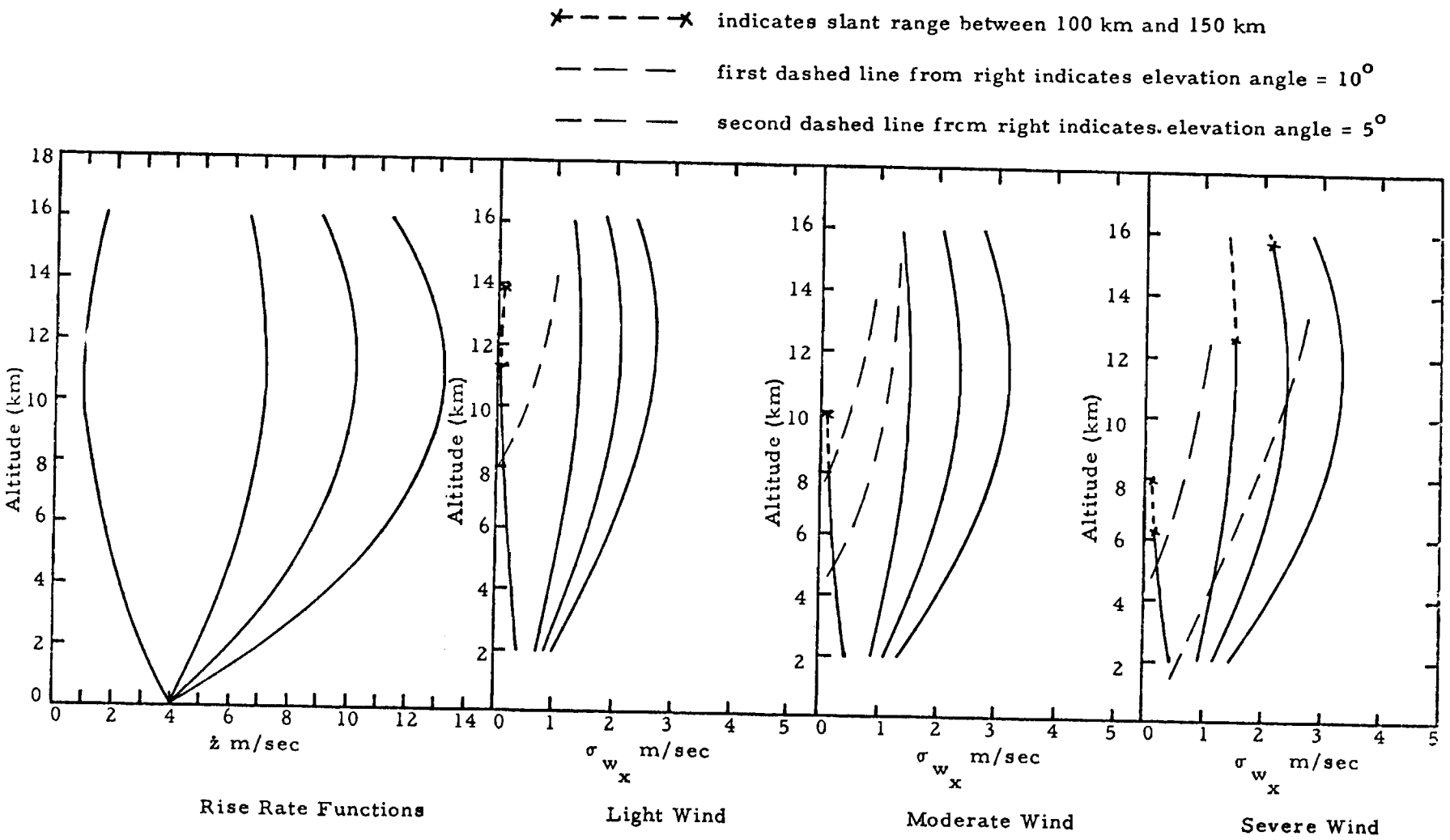

Figure 33. Error in Wind Magnitude for Linear Rise Rate Functions.

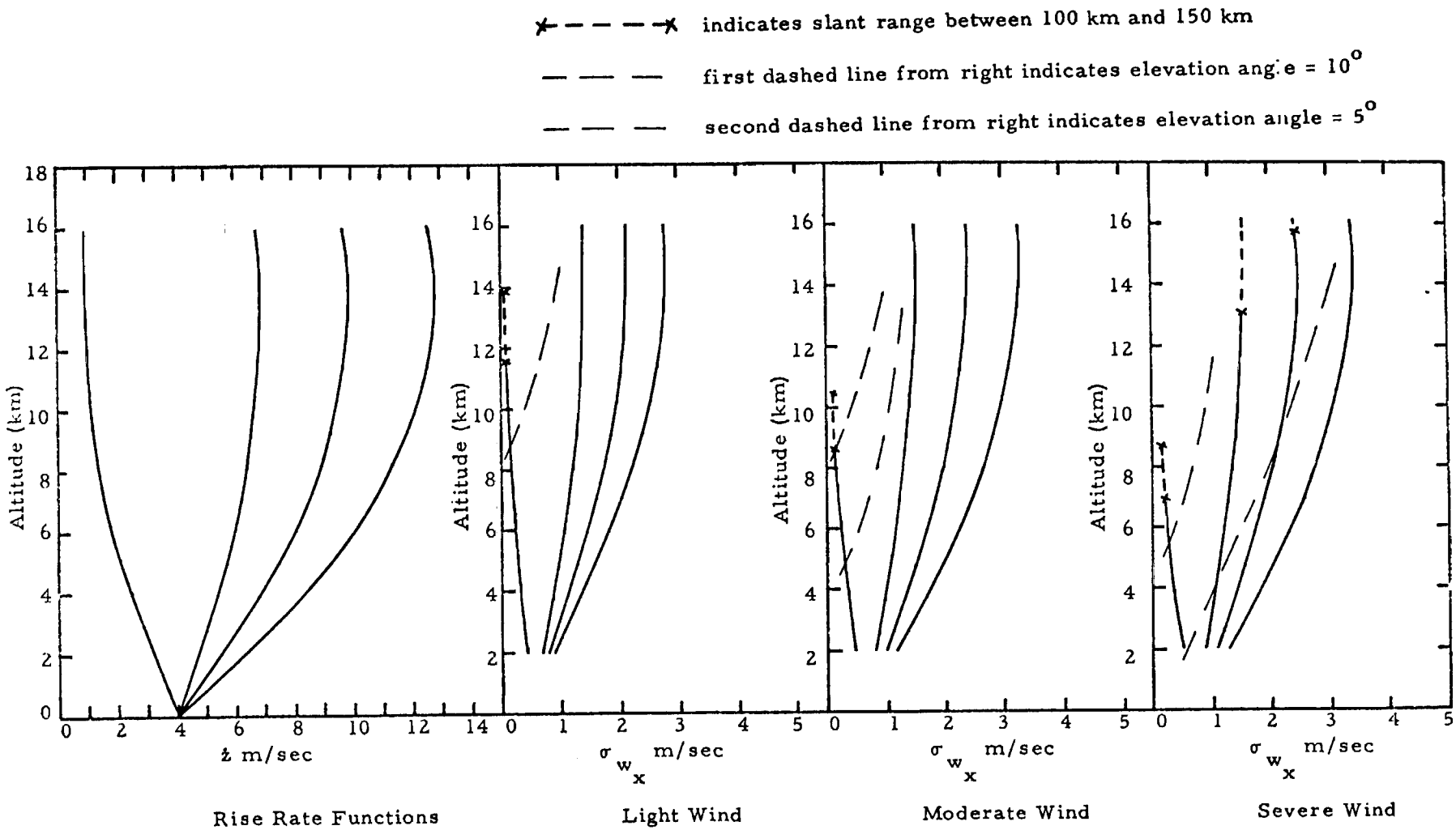

Figure 34. Error in Wind Magnitude for Linear Rise Rate Functions.

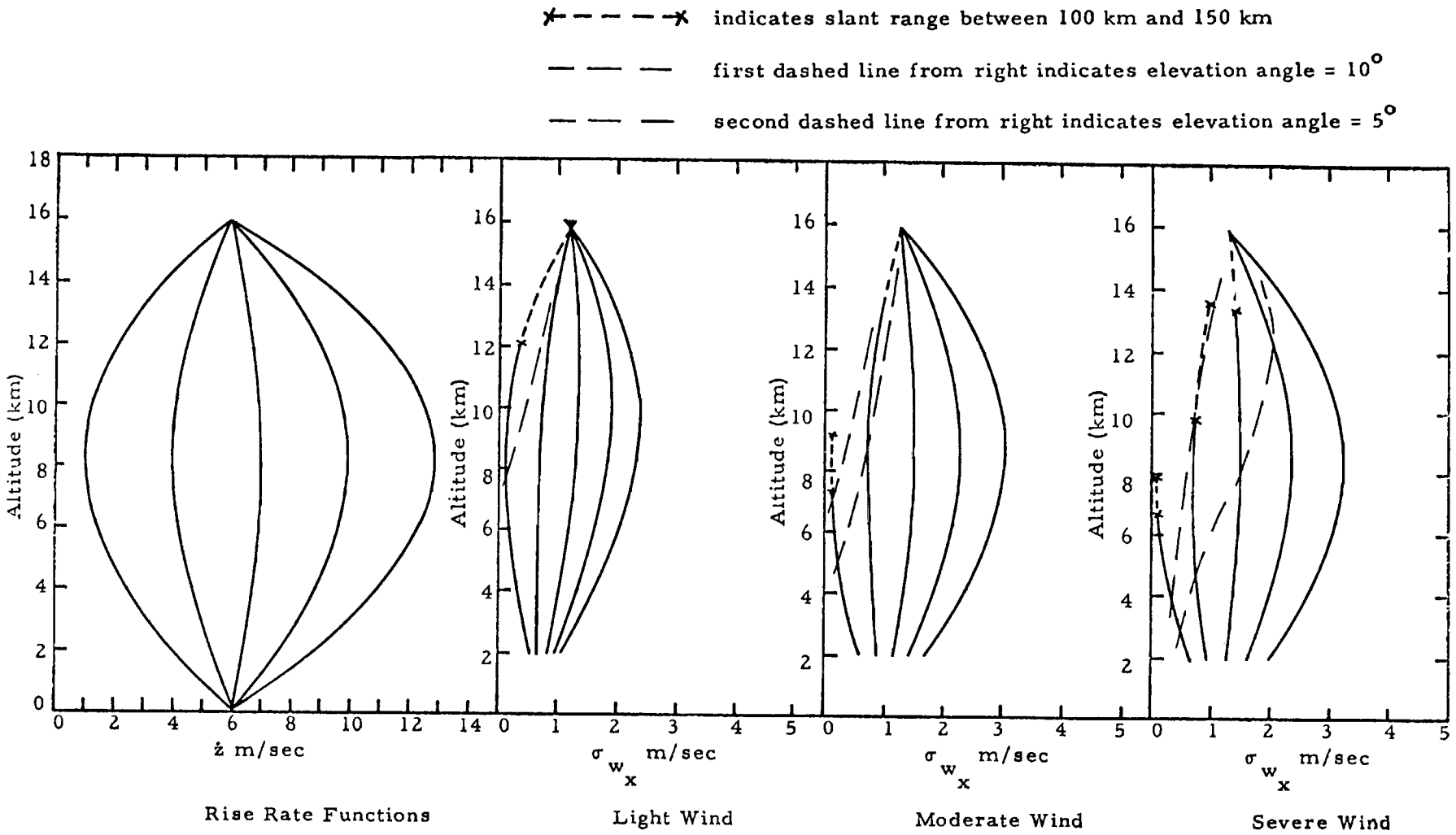

Figure 35. Error in Wind Magnitude for Linear Rise Rate Functions.

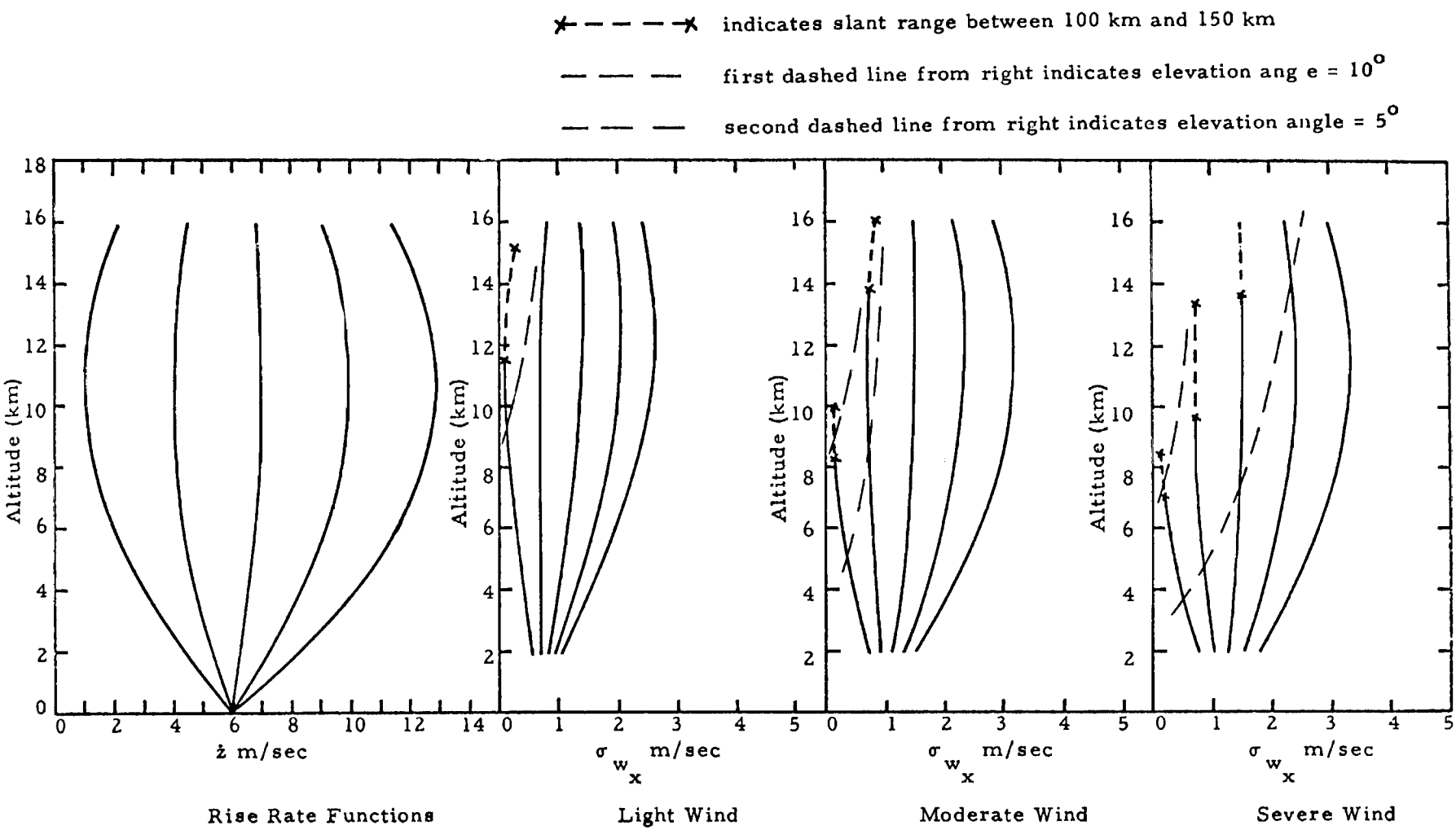

Figure 36. Error in Wind Magnitude for Linear Rise Rate Functions.

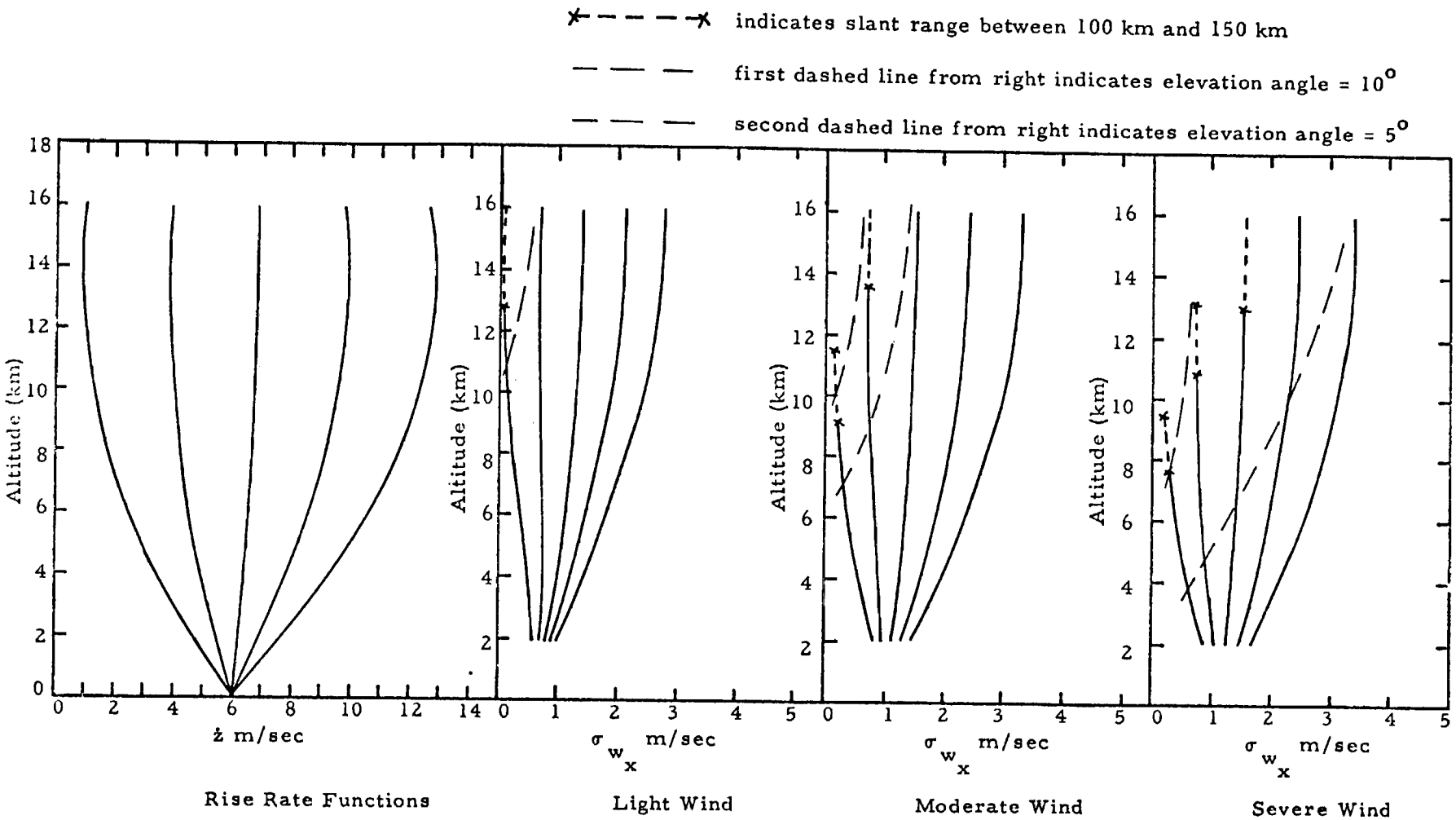

Figure 37. Error in Wind Magnitude for Linear Rise Rate Functions.

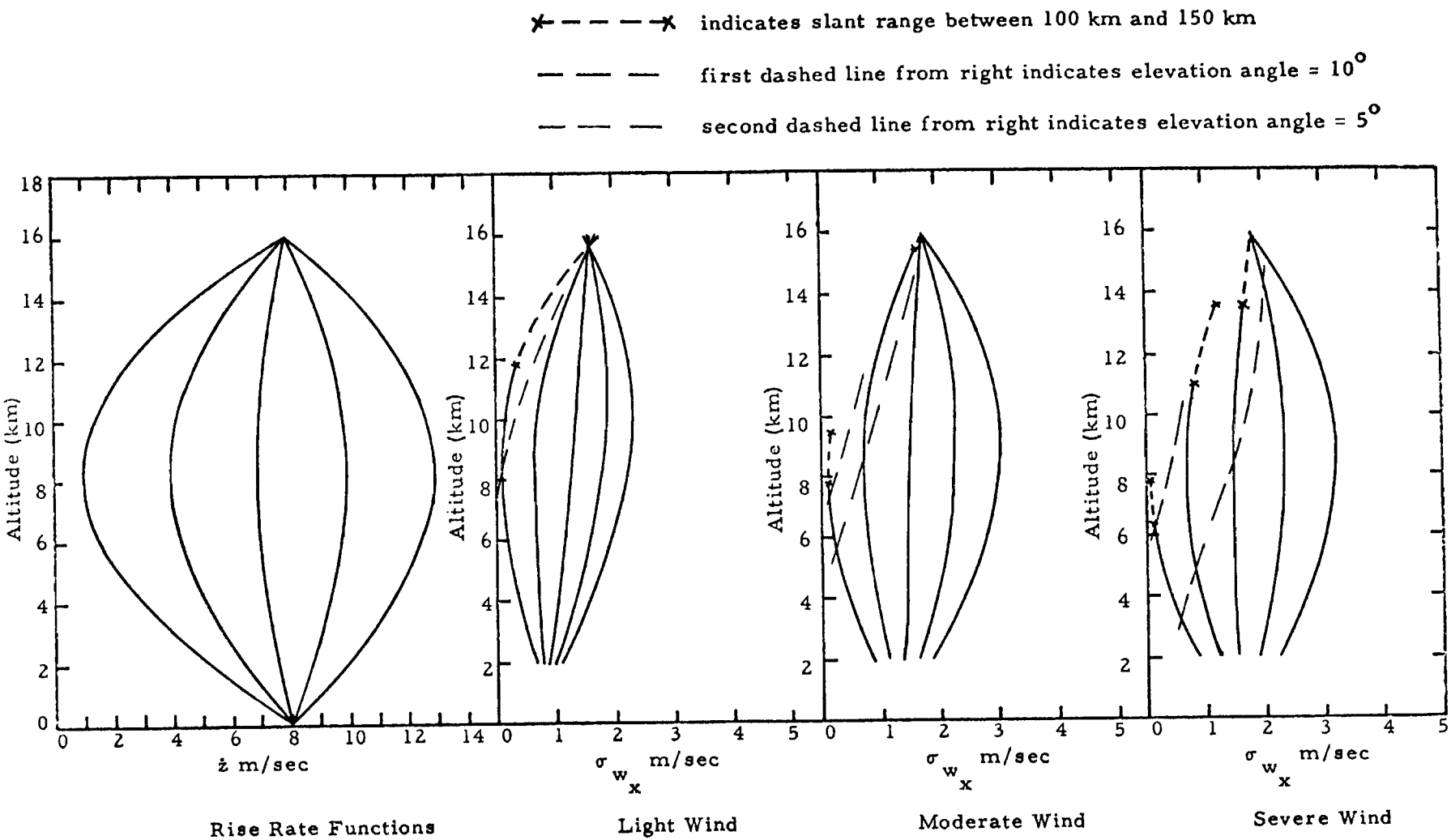

Figure 38. Error in Wind Magnitude for Linear Rise Rate Functions.

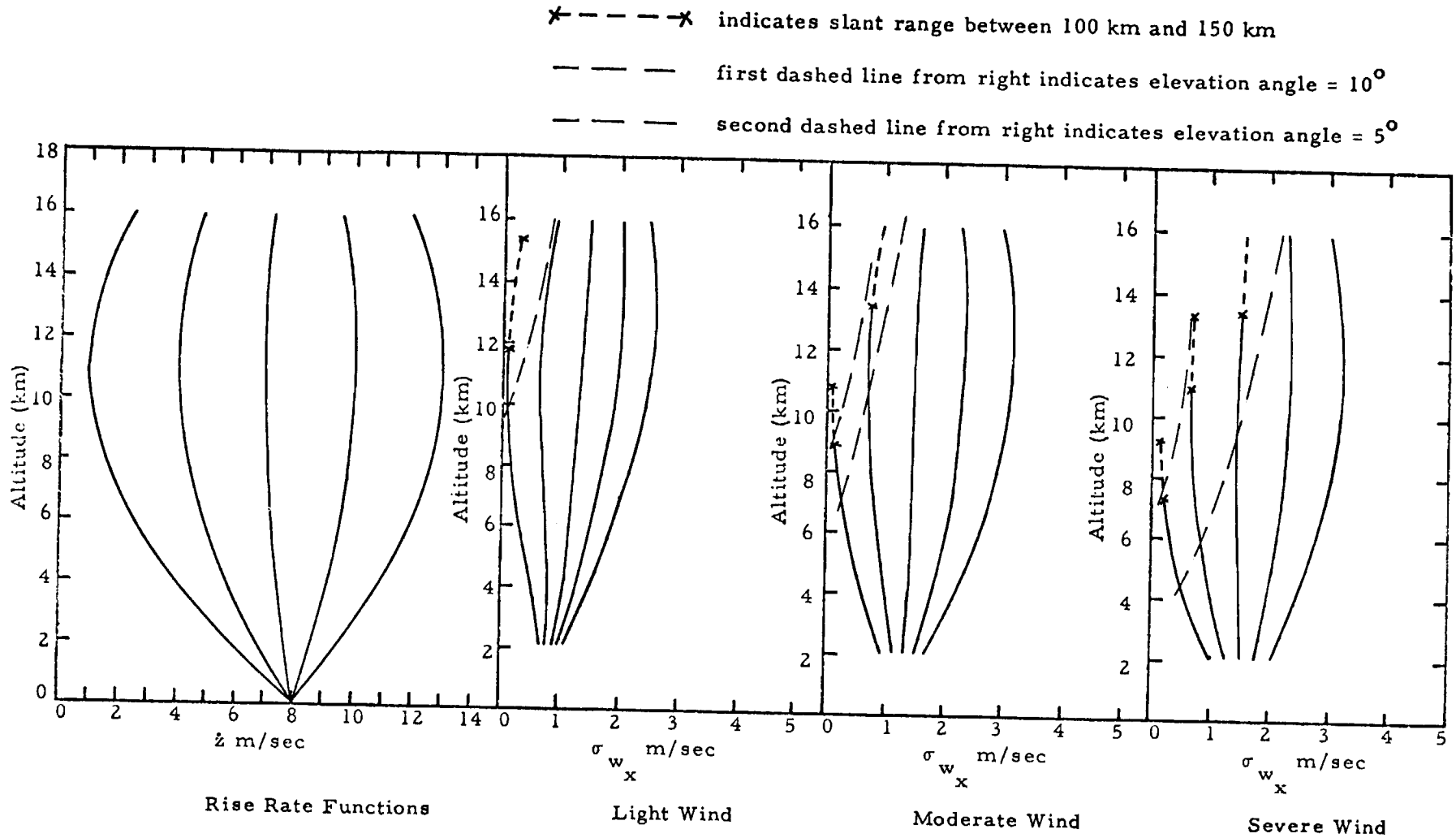

Figure 39. Error in Wind Magnitude for Linear Rise Rate Functions.

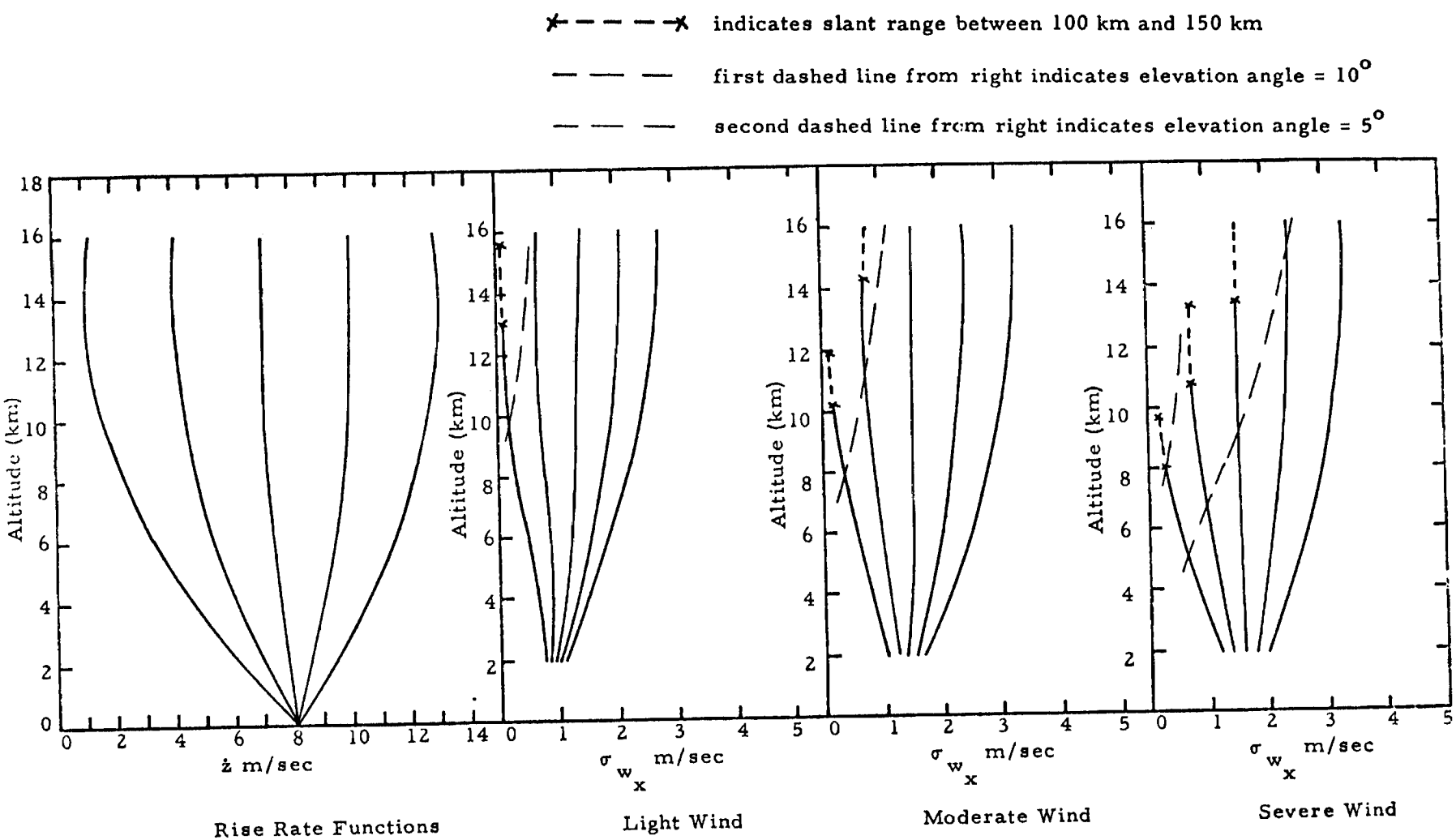

Figure 40. Error in Wind Magnitude for Linear Rise Rate Functions.

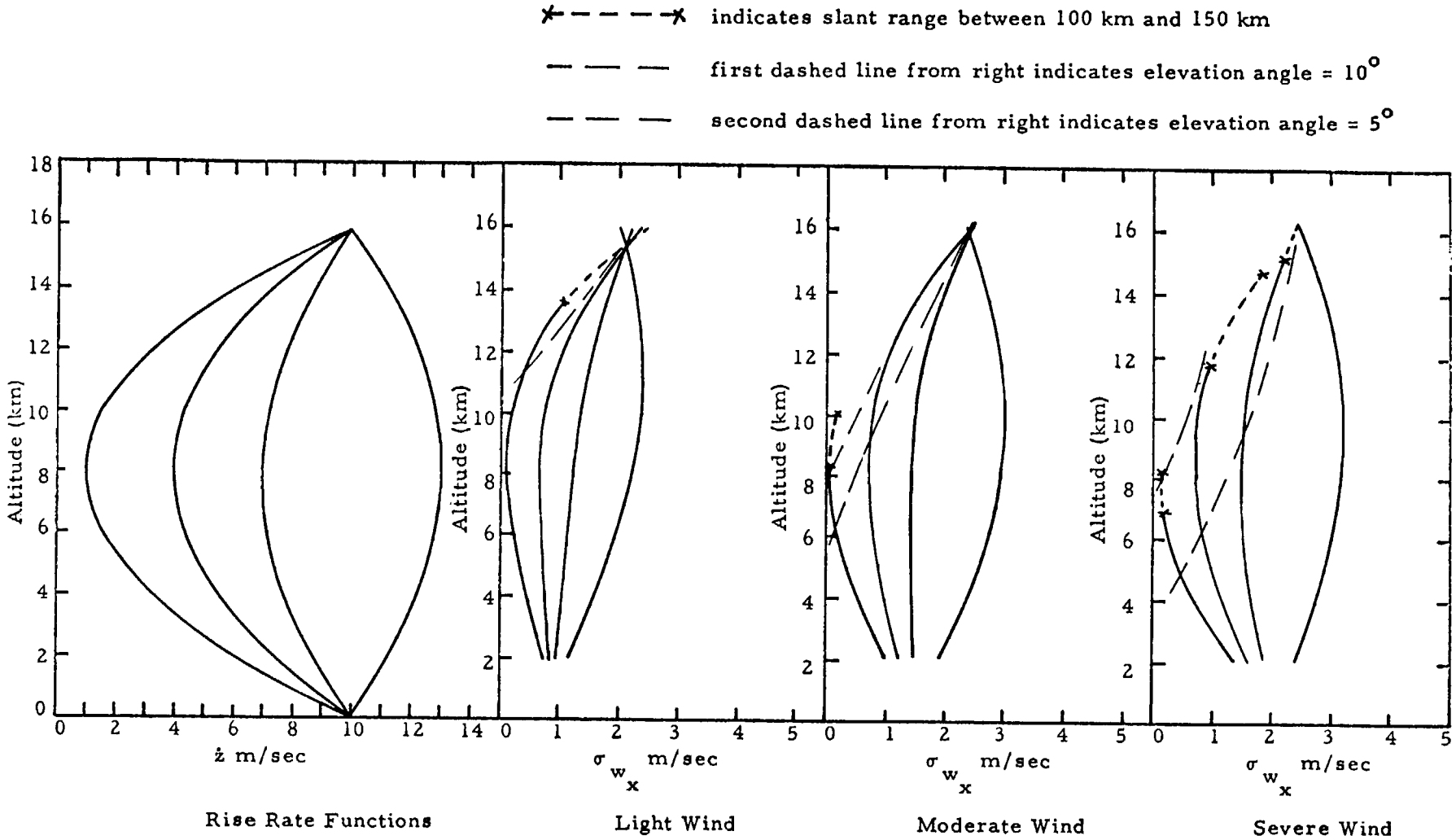

Figure 41. Error in Wind Magnitude for Linear Rise Rate Functions.

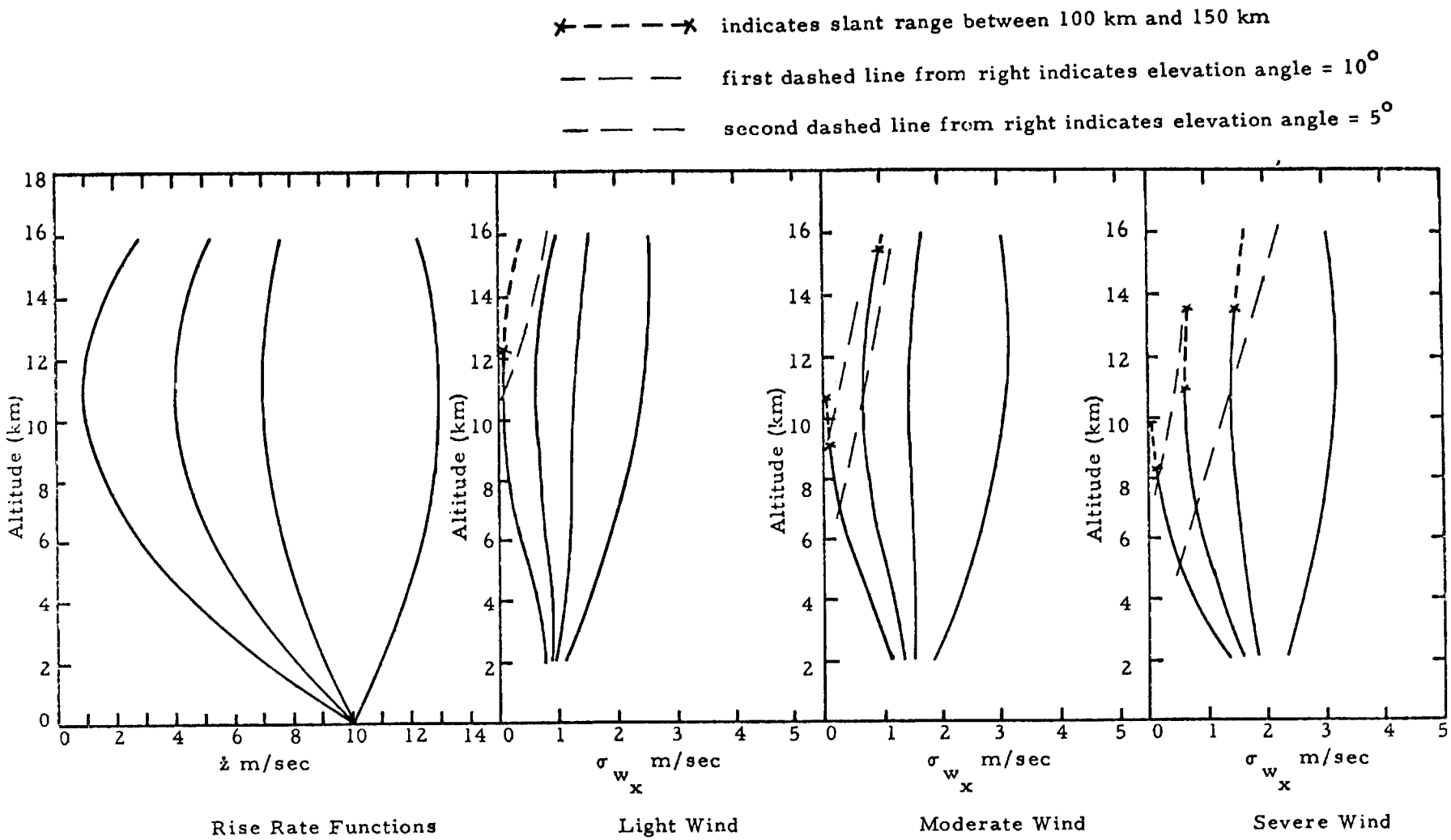

Figure 42. Error in Wind Magnitude for Linear Rise Rate Functions.

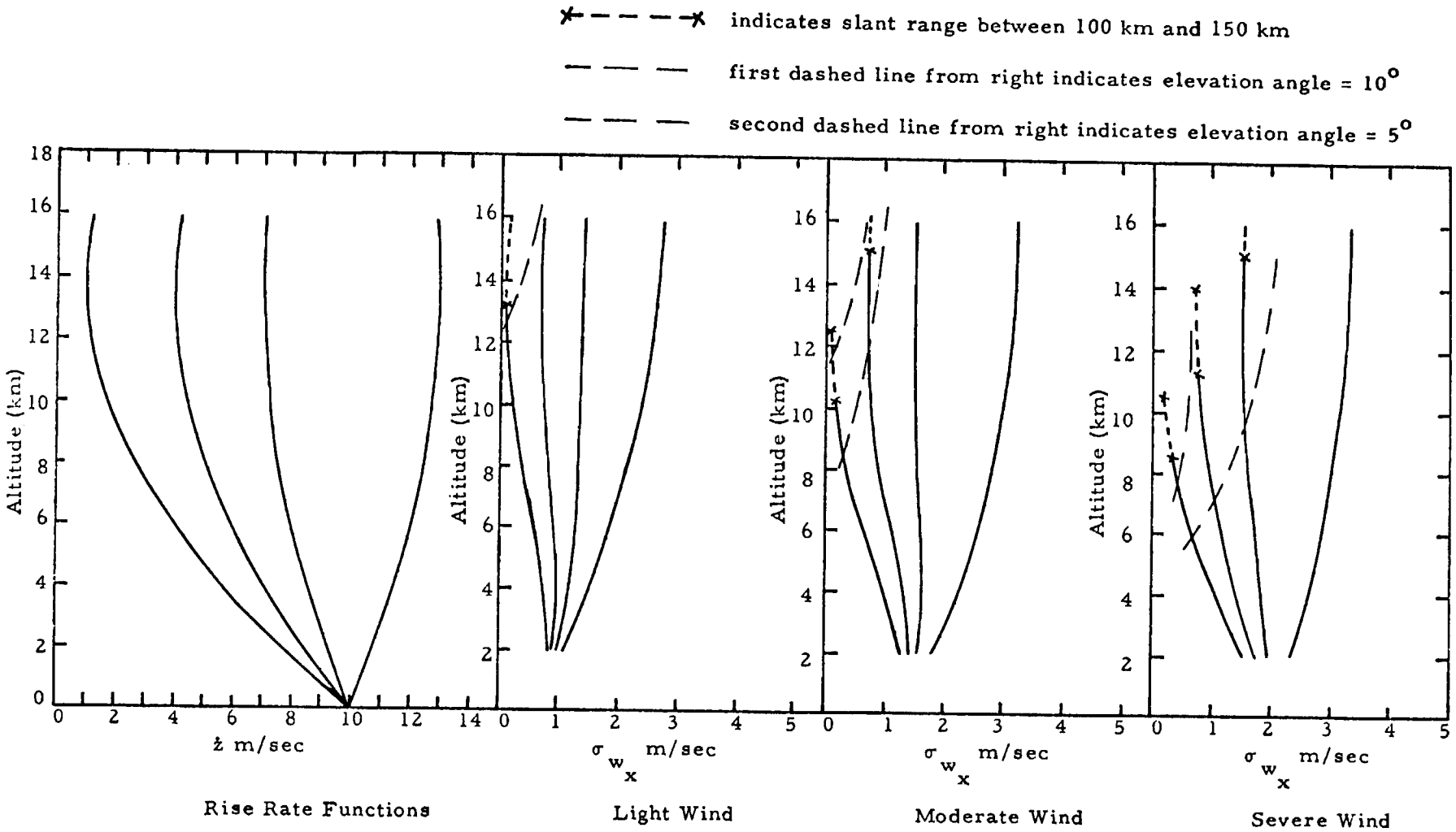

Figure 43. Error in Wind Magnitude for Linear Rise Rate Functions.

Effect of Smoothing Interval on Wind Accuracy

Recalling Equation (17a) the smoothing interval, S, is given by

$$S = (N-1)\dot{z}\,\Delta t \tag{17a}$$

and number of points, N, associated with the smoothing interval, S, as:

$$N = \frac{S}{\dot{z}\,\Delta t} + 1 \quad . \tag{17b}$$

Substituting (17a) into the wind error equation for a constant directional wind field (Equation (4)) gives the wind error in terms of the smoothing interval. That is:

$$\sigma_{wx}^2 = \sigma_{\dot{x}}^2 = \frac{12\,\sigma_x^2}{\left(\frac{S}{\dot{z}\,\Delta t} + 1\right)\left(\frac{S}{\dot{z}\,\Delta t} + 2\right)\left(\frac{S}{\dot{z}\,\Delta t}\right)\Delta t^2} \quad .$$

If the smoothing interval, S, is changed to S' then the ratio of wind errors from the S' interval to the S interval is:

$$\frac{\sigma_w(S')}{\sigma_w(S)} = \left[\frac{\left(\frac{S}{\dot{z}\,\Delta t} + 1\right)\left(\frac{S}{\dot{z}\,\Delta t} + 2\right)(S)}{\left(\frac{S'}{\dot{z}\,\Delta t} + 1\right)\left(\frac{S'}{\dot{z}\,\Delta t} + 2\right)(S')}\right]^{1/2} \quad . \tag{28}$$

For the case when the original smoothing interval S is 25 meters (Figures 23 through 27 and 29 through 43) and $\Delta t = 0.5$ second, Equation (28) becomes:

$$\frac{\sigma_w(S')}{\sigma_w(25)} = \left[\frac{\left(\frac{50}{\dot{z}} + 1\right)\left(\frac{50}{\dot{z}} + 2\right)(25)}{\left(\frac{2S'}{\dot{z}} + 1\right)\left(\frac{2S'}{\dot{z}} + 2\right)(S')}\right]^{1/2} \quad . \tag{29}$$

Equation (29) defines the multiplicative factor that transforms wind errors from any of the previous Figures 24 through 27, 29 through 43, for 25 meter smoothing into wind errors for any arbitrary smoothing interval S' Equation (29) is plotted as a function of S' and $\dot{z}$ in Figure 44.

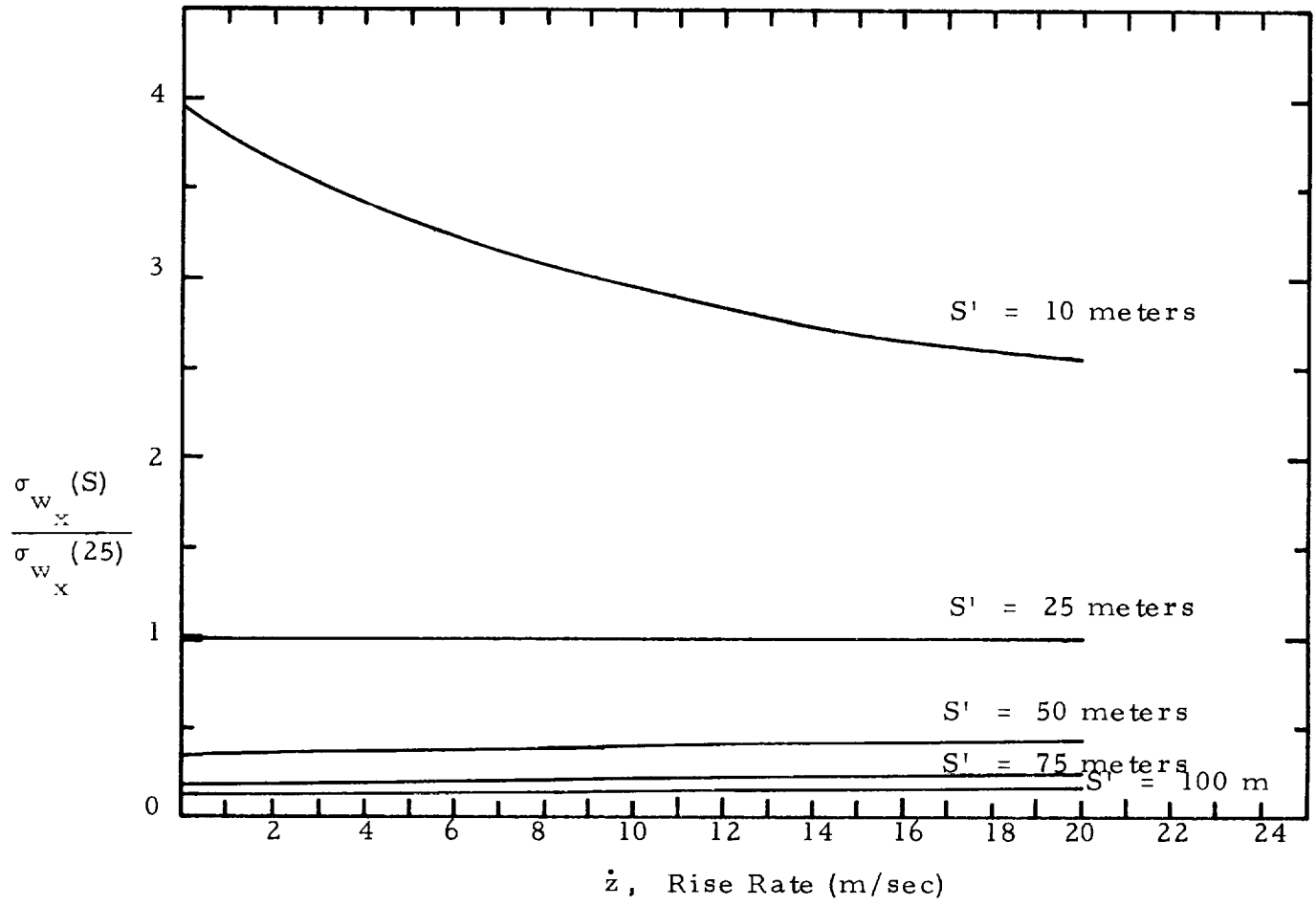

Figure 44. Multiplicative Factor to Convert Wind Error for 25 Meter Smoothing into Wind Error for 10 Through 100 Meter Smoothing.

The following example illustrates the use of Figure 44 to determine wind error for various smoothing intervals. For the linear rise rate function number 1 (Figure 26) the rise rate is $\dot{z}$ = 4 meters per second at 9 kilometers. The corresponding wind error for 25 meter smoothing in a moderate wind field is 0.7 meter per second. If the smoothing interval were ten meters then the wind error would be 0.7 x 3.4 = 2.38 m/sec where the multiplicative factor 3.4 is derived from the S' = 10 meter line from Figure 44. For 75 meter smoothing, the wind error would be 0.7 x .20 = .14 meter per second.

Figure 44 shows the multiplicative factor $\sigma_w(S)/\sigma_w(25)$ to be, in most cases, a weak function of $\dot{z}$. The multiplication factor can be approximated independently of $\dot{z}$ by ignoring the lower order terms of Equation (29). Equation (29) then simplifies to

$$\frac{\sigma_w(S)}{\sigma_w(25)} \approx \left[\frac{25}{S}\right]^{3/2}$$

which is independent of $\dot{z}$. Using the previous example and the approximated multiplication factor, the ten meter smoothing wind error would be 0.7 x 3.95 = 2.77 meters per second and the 75 meter smoothing wind error 0.7 x .19 = .13 meter per second.

Effect of the Time Constant on Wind Accuracy

The wind errors shown in Figures 23-27 and 29-43 assume typical FPS-16 coordinate errors of 0.1 mil in azimuth and elevation and five meters in slant range. A time spacing of $\Delta t = 0.5$ second between independent points is also assumed. The amount of decrease in wind error that would result under ideal tracking conditions where the time constant Δt could be as small as 0.1 second can be shown as follows. If the time constant is changed from Δt to $\Delta t'$ while the smoothing interval remains fixed, then the number of points in the smoothing interval will also change. The relationship between the time constant, smoothing interval, and number of points is:

$$S = (N-1)\,\Delta t \quad .$$

Holding S fixed while changing Δt and N to $\Delta t'$ and N' gives the equality

$$(N-1)\Delta t = (N'-1)\Delta t'$$

or

$$N' = (N-1)\frac{\Delta t}{\Delta t'} + 1 \quad . \tag{30}$$

The ratio of wind error when the time constant is $\Delta t'$ to wind error when the time constant is Δt is:

$$\frac{\sigma_w(\Delta t')}{\sigma_w(\Delta t)} = \left[\frac{\frac{12\sigma_x^2}{N'(N'^2-1)\Delta t'^2}}{\frac{12\sigma_x^2}{N(N^2-1)\Delta t^2}} \right] \quad . \tag{31}$$

Substituting Equation (30) into (31) gives

$$\frac{\sigma_w(\Delta t')}{\sigma_w(\Delta t)} = \left[\frac{N(N^2-1)\Delta t}{\left[(N-1)\frac{\Delta t}{\Delta t'} + 1\right]\left[(N-1)\frac{\Delta t}{\Delta t'} + 2\right](N-1)\Delta t'} \right]^{1/2} \tag{32}$$

where N is the number of points in S with time spacing Δt. Equation (32) can be approximated by

$$\frac{\sigma_w(\Delta t')}{\sigma_w(\Delta t)} \approx \left[\frac{\Delta t'}{\Delta t}\right]^{1/2} \qquad (33)$$

which is independent of N.

A plot of Equation (32) for a $\Delta t = 1/2$ and various values of $\Delta t'$ is given in Figure 45. The following example illustrates the use of Figure 45. For the linear rise rate function number 1 (Figure 26) the wind error for 25 meter smoothing in a moderate wind field at 9 km is 0.7 m/sec. The rise rate at this altitude is $\dot{z}$ = 4 meters per second and the time constant is $\Delta t = 1/2$. The number of points in the 25-meter smoothing interval is

$$N = \frac{S}{\dot{z}\,\Delta t} + 1 = 13.5 \quad .$$

If the time constant is changed to $\Delta t'$ = 0.1 second, the multiplicative factor from Figure 45 for N = 13.5 is 0.49. Thus, the wind error resulting if the time constant were 0.1 second is 0.7 x 0.49 = 0.34 meter per second. Similarly, for a time constant of two seconds, the resulting wind error would be 1.11 meters per second. If the approximation formula, Equation (33), were used, the resulting wind errors for Δt = 0.1 and Δt = 2.0 seconds would be 0.7 x 4.5 = 0.31 meter per second and 0.7 x 2 = 1.4 meters/second.

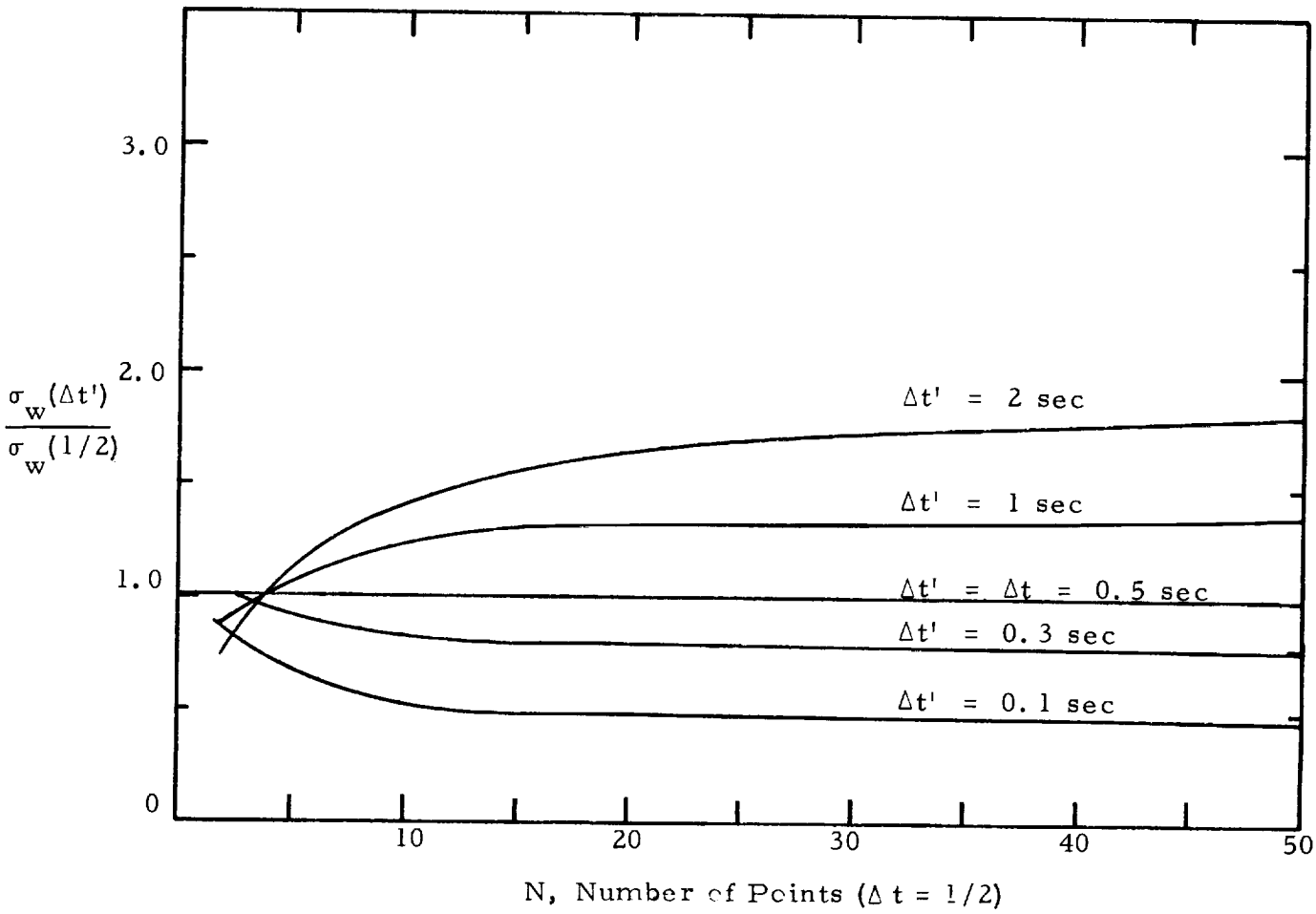

Figure 45. Multiplicative Factor to Convert Wind Error When the Time Constant is 0.5 Second into Wind Error When the Time Constant has Other Values.

BALLOON DIMENSIONS

The previous sections have shown the wind accuracy that will result from various rise rate functions under given wind conditions. It is now realistic to examine what balloon dimensions are required to provide a specified rise rate function. This question cannot be answered without first specifying what type balloon is being considered (e.g., a constant volume spherical balloon, expandable balloon, etc.). To answer this question for expandable spherical balloons the following approach can be pursued. It will be shown in this section that to achieve a desired rise rate at a specified altitude there is only one radius smooth (or one radius roughened) spherical balloon that can achieve these results, consequently, a balloon can be designed to provide a specified rise rate profile by determining the balloon radius needed to achieve the rise rates specified by the profile at various altitudes. A balloon manufacturer can then determine what type expandable balloon will achieve the proper radius at the proper altitude. For other type balloons other methods can be used to provide a specified rise rate profile. A change in the skin thickness, an additional ballast, or a relief valve could change the rise rate profile. In fact, any change in a parameter of the rise rate equation (derived in this section) would effect the entire rise rate profile. A study of the effect produced by a variation in each parameter of the radius equation would be valuable in determining what parameters can best be manipulated to achieve various types rise rate functions. The discussion presented in the following section has stopped short of a sensitivity analysis of the rise rate equation. What is presented is a means of determining what radius balloon will provide a specified rise rate at a specified altitude. The altitudes specified are 10 km and 14 km. The results have direct application for expandable balloon design for smooth and roughened spheres. In addition, the technique presented is intended to serve as a guide to anyone who wishes to consider the variation of other parameters in the rise rate equation.

Balloon Radius Versus Rise Rate - The equation of motion in the vertical direction of a rising sphere is given to a good approximation as:

$$(m_{skin} + m_{gas})\ddot{z} = -\frac{1}{2}\rho\, C_D\, A\dot{z}^2 - \rho\, vol\, g + (m_{skin} + m_{gas})g \qquad (34)$$

where

m_{skin}, m_{gas} are mass of the balloon skin and mass of the contained gas, respectively,

vol is volume of the balloon,

$\dot{z}$, $\ddot{z}$ are vertical velocity and acceleration,

g is gravitational acceleration = 9.8 m/sec^2,

ρ is density of air,

C_D is drag coefficient,

and

A is the cross-sectional area of the balloon.

Over small regions of the atmosphere, the density can be considered constant and thus the balloon will approach an equilibrium or terminal velocity when the acceleration approaches zero.

Under this condition, Equation (34) becomes

$$-\frac{1}{2}\rho\, C_D A\dot{z}^2 - \rho\, vol\, g + (m_{skin} + m_{gas})g = 0 \quad . \qquad (35)$$

The skin mass can be written as

$$m_{skin} = \rho_{skin}\, \Delta s\, A_s \qquad (36)$$

where Δs is the thickness of the skin and A_s is the surface area.

Smooth Spherical Balloon - For a smooth spherical balloon, the surface area is:

$$A_s = 4\pi r^2 \quad .$$

Equation (36) for a smooth sphere becomes

$$m_{skin} = \rho_{skin}\, \Delta s\, 4\pi r^2 \quad . \qquad (37)$$

The mass of the gas is given by

$$m_{gas} = \rho_{gas} vol \quad . \tag{38}$$

For a sphere, Equation (38) is given by

$$m_{gas} = \frac{4}{3} \pi r^3 \rho_{gas} \quad . \tag{39}$$

The cross-sectional area A defined in Equation (35) is given for a sphere as:

$$A = \pi r^2 \quad . \tag{40}$$

A substitution of Equations (37), (39), and (40) into Equation (35) and solving Equation (35) for r, the radius of the sphere, gives the radius equation for smooth spheres:

$$r = \frac{-C_D \dot{z}^2 + 8 \Delta s \, g \frac{\rho_{skin}}{\rho}}{\frac{8}{3} g \left(1 - \frac{\rho_{gas}}{\rho} \right)} \quad . \tag{41}$$

Equation (41) can be used to estimate the radius of a smooth sphere required to achieve a specified rise rate ($\dot{z}$). The quantities that must be known or estimated to solve Equation (41) for r are: a) the density of the material used to make the sphere, b) the thickness of this material, c) an estimate of the drag coefficient of the sphere, and d) the density of the air at the altitude where the specified rise rate is desired. Of these quantities, only (c), an estimate of the drag coefficient, provides any degree of difficulty. The drag coefficient for a slow-moving sphere (Mach$\approx$0) is sketched as a function of Reynolds number in Figure 46. The sharp change in the drag curve occurs at the approximate Reynolds number of 2.5×10^5. An ascending sphere will decrease in Reynolds number as it ascends. Thus, it will traverse the drag curve sketched in Figure 46 from right to left. At Reynolds numbers greater than the critical value (2.5×10^5), the flow around the sphere is turbulent and a smooth sphere will experience random self-induced aerodynamic oscillations. These random oscillations make small scale wind determination impractical with a smooth sphere. After passing through the critical Reynolds

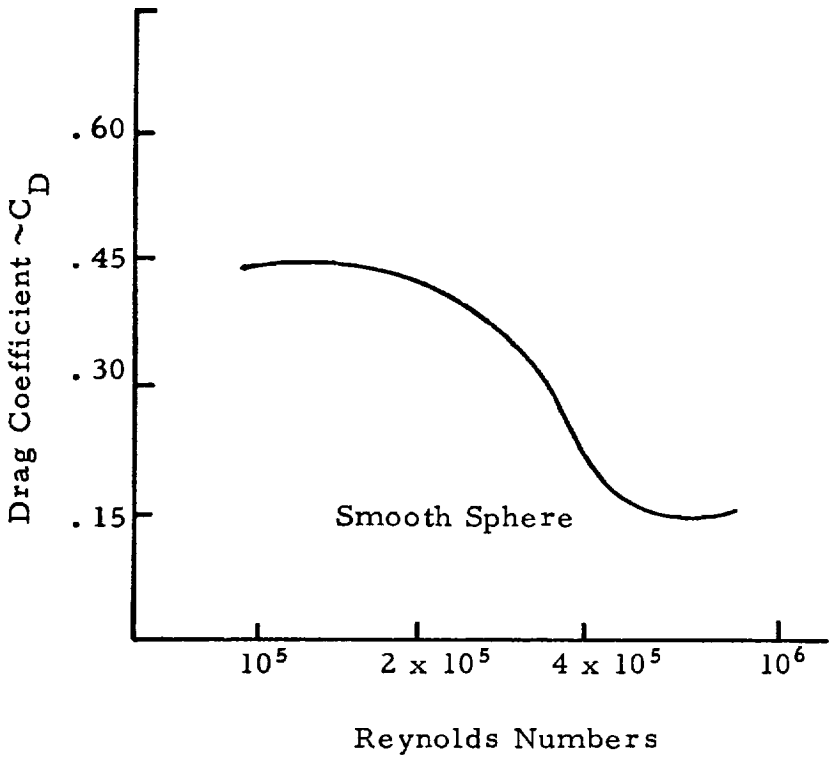

Figure 46. Drag Curve for a Smooth Sphere.

number, the flow around the sphere becomes laminar and the self-induced motions sharply diminish. Small scale wind measurements are again possible. For the sake of design engineering, a satisfactory estimate of the drag coefficient function can be taken as:

$$\begin{aligned} C_D &= .45 \text{ for } R \leq 2 \times 10^5 \\ C_D &= .30 \text{ for } 2 \times 10^5 < R < 4 \times 10^5 \\ C_D &= .15 \text{ for } R \geq 4 \times 10^5 \end{aligned} \qquad (42)$$

This function can be used to estimate C_D if Reynolds number can be determined.

Reynolds number is given by the expression

$$R = 2 \rho \dot{z} r/\mu \tag{43}$$

where μ is the coefficient of viscosity of air and is a weak function of altitude. To achieve a desired $\dot{z}$ at a specified altitude, the Reynolds number can be determined from Equation (43) for any proposed radius. The determination of R allows the estimation of C_D from Equations (42) which in turn is needed in Equation (41).

An example will illustrate how Equation (41) can be used to determine the balloon radius needed to achieve a desired rise rate at a specified altitude. The following assumptions will be made about the balloon:

a) The balloon is a smooth sphere of radius r.

b) The skin is mylar of thickness 1/4 mil = 6.35×10^{-6}m.

c) The sphere is filled with helium at ambient pressure and temperature.

d) No additional mass is attached to the skin.

Under these assumptions, the evaluation of Equation (41) for a rise rate of $\dot{z}$ = 10 meters per second at 10 kilometers altitude is illustrated below:

$\dot{z} = 10$ m/sec

$z = 10$ kilometers

$\rho_{10km} = 414$ gr/m^3

$\Delta s = 6.35 \times 10^{-6}$

$g = 9.8$ m/sec^2

$\rho_{helium}/\rho = 4/29$

$\rho_{mylar} = 1.2 \times 10^6$ gr/m^3 .

$C_D = f(R)$ and is either .45, .30, or .15, depending upon r. Equation (41) can be evaluated for each of the three values of C_D to determine three values of a radius r. For each radius r, an associated Reynolds number can be calculated. The Reynolds number then uniquely determines the C_D corresponding to that radius. If the corresponding radius and C_D match the original chosen C_D for that radius, a valid combination has been found. If not, the originally chosen C_D and radius are an inconsistent combination that will

not solve Equations (41), (42), and (43) simultaneously. That is, from Equation (41),

$$r = 2.06 \quad \text{for } C_D = .45$$
$$r = 1.40 \quad \text{for } C_D = .30$$
$$r = .73 \quad \text{for } C_D = .15 \quad .$$

The Reynolds numbers associated with each of the above radii are derived from Equation (43) as:

$$r = 2.06 \quad R = 2r\rho\dot{z}/\mu = 1.2 \times 10^6 > 4 \times 10^5 \rightarrow C_D = .15$$
$$r = 1.40 \quad R = 7.9 \times 10^5 > 4 \times 10^5 \rightarrow C_D = .15$$
$$r = .73 \quad R = 4.1 \times 10^5 > 4 \times 10^5 \rightarrow C_D = .15 \quad .$$

Applying Equations (42), the only consistent triplet of r, R, and C_D is:

$$r = .73 \quad R = 4.1 \times 10^5, \text{ and } C_D = .15 \quad .$$

Thus, a 0.75 meter radius smooth sphere, made of 1/4 mil mylar, filled with helium, with no ballast or additional mass, will, at ten kilometers, have a rise rate of 10 m/sec. This sphere, however, will experience difficulties in obtaining wind measurements since it will be in a turbulent flow condition and exhibit random aerodynamic oscillations.

The radius necessary to achieve other rise rates at altitudes of ten and 14 kilometers under the same four assumptions (a, b, c, d) is given in Tables 3 and 4. The radii given in these tables are the only radii that will provide the desired rise rates under the stated assumptions.

As seen in Tables 3 and 4, large rise rates of 10 to 20 m/sec are possible with smooth spheres of modest diameters. One difficulty with using spheres of these dimensions for small-scale wind determination is the turbulent flow condition associated with the $C_D = .15$. The random aerodynamic motions associated with turbulent flow make all but the gross wind structure impossible to observe from the trajectory of the sphere.

TABLE 3

RADIUS AS A FUNCTION OF $\dot{z}$ AT 10 KILOMETERS ALTITUDE FOR SMOOTH SPHERE

Rise Rate ($\dot{z}$ ~ m/sec)

Drag Coefficient	2	4	6	10	15	20
.15				.73	1.56	2.73
.30			.54			
.45	.14	.38				

TABLE 4

RADIUS AS A FUNCTION OF $\dot{z}$ AT 14 KILOMETERS ALTITUDE FOR SMOOTH SPHERE

Rise Rate ($\dot{z}$ ~ m/sec)

Drag Coefficient	2	4	6	10	15	20
.15					1.61	2.78
.30						
.45	.20	.44	.84			

Rough Spherical Balloons - Roughening cones added to the smooth sphere have shown, in the case of the Jimsphere, that the random motions of a smooth sphere can be transformed into regular oscillations over a very small frequency band. These oscillations can then be removed from the trajectory by a properly designed filter. However, a secondary effect of adding the roughening cones is a change in the drag coefficient curve. For the Jimsphere, the drag coefficient has been derived by Fichtl, DeMandel, and Krivo [12] to be as shown in Figure 47. Thus, the roughening elements in increasing the sphere stability also increase the drag coefficient at supercritical Reynolds numbers. Thus, the entries in Tables 3 and 4 would not be valid for roughened spheres because of the different drag coefficient curve. For engineering application, the drag coefficient curve for the roughened sphere will be taken as:

$$\begin{aligned} C_D &= .47 \quad \text{for } R \leq 1.2 \times 10^5 \\ C_D &= .60 \quad \text{for } 1.2 \times 10^5 < R < 2.5 \times 10^5 \\ C_D &= .72 \quad \text{for } R \geq 2.5 \times 10^5 \end{aligned} \qquad (44)$$

The skin mass of the roughened sphere also differs from that of a smooth sphere because of the roughening elements. It will be assumed that the skin surface area of a rough sphere is 1.4 times that of the corresponding smooth sphere of the same diameter. The other balloon associated variables m_g and A needed to derive the radius equation for roughened spheres can be taken as the corresponding parameters for smooth spheres.

The radius equation for roughened spheres is

$$r = \frac{-C_D \dot{z}^2 + 11.2 \, \Delta s \, g \, \frac{\rho_{skin}}{\rho}}{\frac{8}{3} g \left(1 - \frac{\rho_{gas}}{\rho} \right)} \qquad .$$

Solving Equations (43), (44), and (45) simultaneously for r determines the radius of roughened spheres necessary to produce given rise rates at specified altitudes. Tables 5 and 6 show the radii required to produce 2 to 20 m/sec rise rates at 10 and 14 kilometers. A comparison between Tables 3 and 4 and Tables 5 and 6 shows that larger radii are required to produce a given

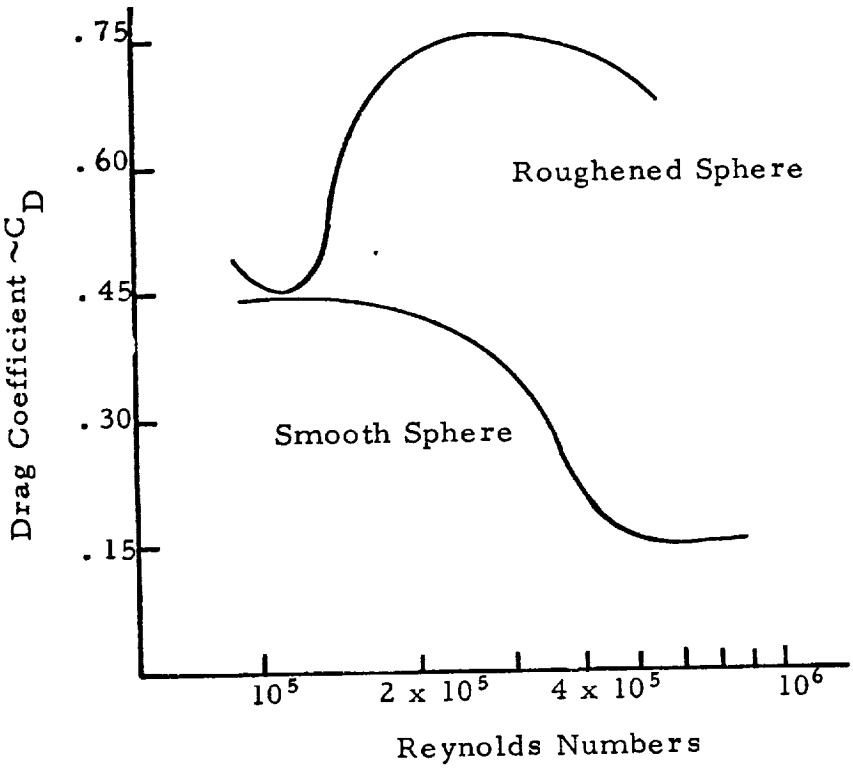

Figure 47. Comparison Between Drag Curve for Smooth and Roughened Sphere.

TABLE 5

RADIUS AS A FUNCTION OF $\dot{Z}$ AT 10 KILOMETERS ALTITUDE FOR ROUGHENED SPHERE

Drag Coefficient	Rise Rate (m/sec) 2	4	6	10	15	20
.47	.17					
.60		.52				
.72			1.24	3.29	7.28	12.87

TABLE 6

RADIUS AS A FUNCTION OF $\dot{Z}$ AT 14 KILOMETERS ALTITUDE FOR ROUGHENED SPHERE

Drag Coefficient	Rise Rate (m/sec) 2	4	6	10	15	20
.47	.25	.50				
.60						
.72			1.31	3.36	7.35	12.94

rise rate from a roughened sphere than from a smooth sphere - particularly for large $\dot{z}$. This is because the drag coefficient is larger for rough spheres than for smooth spheres, especially at supercritical Reynolds numbers.

Perhaps more practical than designing a large diameter balloon to measure winds is to design a streamlined-non-spherical balloon possessing a low drag coefficient at large Reynolds numbers and that does not possess the random aerodynamic motions associated with its flow conditions. The foregoing analysis that was performed for smooth and roughened spheres can also be undertaken for other non-spherical type balloons. All that is required is

a) A knowledge of the drag curve for the balloon.

b) An expression for the volume of the balloon.

c) An expression for the surface area of the balloon.

d) An expression for the cross-sectional area of the balloon.

Of these quantities, only the drag coefficient curve may be difficult to come by. An expression for each of the other quantities can certainly be derived.

Wind Sensing Capability of Fast Rising Balloons - The previous section discussed balloon diameters required to achieve specified rise rates. Of equal importance is the ability of the balloon to respond to the wind field. That is, can one assume that the horizontal velocity of the balloon is the wind velocity, or does the balloon's response sharply lag the wind response? One way of attacking this problem is to assume a sinusoidal varying wind field versus altitude of the form:

$$W_x = A \sin(\omega t) \quad .$$

Under this assumed wind field and assuming the balloon is a point mass, it is possible to solve the equations of motion for the balloon velocity. The amplitude of the balloon velocity oscillation can then be ratioed to the amplitude of the sinusoidal wind field to determine the percentage response of the wind field shown in the velocity of the balloon.

If the sinusoidal wind field $W_x = A \sin \omega t$ is substituted into the horizontal equations of motion and the resulting differential equation integrated for the balloon velocity, the result is (Ref. [1], p. 78):

$$\dot{x} = \frac{b}{K_1} e^{t/K_1} + A' \sin (\omega t + \varphi_B) \tag{46}$$

where

b is a constant of integration,

$$\varphi_B = \arctan \left(\frac{\omega(K_1 - K_2)}{1+K_1 K_2 \omega^2} \right) ,$$

$$K_1 = \frac{(m+m')\dot{z}}{g(m-\rho \text{ vol})} ,$$

$$K_2 = \frac{m'\dot{z}}{g(m-\rho \text{ vol})} ,$$

m' = the apparent mass of the balloon,

and

$$A' = \frac{A[1 + \omega^2 (K_1^2 + K_2^2 + K_1^2 K_2^2 \omega^2)]^{1/2}}{1 + K_1^2 \omega^2} .$$

The first term of Equation (46) is the transient part of the solution and rapidly approaches zero as t increases. The second term represents the steady state solution. The ratio of the amplitude of the steady state balloon velocity to the amplitude of the wind velocity is therefore:

$$D_B = \frac{A'}{A} = \frac{[1 + \omega^2 (K_1^2 + K_2^2 + K_1^2 K_2^2 \omega^2)]^{1/2}}{1 + K_1^2 \omega^2} . \tag{47}$$

Equation (47) gives the percentage response of the amplitude of the balloon velocity to wind velocity for the frequency $\omega/2\pi$. The frequency is related to the wavelength through the rise rate of the sensor by:

$$\lambda = (2\pi/\omega)\dot{z}$$

where λ is the wavelength

The velocity response of a balloon to the wavelength λ can be calculated from Equation (47) as a function of the balloon rise rate and the balloon

dimension needed for evaluating K_1 and K_2. It is interesting to note that the balloon response does not depend upon the drag coefficient, except indirectly through its effect on the rise rate. Thus, other dimensions being equal (i.e., mass, diameter) a smooth and roughened sphere of the same rise rate would have the same horizontal response to the wind field. The actual velocity response of the smooth and roughened spheres represented in Tables 3, 4, 5, and 6, at 10 and 14 kilometers, have been calculated for wavelengths of 50 to 100 meters and are presented in Tables 7, 8, 9, and 10. The tables were derived under the assumptions that the balloon is a point mass. The diameter of large balloons may be a significant percentage of the wavelength being examined and thus the point mass assumption is dubious. For example, a 10 meter radius balloon has a diameter equal to 40% of a 50 meter wavelength. These results show excellent balloon response to 50 and 100 meter wave structure. Even the fast rising balloons of large radii show response to at least 79% to 50 meter wave structure. Thus, the response of any of the balloons considered, either smooth or roughened, is most satisfactory and is not a limiting factor in designing a fine scale wind measurement balloon system.

Summary and Conclusions - The error in the magnitude of the horizontal wind field as computed for balloons with linear and quadratic rise rates ascending through a light, moderate, or severe wind field has been derived. The linear and quadratic rise rate functions chosen span the set of all practical rise rate functions for a rising balloon. Figures are presented which show the wind error versus altitude for each rise rate, and each wind field, assuming 25-meter linear smoothing. Nominal FPS-16 radar errors of 0.1 mil in azimuth and elevation, five meters in slant range, and a time constant $\Delta t = 0.5$ second are assumed throughout. The wind errors derived under these assumptions can be adjusted in the case when the smoothing interval is not 25 meters, or the time constant is not 0.5 second. Exact and approximate expressions for these adjustments have been determined. The results and figures presented are useful in determining the ultimate capability

TABLE 7

RATIO OF BALLOON VELOCITY TO WIND VELOCITY FOR VARIOUS SMOOTH SPHERES AT 10 KILOMETERS ALTITUDE

Rise Rate ($\dot{z}$ ~ m/sec)

	2	4	6	10	15	20
Smooth Sphere (C_D = .15)				r = .73 $D_B = .92_1$ / $.81_2$	r = 1.56 $D_B = .85_1$ / $.77_2$	r = 2.73 $D_B = .80_1$ / $.77_2$
Smooth Sphere (C_D = .30)			r = .54 $D_B = .98_1$ / $.94_2$			
Smooth Sphere (C_D = .45)	r = .14 $D_B = .99_1$ / $.98_2$	r = .38 $D_B = .99_1$ / $.98_2$				

1 Indicates a Vertical Wavelength of 100 Meters.

2 Indicates a Vertical Wavelength of 50 Meters.

TABLE 8

RATIO OF BALLOON VELOCITY TO WIND VELOCITY FOR VARIOUS SMOOTH SPHERES AT 14 KILOMETERS ALTITUDE

Rise Rate ($\dot{z}$ ~ m/sec)

	2	4	6	10	15	20
Smooth Sphere ($C_D = .15$)					$r = 1.61$, $D_B = .81_1$ / $.73_2$	$r = 2.78$, $D_B = .78_1$ / $.74_2$
Smooth Sphere ($C_D = .45$)	$r = .20$, $D_B = .98_1$ / $.93_2$	$r = .44$, $D_B = .99_1$ / $.96_2$	$r = .84$, $D_B = .98_1$ / $.93_2$			

1 Indicates a Vertical Wavelength of 100 Meters.

2 Indicates a Vertical Wavelength of 50 Meters.

TABLE 9

RATIO OF BALLOON VELOCITY TO WIND VELOCITY FOR VARIOUS ROUGHENED SPHERES AT 10 KILOMETERS ALTITUDE

	Rise Rate ($\dot{z}$ ~ m/sec)					
	2	4	6	10	15	20
Rough Sphere (C_D = .47)	r = .17 $D_B = .99_1$ $.99_2$					
Rough Sphere (C_D = .60)		r = .52 $D_B = .99_1$ $.98_2$				
Rough Sphere (C_D = .72)			r = 1.24 $D_B = .99_1$ $.96_2$	r = 3.29 $D_B = .95_1$ $.88_2$	r = 7.28 $D_B = .88_1$ $.81_2$	r = 12.87 $D_B = .83_1$ $.79_2$

1 Indicates a Vertical Wavelength of 100 Meters.

2 Indicates a Vertical Wavelength of 50 Meters.

TABLE 10

RATIO OF BALLOON VELOCITY TO WIND VELOCITY FOR VARIOUS ROUGHENED SPHERES AT 14 KILOMETERS ALTITUDE

	Rise Rate ($\dot{z} \sim$ m/sec)					
	2	4	6	10	15	20
Rough Sphere ($C_D = .47$)	$r = .25$ $D_B = .99_1$ $.98_2$	$r = .50$ $D_B = .99_1$ $.96_2$				
Rough Sphere ($C_D = .60$)						
Rough Sphere ($C_D = .72$)			$r = 1.31$ $D_B = .99_1$ $.95_2$	$r = 3.36$ $D_B = .95_1$ $.87_2$	$r = 7.35$ $D_B = .87_1$ $.80_2$	$r = 12.94$ $D_B = .82_1$ $.79_2$

1 Indicates a Vertical Wavelength of 100 Meters.

2 Indicates a Vertical Wavelength of 50 Meters.

of rising balloon systems for measuring wind from the surface to 18 kilometers. Using the figures presented, one can estimate the wind accuracy that can be achieved by any type rising balloon by knowing only its rise rate behavior versus altitude. In addition, the figures can be used in balloon design to determine what rise rate function is needed to achieve specified accuracies.

Having specified a desired rise rate at a given altitude, the radius of a smooth and roughened sphere needed to achieve this rise rate has been derived. Since the equilibrium rise rate depends largely upon drag coefficient, it was necessary to assume two drag coefficient curves - one for a smooth and one for a roughened sphere. The curves chosen were from Hoerners [1] for the smooth sphere; and the drag coefficient curve for the Jimsphere [12] was assumed for a roughened sphere. Tables 3-6 show the balloon radius for smooth and roughened spheres needed to achieve two meter per second to 20 meter per second rise rates at 10 and 14 kilometer altitudes. Due to the higher drag coefficient for roughened spheres, a much larger radius is required for roughened spheres to achieve the faster (10 m/sec to 20 m/sec) rise rates.

The wind errors estimated in this report are in actuality balloon velocity errors since it is assumed that the balloon is a perfect wind sensor. That is, balloon velocity equals wind velocity. It has been shown in Tables 3-6 that large radii balloons are required to achieve ten meter per second or faster rise rates. It is important to know if these balloons, as well as smaller radii balloons, are good wind sensors. It has been shown in Tables 7-10 that all of the different radii balloons given in Tables 3-6 are indeed excellent wind sensors. Even the large diameter rough spheres show at least a 79% response to a fifty-meter wave. Consequently the balloon response provides no constraints in designing a fine scale wind measurement balloon system.

The tables relating rise rate to radius have important applications to the design of a rising balloon system. The proper perspective in

interpreting these tables, however, is essential. Careful attention must be paid to the assumptions under which the rise rate vs. radius tables were generated. The basic assumptions were that the drag curves depicted for smooth and rough spheres are reasonably accurate and that the spheres are non-exandable, 1/4 mil mylar skin, helium-inflated to ambient pressure, with no additional mass, ballast or instrument package. Any change in one of these assumptions would produce a different set of rise rate vs. radius tables. Consequently, by varying these assumptions, other means of obtaining a specified rise rate are feasible. For example, to achieve a fast rise rate, a more desirable means may be the design of a stream-lined balloon with a low drag coefficient. Other possible means would be the design of an expanding balloon, or perhaps an evaporating mass balloon (i.e., a balloon which loses mass, as well as gas, as it ascends). The techniques derived in this report can be used to provide rise rate versus radius tables under these and other assumptions. Before designing an advanced balloon measurement system, one should carefully compare and evaluate rise rate versus radius tables for various type balloon structures.

There are other practical considerations in balloon design and evaluation which have not been discussed in this report and are nevertheless of considerable importance. Cost, for example, is always of fundamental importance in the design of any system. Some of the large radius balloons discussed in this report are impractical for routine operational systems because the cost of the helium to fill these balloons would be exorbitant. Another practical consideration is the free-lift buoyancy force of a fast rising balloon. Large diameter balloons could provide a buoyancy force in excess of the weight of the man anchoring the balloon.

REFERENCES

1. Zartarian, G., and J. H. Thompson, "Validity of Detailed Balloon Soundings in Booster Vehicle Design," Scientific Report No. 1, AFCRL-68-0606, Kaman Avidyne, October 1968.

2. Reed, Wilmer H., III, "Dynamic Response of Rising and Falling Balloon Wind Sensors with Application to Estimates of Wind Loads on Launch Vehicles," NASA TN D-1821, National Aeronautics and Space Administration, October 1963.

3. Eckstrom, C. V., "Theoretical Study and Engineering Development of Jimsphere Wind Sensor," Final Report, NAS8-11158, G. T. Schjeldahl Co., July 1965.

4. Luers, J., and N. Engler, "On Optimum Methods for Obtaining Wind Data from Balloon Sensors," Journal of Applied Meteorology, Vol. 6, No. 5, October 1967, pp. 816-823.

5. DeMandel, R., and S. Krivo, "Capability of the FPS-16/Jimsphere System for Direct Measurement of Vertical Air Motions," NASA CR-61232, National Aeronautics and Space Administration, 1968.

6. Fichtl, G. H., "The Responses of Balloon and Falling Sphere Wind Sensors in Turbulent Flows," NASA TN D-7049, National Aeronautics and Space Administration, February 1971.

7. Murrow, H. N., and R. M. Henry, "Self-Induced Balloon Motions," Journal of Applied Meteorology, Vol. 4, No. 1, February 1965, pp. 131-138.

8. Scoggins, J. R., "Spherical Balloon Wind Sensor Behavior," Journal of Applied Meteorology, Vol. 4, No. 1, February 1965, pp. 139-145.

9. Rogers, R. R., and H. G. Camnitz, "Project Baldy, an Investigation of Aerodynamically-Induced Balloon Motions," Final Report, NAS8-11140, Cornell Aeronautical Laboratory, Inc., 1965.

10. MacCready, P. B., Jr., and H. R. Jex, "Study of Sphere Motion and Balloon Wind Sensors," NASA TM X-53089, National Aeronautics and Space Administration, July 1964.

11. MacCready, P. B., Jr., and R. E. Williamson, "The Motion of Ascending and Descending Spheres," NASA CR-61102, National Aeronautics and Space Administration, September 1965.

12. Fichtl, G.H., R.E. DeMandel, and S.J. Krivo, "Aerodynamic Properties of Rough Spherical Balloon Wind Sensors," NASA TN D-6373, National Aeronautics and Space Administration, July 1964.

13. Barton, D. K., Radar System Analysis, Prentice-Hall, 1964.

14. Scoggins, J.R., "Sphere Behavior and the Measurement of Wind Profiles," NASA TN D-3994, June 1967.

15. Engler, N.A., J.K. Luers, and J.W. McCloskey, "An Analysis of the AN/FPS-16 ROSE System," Scientific Report No. 2, AFCRL-67-0534, University of Dayton Research Institute, November 1967.

16. Engler, N.A., J. K. Luers, J.W. McCloskey, and J.D. Strange, "Tracking Errors in Detailed Wind Soundings," Scientific Report No. 1, AFCRL-69-0213, University of Dayton Research Institute, April 1969.

17. Luers, J.K., "A Method of Computing Winds, Density, Temperature, Pressure, and Their Associated Errors from the High Altitude ROBIN Sphere Using an Optimum Filter," AFCRL-70-0366, University of Dayton Research Institute, July 1970.

18. Scoggins, J.R., "An Evaluation of Detail Wind Data as Measured by the FPS-16 Radar/Spherical Balloon Technique," MTP-AERO-62-38, National Aeronautics and Space Administration, April 1962.

19. Daniels, G.E., Ed., "Terrestrial Environment (Climatic) Criteria Guidelines for Use in Space Vehicle Development, 1969 Revision," NASA TM X-53872, National Aeronautics and Space Administration, September 8, 1969; March 15, 1970.